Modeling the Sensitivity of Total Phosphorus in an Urban Stream to Climate Variability

A Thesis

Submitted by

Katherine M. Munson

In partial fulfillment of the requirements

For the degree of

Master of Science

in

Civil and Environmental Engineering

TUFTS UNIVERSITY

May 2015

Committee Members:

Professor John Durant (Advisor)

Professor Richard Vogel

Dr. Patrick Herron

Abstract

A study was performed to investigate the sensitivity of river phosphorus loading to changes in precipitation, temperature, and flow rate. This research performs sensitivity analyses using elasticity principles similar to those employed by economists (i.e., price elasticity of demand) to uncover climate-nutrient-loading relationships. Here, the concept of elasticity is implemented in a water quality context to identify the sensitivity of total phosphorus (dissolved and particulate) loading in an urban stream to several climate variables using multivariate approaches. Previous analyses have used single parameter elasticity methods to represent the general relationship between nutrient loading and a variable of interest, but these methods cannot reflect the complicated nonlinear relationships inherent among nutrients, precipitation, temperature, and streamflow. Instead, the multivariate analysis presented in this study relies on the combined interactions among precipitation, temperature, and streamflow to successfully distinguish their individual impacts on nutrient loading. This study presents field data results and develops models that can be used to estimate phosphorus loads while determining the sensitivity of total phosphorus loading to changes in climate variables. It was found that total phosphorus loading at Alewife Brook depends significantly on season, rainfall, combined sewer overflow incidents, and flow rate. These results were significant for the development of a nutrient loading model that predicted a 3.6% to 7.4% increase in total phosphorus loading at Alewife Brook if small increases in precipitation, temperature, flow rate, and combined sewer overflow incidents occur. These results could be useful for developing models to better predict water quality responses to climate variability.

Acknowledgements

This work was supported by a Tufts Community Research Center (TCRC) grant from Tisch College at Tufts University as well as a Water Systems Science and Society (WSSS) fellowship from the Tufts Institute of the Environment.

I would like to thank my advisor, Professor John Durant, for his guidance and intellectual contributions to field project procedures and model development. Thanks to Professor Rich Vogel for assistance with modeling and statistical analysis, as well as his enthusiastic encouragement. I'd like to thank Dr. Patrick Herron for his professional guidance through both the sampling process and external thesis direction. I would also like to thank my research assistant Ruhui Zhao for valuable assistance in the field and in the laboratory. Finally, a special thanks to my parents for their kindness and support.

Table of Contents

List of Figures

List of Tables

Introduction

Watersheds are dynamic systems, changing over minutes, years, decades or centuries. One component of watersheds that is constantly fluctuating is water quality. In addition to changes in infrastructure, population, and land use, changing weather patterns may greatly influence water quality (Wilby, 1993; Mimikou et al., 2000; Whitehead et al., 2009). Over the past few decades, the impacts of a changing climate on water quantity have been studied at length (Frederick and Major, 1997; Kundewicz et al., 2007; Milly et al., 2008); however, the influence of climate variability on water quality has only recently been considered (Kundewicz et al., 2007; Whitehead et al., 2009; Delpa et al., 2009).

Water quality within hydrologic systems evolves due to a variety of influences such as changes in precipitation intensity, temperature, storm frequency, wind speed, atmospheric deposition, groundwater recharge, and streambed erosion. Concentrations of pollutants often vary seasonally based on seasonal changes in streamflow (Lipp, 2001; Praskievicz and Chang, 2009). Particularly during storm events, substantial quantities of contaminants flow into rivers and streams, causing pollutant loads to increase. In areas containing nutrient-laden sediments, increases in streamflow rates will influence resuspension of particulate matter from bottom sediments, increasing nutrient loads carried by rivers. In particular, projected changes in winter rainfall are expected to enhance nutrient loading to freshwaters in the temperate zone (IPCC, 2007).

Nutrient pollution is one of America's most widespread environmental problems (Gilinsky, 2009; Barvenik, 2009). In particular, nutrient pollution (nitrogen and

phosphorus) supports the rapid growth of potentially harmful algal blooms which, during decomposition, can decrease the dissolved oxygen necessary to support aquatic life (Conley et al., 2009). Some algal blooms are even harmful to humans who come in contact with polluted water or consume tainted fish (Anderson et al., 2002). The presence of excess nitrogen and phosphorus can lead to eutrophication, which the EPA and USGS agree is the most ubiquitous water quality impairment in the United States, accounting for approximately 60% of impaired river reaches across the nation (U.S. EPA, 1998).

Nutrient loads can be generated from several sources in an urban environment, including stormwater runoff, leaking municipal infrastructure, pet and urban wildlife waste, phosphate-containing cleaning agents, atmospheric deposition, soil erosion, sediment resuspension, and sanitary and combined sewer overflows (Mallin et al., 2009). Suspended sediments readily adsorb phosphate[1], which can desorb during dynamic conditions produced by storms (Burkholder et al., 1992). When combined with escalated runoff and erosion caused by increased impervious coverage, sediment resuspension can exacerbate nutrient conditions within a stream (Mallin et al., 2009). However, many of these inputs are often difficult to measure and regulate because they come from large, ill-defined land areas and are affected by variability in weather events (Kleeburg and Dudel, 1997).

There is broad consensus that human actions are altering the global nutrient cycle, causing nitrogen and phosphorus to accumulate in the soil due to fertilizer use, animal feeds, agricultural crops, mining, and other activities (Vitousek et al., 1997; Galloway, 1998; Gruber and Galloway, 2008). It is estimated that net phosphorus storage in

[1] A compound consisting of phosphorus and oxygen that plays a major role in biological processes of many organisms

terrestrial and freshwater ecosystems is at least 75% greater than preindustrial levels (Bennet, 2001). High impervious surface coverage in urban areas exacerbates runoff of nutrients from lawns, gardens, and landscaped areas by increasing the "flashiness" or erratic and rapid inputs of runoff into rivers (Holland et al., 2004). It is projected that if current practices continue, nonpoint source pollution of surface waters is likely to increase over time (Carpenter, 1998).

Because the climatic system and the freshwater resource system are so closely linked, a change in one of these is likely to induce change in another (Kundzewicz, 2007). Often, water pollution is directly associated with anthropogenic activities such as urban, industrial, or agricultural growth, and climate change has the potential to further degrade surface water quality when combined with these activities (Delpa, 2009). The impacts of climate change on water quality primarily occur through hydrological changes (Praskievicz and Chang, 2009). It is widely accepted that increases in temperature, observed at all spatial scales, drive many of the observed changes we are now seeing in water quality (Kundzewicz, 2010). These changes in temperature directly impact soil temperature, season length, and precipitation, all of which contribute to increased pollution of rivers and streams.

Variability in climate may have significant impacts on the water cycle and nutrient losses, modifying nutrient transformation and transport characteristics (Bouraoui et al., 2004). Temperature is positively correlated with microbial processes, which increase phosphate activity and nutrient mobilization in soils (Delpa, 2007; Sardans et al., 2008). A moderate increase in soil temperatures could lead to a large increase in the amount of nutrients available for runoff during storm events. Seasonality has an important impact on nutrient patterns within water bodies (Zhu et al., 2005). Climate

scientists report with high confidence that the United States will experience a significant increase in the number of hot days by the end of this century (Gleason et al., 2007). Changes in temperature lead to changes in land use management, such as rates and timing of lawn fertilization (Howden et al, 2007). If surface temperature warming increases the number of warm days per year, then the period in which people are fertilizing their lawns may lengthen. As a consequence, rainfall runoff could potentially carry a larger annual quantity of nutrients into rivers. Increase in runoff and erosion due to greater precipitation intensity will likely result in an increase of pollutant transport, especially after long periods of dry weather (Delpa, 2007). As weather extremes become more frequent and severe, intense precipitation may overload sewer systems, introducing yet another source of pollution into waters. Additionally, flooding as a result of increased severity of storms has the potential to increase erosion of nutrient-laden soil, which adds to degradation of water quality.

The potential for climate-induced changes in water quality motivates the need for an investigation into the sensitivity of the water quality of individual watersheds to changes in climate variables. Climate-streamflow relationships have been used to determine precipitation and temperature elasticity[2] of streamflow, providing a nonparametric[3] measure of the sensitivity of streamflow to changes in climate (Sankarasubramanian et al., 2001; Chiew et al., 2007). Elasticity is a term that represents a form of sensitivity analysis that has a specific mathematical interpretation. This term can be generally defined as the proportional change in one variable, *x*, divided by the

[2] How sensitive a variable is to changes in another variable – in this instance how sensitive streamflow is to changes in precipitation and temperature

[3] Not involving any assumptions as to the form or parameters of a distribution

proportional change in another variable, *y*, where $\varepsilon_x(x,y) = \frac{dy/y}{dx/x} = \frac{dy}{dx}\frac{x}{y}$. The interpretation of this definition of elasticity is simple. If elasticity, $\varepsilon_x(x,y)$, is equal to 2%, then a 1% increase in *x* will yield a 2% increase in *y*. Discussion concerning the interpretation and estimation of elasticity dates back to the early 1900s in economic literature, but has recently received attention from water resources researchers in the past couple of decades.

This climate-streamflow sensitivity methodology introduced by Sankarasubramanian et al. (2001) was extended to develop climate-water quality relationships using extensive sampling records to describe the magnitude of stream water quality responses to climate change (Jiang et al., 2014). However, these models consider sensitivity of water quality to temperature separate from its sensitivity to precipitation. Saltelli and Annoni (2010) emphasize the shortcomings of such an approach to sensitivity analyses, presenting a generalized proof that demonstrates the inefficiency of one-at-a-time- (OAT) methods.

In lieu of OAT approaches, a multivariate analysis to determine sensitivity of water quality to changes in climate is desired. Many multivariate models describe the relationship between water quality and other factors (i.e., Koklu et al. 2010; Nasir et al., 2011; Mustapha and Abdu 2012). However, to our knowledge, these studies do not interpret the meaning of the coefficients of such models as elasticities. Multivariate methods to determine elasticity of streamflow to changes in climate have been developed in recent years. For instance, Fu et al. (2007) extended the single parameter precipitation elasticity of streamflow index introduced by Sankarasubramanian et al. (2001) into a two parameter climate elasticity index, as a function of both precipitation and temperature.

This two parameter climate elasticity methodology was used by Ma et al. (2010) and then compared to a geomorphology-based hydrological model to estimate the impact of climate variability on the inflow into a reservoir responsible for domestic water supply in Beijing. The work of Ma et al. (2010) was extended to include a variable for interannual variability of soil moisture storage to represent the sensitivity of runoff to changes in soil moisture storage, precipitation, and temperature simultaneously (Xu et al., 2012). Gardner et al. (2009) used multivariate elasticity techniques to estimate changes in runoff as a function of changes in precipitation, temperature, and potential evapotranspiration. Tsai and Vogel (2010) incorporated climate influences (i.e. precipitation and temperature), land use changes, and well withdrawals in elasticity analyses to determine sensitivity of streamflow to changes in these variables using standardized departures about mean-ordinary least squares (SDM-OLS) techniques. Allaire et al. (2015) presented a multivariate approach to model complex hydrological interactions among climate, land use, and water use variables while avoiding the limitations of OAT methods.

Saltelli and Annoni (2010) and Allaire et al. (2015) and many others have shown that a complete sensitivity analysis should consider interaction effects among input uncertainties and evaluate the effect of an input while other inputs are allowed to vary at the same time. Economists have implemented this methodology extensively in an attempt to reduce omitted variable bias (OVB), which occurs when a model incorrectly leaves out one or more important causal factors thus over- or under-estimating the effect of one of the other factors. However, the climate elasticity of water quality methods introduced by Jiang et al. (2014) do not account for OVB in the bivariate estimation of the sensitivity of water quality variables to changes in precipitation and temperature.

The primary goal of this thesis is to demonstrate that one can only understand the interactions among temperature, precipitation, streamflow, and nutrient loads in an urban watershed if these factors are considered in an integrated fashion. We hope to demonstrate the efficiency of using multivariate approaches to estimate elasticity that result from models with high explanatory value and reduced OVB. The methodology introduced in this study is quite general and should have application to a wide range of problems relating to water quality management that seek to evaluate the evolution of water quality response of a watershed to many different climate factors. A case study is introduced to highlight the influence of precipitation, temperature, and surface water discharge on total phosphorus loading within Alewife Brook, a tributary to the Mystic River near Boston, MA.

Methodology

Climate Elasticity of Streamflow

Previous studies have examined the sensitivity of streamflow to changes in precipitation by introducing the concept of precipitation elasticity (Schaake, 1990; Sankarasubramanian et al, 2001; Chiew, 2006). The precipitation elasticity of streamflow is defined as the proportional change in streamflow, *Q*, divided by the proportional change in precipitation, *P*:

$$\varepsilon_P = \frac{dQ/Q}{dP/P} = \frac{dQ}{dP}\frac{P}{Q} \quad (1)$$

Sankarasubramanian et al. (2001) presented a nonparametric estimator of precipitation elasticity defined at the mean value of the climate variable so that

$$\bar{\varepsilon}_P = \frac{dQ}{dP}\frac{\bar{P}}{\bar{Q}} \quad (2)$$

where $\bar{P}$ and $\bar{Q}$ denote the mean values of precipitation and streamflow, respectively.

Based upon the nonparametric elasticity estimator recommended by Sankarasubramanian et al. (2001), Jiang et al. (2014) developed elasticity estimators for several water quality parameters (e.g. nutrients, turbidity, dissolved oxygen) with respect to air temperature and precipitation at the monthly scale (equation (3)), where WQ_t represents the water quality variable at time *t*, $\overline{WQ}$ represents the mean value of water quality variables, P_t represents the monthly precipitation value at time t, and $\bar{P}$ represents the mean precipitation value for all of the data assessed.

$$\varepsilon_P = median\left(\frac{WQ_t - \overline{WQ}}{P_t - \bar{P}}\frac{\bar{P}}{\overline{WQ}}\right) \quad (3)$$

The advantage of using this elasticity estimator is that the use of the median minimizes the impacts from outliers, such as extreme events. However, the present study argues that certain water quality measurements, such as nutrient loads, are greatly influenced by weather extremes, and thus outliers are an integral part of estimating sensitivity of water quality to changes in climate.

One limitation of the Sankarasubramanian et al. (2001) and Jiang et al. (2014) methods is that they are only able to determine sensitivity of streamflow or water quality to changes in a single explanatory variable. However, water quality is influenced by simultaneous changes in precipitation, temperature, streamflow, and sometimes extreme events, seasonal cycling, and other possible explanatory variables. A multivariate approach is necessary to capture complex interactions among climate variables that influence total phosphorus concentrations. The following section describes two general approaches to estimation of the multivariate elasticity of nutrient loads.

Multivariate Climate Elasticity of Nutrient Water Quality

In an effort to determine the generalized sensitivity of nutrient loading to changes in precipitation, temperature, and streamflow, we consider the total differential of nutrient load (L) resulting from simultaneous changes in precipitation (P), temperature (T), and flow rate (Q)

$$dL = \frac{\partial L}{\partial P} dP + \frac{\partial L}{\partial T} dT + \frac{\partial L}{\partial Q} dQ \tag{4}$$

Based on the recommendation of Sankarasubramanian et al. (2001), the mean values of each variable were used to estimate the differentials, leading to

$$L - \bar{L} = \frac{\partial L}{\partial P}(P - \bar{P}) + \frac{\partial L}{\partial T}(T - \bar{T}) + \frac{\partial L}{\partial Q}(Q - \bar{Q}) \tag{5}$$

Each term is divided by the mean load, $\bar{L}$, and the three terms on the right hand side are multiplied by unity in the form of $\frac{\bar{P}}{\bar{P}}, \frac{\bar{T}}{\bar{T}}$, and $\frac{\bar{Q}}{\bar{Q}}$ respectively, to result in

$$\left(\frac{L-\bar{L}}{\bar{L}}\right) = \frac{\partial L}{\partial P}\frac{\bar{P}}{\bar{L}}\left(\frac{P-\bar{P}}{\bar{P}}\right) + \frac{\partial L}{\partial T}\frac{\bar{T}}{\bar{L}}\left(\frac{T-\bar{T}}{\bar{T}}\right) + \frac{\partial L}{\partial Q}\frac{\bar{Q}}{\bar{L}}\left(\frac{Q-\bar{Q}}{\bar{Q}}\right) \tag{6}$$

Lower case variables *l*, *p*, *t*, and *q*, are defined as the four respective terms in parentheses in the above equation, or the percentage change from the mean, so that

$$l = \bar{\varepsilon}_P * p + \bar{\varepsilon}_T * t + \bar{\varepsilon}_Q * q \tag{7}$$

where

$$\bar{\varepsilon}_P = \frac{\partial L}{\partial P}\frac{\bar{P}}{\bar{L}}, \quad \bar{\varepsilon}_T = \frac{\partial L}{\partial T}\frac{\bar{T}}{\bar{L}}, \quad \text{and} \quad \bar{\varepsilon}_Q = \frac{\partial L}{\partial Q}\frac{\bar{Q}}{\bar{L}}$$

are the precipitation, temperature, and streamflow elasticity of nutrient water quality, respectively. The objective is to use ordinary least squares (OLS) regression methods to fit the multivariate linear model resulting in minimum variance, unbiased estimates of the three elasticity estimates by fitting a linear model to (7) without an intercept term. The model parameter estimates are then the elasticity estimates shown in (7).

Because the linear multivariate model in (7) is based on the definition of the total differential, we avoid uncertainty regarding the use of a correct model form. In other words, there are no model assumptions made in the above derivation concerning the relationship between the dependent variable of interest, L, and the various independent variables, P, T, and Q. This unique feature distinguishes our approach to sensitivity analysis from most previous approaches, which are based on model assumptions (Fu et al.,2007; Ma et al., 2010; Mustapha and Abdu, 2012). The resulting model in (7) is linear, and can be solved using multivariate OLS regression. OLS is an attractive estimation method because resulting estimates of elasticities are unbiased and provide standard errors and confidence intervals so that hypothesis testing can take place. This opens the possibility for corrections for heteroscedastcity[4] (Stedinger and Tasker, 1985; Kroll and Stedinger, 1998), autocorrelated model errors[5] (Draper and Smith, 1981) and other violations of OLS model assumptions (Johnston, 1984). The explanatory power of the

[4] Heteroscedasticity occurs when the variance of error terms differ across observations

[5] Autocorrelated errors are detected in the observable residuals of a regression model and indicate that the error terms are correlated such that OLS estimators are no longer the best linear unbiased estimators

regression (i.e., the value of R^2) is not preeminent for estimation of elasticity, which relies on unbiased model parameters rather than high explanatory value. Instead, OVB is the key issue that tends to be lessened as R^2 increases. For the purposes of elasticity estimation, residuals of the model must be independent and normally distributed with a constant variance to enable statistical inference of resulting elasticity estimates. However, we strive to build a model that provides unbiased elasticity estimates while simultaneously having high explanatory value.

Furthermore, additional explanatory variables may be added to the analysis as long as they are representative of the dependent variable. Once additional explanatory variables are added, an analysis of the model sum of squared errors may be used to determine which explanatory variables have the greatest impact on nutrient loading. Here either F-tests[6] or t-tests[7] are suited to such analyses.

Each elasticity estimate has a physical meaning. For example, if an elasticity estimate is near 0, the variable has little to no impact on water quality. If the elasticity is near ±1, the relation is linear. Jiang et al. (2014) classify climate elasticity of water quality by the following rules: (1) inelastic when the absolute value of the elasticity variable is < 0.1; (2) relatively elastic when $0.1 \leq$ absolute value of the elasticity variable is < 0.5; (3) strongly elastic when absolute value of the elasticity variable is ≥ 0.5; and (4) unit elastic (percentage change in the water quality variable is equal to the percentage change in the climate variable) when absolute value = 1.0.

Outlined above is a nonparametric approach that provides an estimate of the elasticity about the mean values of the selected variables as defined in (2) and (7). The

[6] Tests overall fit of a regression model
[7] Tests statistical significance of individual parameters of a regression model

approach is nonparametric because it is derived from the chain rule and thus makes no model assumptions about the structural relationship between the independent and dependent variables. The following section presents a parametric approach frequently used in economics, which makes a critical assumption about the structure of the relationship between the independent and dependent variables. This approach leads to elasticity estimates that are not computed about the mean values of the variables, as shown in the form given in (1).

In the field of economics, the concept of elasticity is widely used to determine the sensitivity of demand for a product to its price. This is termed price elasticity and is an approach that generally does not depend on mean values such as the elasticity in (1), but assumes a log-linear model relating the independent and dependent variables

$$L = \theta * P^{\varepsilon_P} * T^{\varepsilon_T} * Q^{\varepsilon_Q} * v \tag{8}$$

where L, P, T, and Q are defined as in (3)-(7), θ, ε_P, ε_T, and ε_Q are model coefficients and v are lognormally distributed model errors. One can easily show by simply taking derivatives that the model coefficients are the elasticity estimates so that

$$\varepsilon_P = \frac{dL}{dP}\frac{P}{L}, \quad \varepsilon_T = \frac{dL}{dP}\frac{T}{L}, \quad \text{and} \quad \varepsilon_Q = \frac{dL}{dP}\frac{Q}{L}$$

These elasticity definitions are more general than in (7) because they are not defined strictly about the mean of the variables. However, estimation of multivariate elasticities using (8) requires an assumption regarding the power law model structure in (8), which was not a requirement for estimation of the elasticities about the mean values in (7).

Case Study

The following case study outlines the water quality response of Alewife Brook, a tributary to the Mystic River near Boston, MA, to changes in climate. The study begins with background information about the watershed which is followed by a review of phosphorus cycling processes, the potential impacts of climate variability on the area, a description of databases used for modeling, and an explanatory data analysis to better understand the behavior of the observations. This information is followed by the application of equations (7) and (8) to determine the generalized precipitation, temperature, and flow rate elasticity estimates of total phosphorus at Alewife Brook.

Background

Like many urban watersheds, the Mystic River watershed in eastern Massachusetts has a long history of industrial uses, including mills, shipyards, automobile plants, tanneries, and other industries that have left their mark on the river and its ecosystem. As a result of such activity, the river has experienced several water quality problems, such as toxic chemical inputs from contaminated waste sites, excess nutrients, noxious aquatic plants, organic enrichment, and low dissolved oxygen (Massachusetts DEP, 2014). Alewife Brook, a tributary to the larger Mystic River, has been identified as a key contributor of phosphorus to the main stem of the river. Phosphorus is believed to originate from a number of sources within the Alewife Brook watershed, including fertilizer and animal waste runoff, erosion and resuspension of phosphorus-laden soil and sediment, leaking municipal sanitary systems, and the

activation of combined sewer overflows dumping raw sewage into the brook during intense and/or lengthy rain events.

The Phosphorus Cycle at Alewife Brook

The biogeochemical cycle of phosphorus at a local scale, like Alewife Brook, is unique among the cycles of other water quality constituents because it has no significant gaseous component. Most of the phosphorus in cycling processes is derived from weathering of phosphorus-containing minerals and soils (Bashkin, 2002) and is released in the dissolved organic form by organic phosphorus contained in particles, particularly during periods of storm runoff (Kalff, 2002). The primary mechanisms of phosphorus transport in rivers are advection and diffusion through zones of phosphorus storage (Withers and Jarvie, 2008). Usually, dissolved organic phosphorus (DOP) concentrations are highest and dissolved inorganic phosphorus (DIP) concentrations are lowest during two periods - May and late August (Van Der Zee and Chou, 2005). This DOP is an important source of biologically available phosphorus, which bacteria and phytoplankton uptake as nourishment (Orrett and Karl, 1987; Bjorkmann and Karl, 1994). DIP, usually in the form of orthophosphate[8], is produced by natural processes and often found in sewage, whereas DOP is formed by biological processes. DOP is often bound to plant or animal tissue and is contributed to sewage by body waste and food residues (Mueller and Helsel, 1996). The first period of elevated DOP coincides with the highest concentrations of both Chlorophyll *a*[9] and particulate organic phosphorus (POP), which sustains plant

[8] The form of phosphorus, both organic and inorganic, which is produced by the digestion process
[9] Chlorophyll *a* absorbs energy and is essential for photosynthesis in blue-green algae

growth. POP concentrations typically decrease substantially by the second period of elevated DOP and DIP begins. During this period, phosphorus is recycled as biomass decays. This general process is conceptualized in Figure 1.

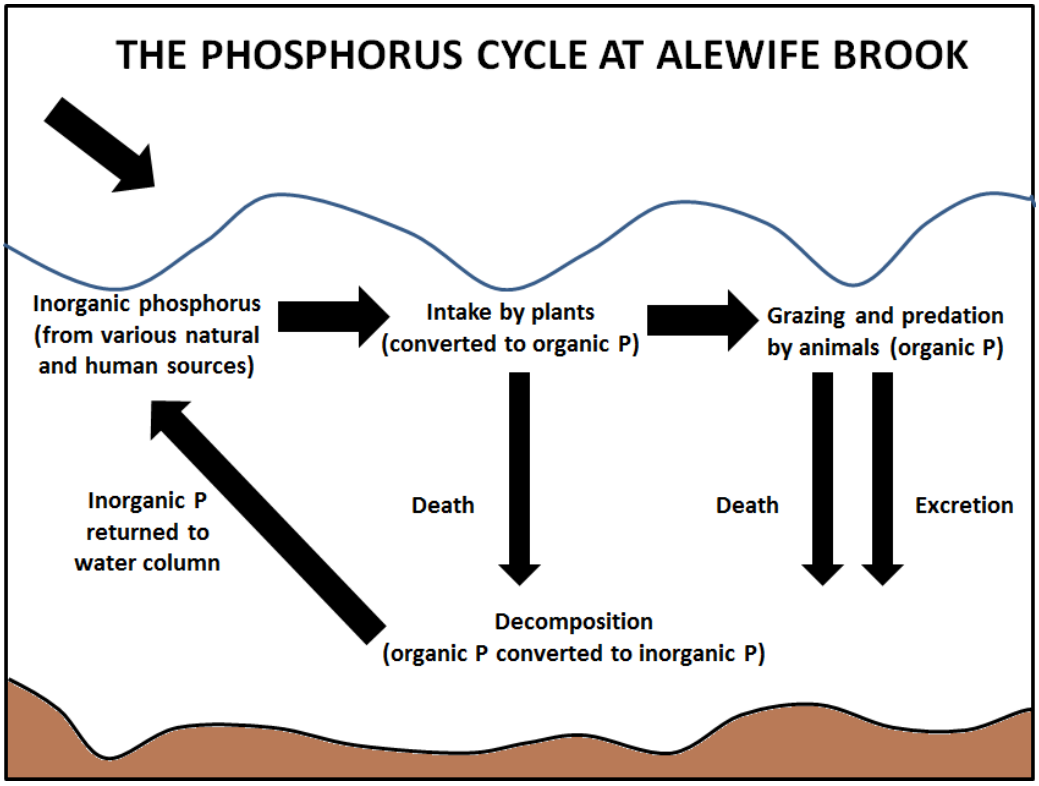

Figure 1. Conceptual Diagram of the Phosphorus Cycle at Alewife Brook

Many parts of Alewife Brook exist underneath a canopy of trees, which make organic matter available to aquatic microbes during the fall when leaves are shed. Plant matter as a result of plant deaths in late summer and early fall decomposes and is retained in the sediments at the bottom of the brook. This decomposed phosphorus matter spreads during storm events to feed a new generation of plants, causing persistent algal blooms in the process. During winter, flows increase due to snowmelt, and less phosphorus is retained in the sediment. Inorganic phosphorus released from the sediments during

springtime allows plants and algae to reproduce quickly, which converts much of the phosphorus to DOP. Decay of this plant matter during the summer months releases DIP back into the ecosystem, causing plants and algae to rapidly grow once again.

Most phosphorus inputs delivered to streams under extreme high flows will be flushed through without entering the stream biogeochemical pathways (Withers and Jarvie, 2008). However, phosphorus tends to be retained within river systems under low flows during spring and summer (e.g. Svendsen and Krovang., 1995; Reddy et al., 1999; Bukaveckas et al., 2005; Némery and Garnier, 2007). Advection in rivers can result in increases in sorption interactions and the mobilization of particulate phosphorus to and from sediments with associated release of dissolved phosphorus from porewaters (Keup, 1968; Casey and Farr, 1982). Macrophytes, or visible plants, contribute to phosphorus cycling through phosphorus uptake during the growing season and release of orthophosphate during decay (Gregg and Rose, 1982; Carpenter and Lodge, 1986). Additionally, plant matter slows water current velocity near the streambed, allowing increased sediment deposition (Gregg and Rose, 1982).

In addition to natural processes, human activities affect the phosphorus cycle. Surface runoff may carry phosphorus in either inorganic phosphorus compounds or organic matter to the brook. We assume that much of the commercial fertilizer used on lawns in the Alewife Brook watershed contains inorganic phosphorus. Organic phosphorus inputs into Alewife Brook likely come from pet and animal excrement, as well as sewage from CSOs. Inputs of phosphorus from surface runoff usually exist in dissolved form, whereas erosion and sediment suspension can transport considerable amounts of phosphorus in particulate form (Mueller and Helsel, 1996). Phosphorus in the Alewife Brook watershed derives from natural soils, sediments, and possibly agricultural

and historical industrial activity (Gawel et al., 2000). During intense rainfall events, erosion of soils and resuspension of sediments return inorganic phosphorus to the water column, making an increased amount of phosphorus available for uptake by plants.

Potential Climate Variation at Alewife Brook

Although increases in average air temperatures and more extreme variation in the amounts and intensity of precipitation have been predicted, the effects of climate change on phosphorus cycling at a local scale are far from clear and are likely to vary from site to site (Schindler, 1997; Meyer et al., 1999; Malmqvist and Rundle, 2002; Huntington, 2006; Withers et al., 2008). Precipitation has a significant impact on phosphorus pollution within the brook because heavy rains can transport sand, silt, clay, and organic particles from the land to surface water. Nearly 45 % of land surfaces within the Alewife Brook sub-watershed are impervious (i.e., either pavement or buildings), allowing phosphorus to be transported from lawns, sidewalks, and streets, and into the brook. Precipitation events also result in greater sanitary sewer inputs to Alewife Brook, as the opportunity for mixing of stormwater and sewer water becomes greater due to over-capacity pipes. Climate models predict that the Northeast U.S. will experience increases in winter precipitation, much of which is expected to fall as rain, as well as an increase in the likelihood and severity of high intensity rain storms (Frumhoff et al., 2007). When precipitation falls as rain, rather than snow, it is able to reach rivers more rapidly. By the end of the century, precipitation in New England is estimated to increase by about 10 % in spring and summer, 15 % in fall, and 20 to 30 % in winter (Frumhoff et al., 2007). As a result of higher winter rainfall, as well as frequency and severity of storms, phosphorus

loading from land to streams is expected to increase in the Northeast (Jeppesen et al., 2009).

Climate change is also expected to increase the frequency of extremely hot days in the Northeast. Boston in particular is projected to experience an increase in the number of days reaching 100°F from an average of one day per year to as many as 24 days per year by the 2100 (Karl et al., 2009). Higher average air temperatures have the potential to cause warming of water temperature in shallow streams (Withers and Jarvie, 2008), like that of Alewife Brook. This warming increases the time period available for biological activity, which may affect phosphorus cycling (Durance and Ormerod, 2007; Harrison et al., 2008). Additionally, the increased frequency of warm days may have a serious impact on phosphorus loading because phosphorus release is much faster at high temperatures than lower temperatures (Li et al., 2013). An explanation for this phenomenon is that as temperature rises, microbial activity increases, degrading organic matter, and mobilizing phosphorus.

Changes in magnitude and frequency of extreme high flows and floods may cause reduced river phosphorus retention capacity, greater seasonal variability in runoff volumes, scouring of streams, and more frequent inputs of storm and combined sewer overflows (Newson and Lewin, 1991; Bouraoui et al., 2002; Wilby et al., 2006; Withers et al., 2008). Although heavily influenced by precipitation, changes in stream flow rate influence erosion at the sediment-water interface. Total phosphorus concentrations during dynamic conditions are often much higher than those during static conditions (Li et al., 2013). Changes in speed or direction of water currents can mobilize particulate matter from bottom sediments, introducing phosphorus into the river. As winter precipitation increases and warmer temperatures melt snow faster, high-flow events are predicted to

occur more frequently. In the Northeast, overall streamflow is projected to become more extreme, especially in the winter (Mauget, 2003; Groisman et al., 2004; Barron et al., 2008). This may increase erosion of the phosphorus-laden soils and sediments that feed Alewife Brook.

In an effort to prepare for such changes in climate, it is essential to determine the sensitivity of water quality at Alewife Brook to changes in precipitation, temperature, and flow rate. Furthermore, this area is often afflicted by an additional input of total phosphorus from incidents of combined sewer overflows (CSOs). Thus, another term for CSOs must be added to the analysis. This can be done through a multivariate estimation of elasticity related to precipitation, temperature, flow rate, and CSO. Elasticity values determined in a multivariate approach will identify how sensitive phosphorus loading is to changes in monthly precipitation, temperature, flow rate, and number of combined sewer overflows per month.

Database

Introduction

Since the year 2000, volunteers have been collecting water samples at Alewife Brook as part of the Mystic River Watershed Association's baseline monitoring program. Samples were collected at regular monthly intervals and analyzed for a number of parameters, including total unfiltered phosphorus (both dissolved and particulate). In 2014, intensive storm-event sampling provided total phosphorus measurements during rainfall events. This combination of baseline and storm event sampling data was used to

model monthly phosphorus loads from 2007-2014. This range was chosen because reliable 15-minute measurements of flow rate at Alewife Brook via a USGS gage (gage #01103025) are available from 2007-2015(http://waterdata.usgs.gov/nwis/uv/? Site_no =01103025). Monthly average temperature and monthly total precipitation data were acquired from the National Climatic Data Center and used for the analysis. Additionally, the number of combined sewer overflow (CSO) discharges per month kept on record by the Mystic River Watershed Association since 2007 was used for this analysis. As shown in Figure 2, the USGS and baseline sampling stations are at the same location. However, the stormwater sampling station was purposely located further downstream from the USGS and baseline stations so that the equipment used to sample was less accessible to the public and therefore less susceptible to vandalism.

Figure 2. Map of Stormwater Sampling Location, USGS Gauge Location, and Baseline Sampling Location at Alewife Brook

Baseline Sampling

Since July 2000, MyRWA has been monitoring trends in water quality with the help of trained volunteers, who collect water samples from fifteen sites across the watershed. These samples were collected manually, using a sample bottle attached to a long pole to grab a small portion of water from the brook. Each sample was analyzed for bacteria, total suspended solids, nutrients (nitrate, nitrite, and total unfiltered phosphorus), conductivity, dissolved oxygen, water temperature, water color, and odor at the Alpha Analytical Laboratory in Westborough, MA. To control for eutrophication, the EPA has established a recommended limit of 0.05 mg/L for total phosphorus in streams that enter lakes and 0.10 mg/L for total phosphorus in flowing waters (U.S. EPA, 1986). As shown in Figure 3, approximately half of the total unfiltered phosphorus measurements taken between the year 2000 and 2014 indicate phosphorus levels above the limit recommended by EPA. Interestingly, the majority of these samples were taken during non-storm conditions.

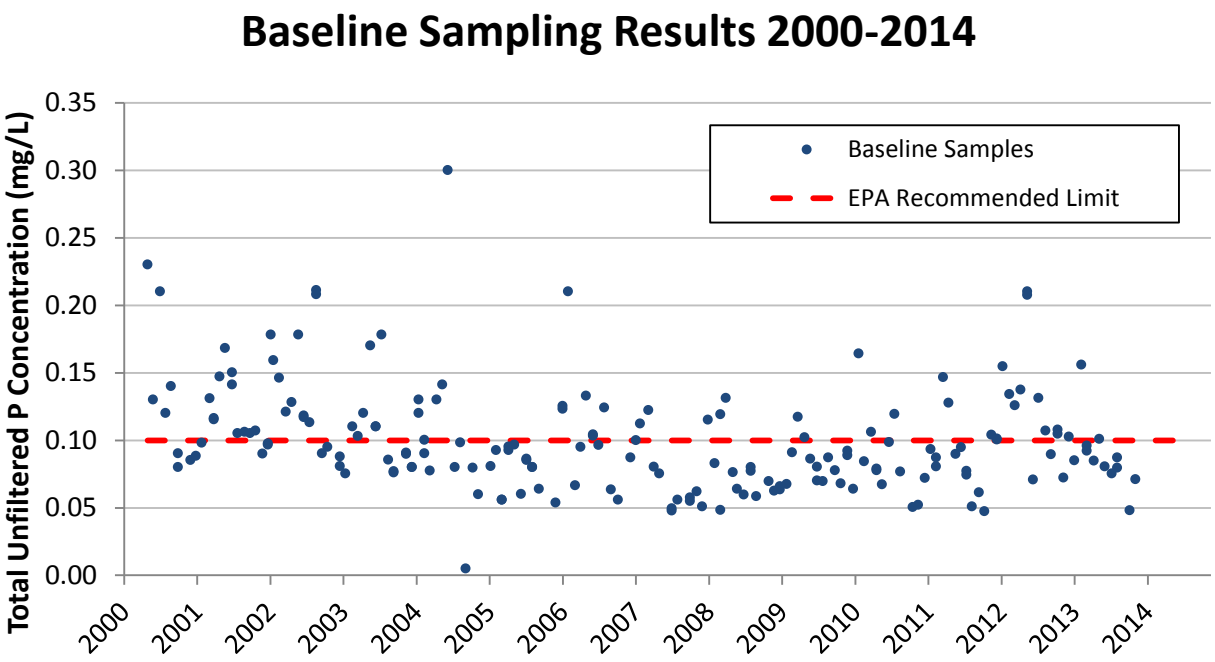

Figure 3. Mystic River Watershed Baseline Sampling Program Data from 2000-2014 (http://mysticriver.org/baseline/)

2014 Storm Sampling

During the 2014 calendar year, samples were collected from April to October and analyzed for total unfiltered phosphorus and turbidity. The events were selected based on weather forecasts for Arlington, MA as reported by various sources including the National Weather Service (NWS), the National Oceanic and Atmospheric Administration (NOAA), and Weather Underground. Forecasted precipitation amounts were tracked using the Quantitative Precipitation Forecasts (QPFs) from the NWS Weather Prediction Center.

Although storm event samples were collected at three locations within the Mystic River basin, this thesis will focus on sampling at Alewife Brook, where an ISCO 6712

autosampler was deployed approximately 600 meters downstream from the USGS streamflow gauge (ID: 01103025) and baseline sampling station ALB006, as shown in Figure 2. Storm events were required to meet the following criteria, adopted from the NPDES Storm Water Sampling Guidance Document (U.S. EPA, 1992):

- Total precipitation depth of the storm must be greater than 0.1 inches
- Storm event must be preceded by at least 72 hours of dry weather (defined as a maximum of 0.01 inches total over the previous 72 hours)
- If possible, total precipitation and duration should be at least 0.15 inches of rainfall within 24 hours
- Continuous flow measurements collected at the sampling point or by a near-by streamflow gage must be available
- Sampling schemes shall be comprised of a minimum of 6 discrete samples spanning the rising limb and peak of the runoff flow hydrograph

Storm-event samples were taken using an ISCO Autosampler (see Appendix A for details). Laboratory methods used to analyze storm event samples were the same as those used to analyze baseline samples. Figure 4 demonstrates the results of the 2014 storm sampling, complete with phosphorus concentration measurements and their corresponding discharges for each storm event. Pictured also is each storm's event mean concentration (EMC). As shown, flow rates were highest for storms in the summer, and constituent phosphorus concentrations were highest in July and September. These two storms with the highest phosphorus concentrations were storms sampled during combined sewer overflow (CSO) events. Specific storm sampling dates and times are found in Appendix B, and additional storm sampling results are found in Appendix C.

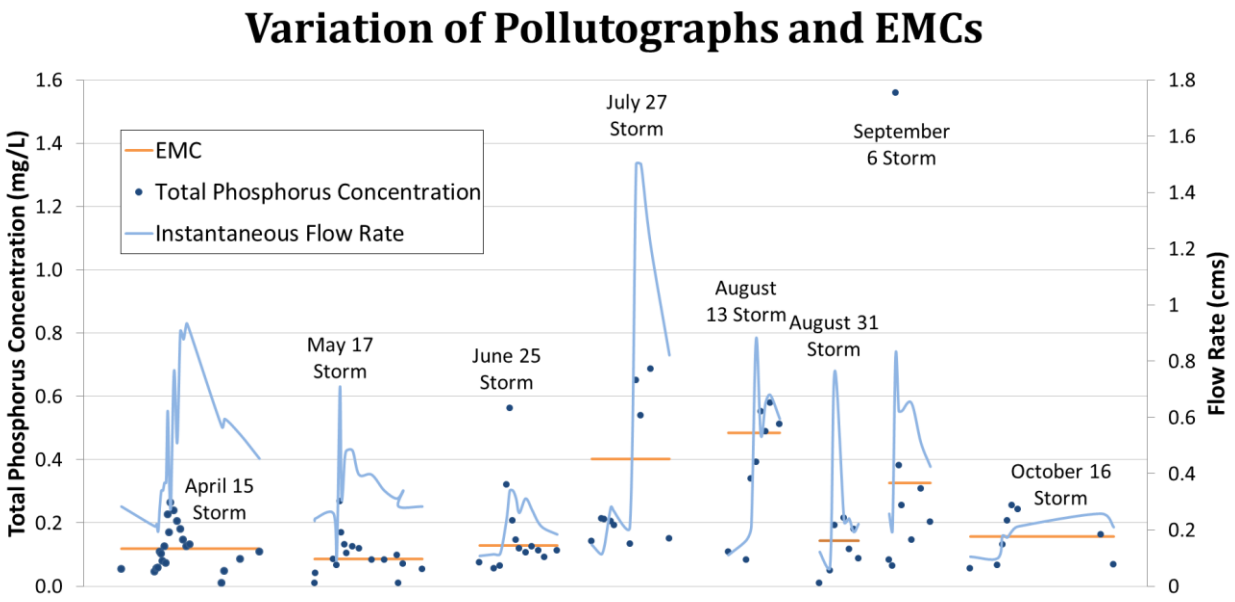

Figure 4. 2014 Storm Sampling Results: Phosphorus Concentrations, event-mean concentration (EMC), and Instantaneous Flow Rates

Higher phosphorus concentrations tend to correspond with higher flow rates, indicating that much of the phosphorus in the brook is likely coming from erosion, sediment resuspension, and runoff over impervious surfaces into the brook. Additional inputs of phosphorus due to combined and sanitary sewer overflows are also likely to increase during high flow events. Even storms corresponding to smaller flow rates indicate high phosphorus measurements in the summer months. This could imply that rising temperatures have the potential to mobilize phosphorus more easily than colder temperatures, allowing higher discharges of phosphorus into the brook. Furthermore, lawn fertilization rates could be increasing in the summer months, leading to increased phosphorus loading into the brook. As shown in Figure 5, all but one of the sampled storms exhibits an EMC greater than the EPA recommended limit.

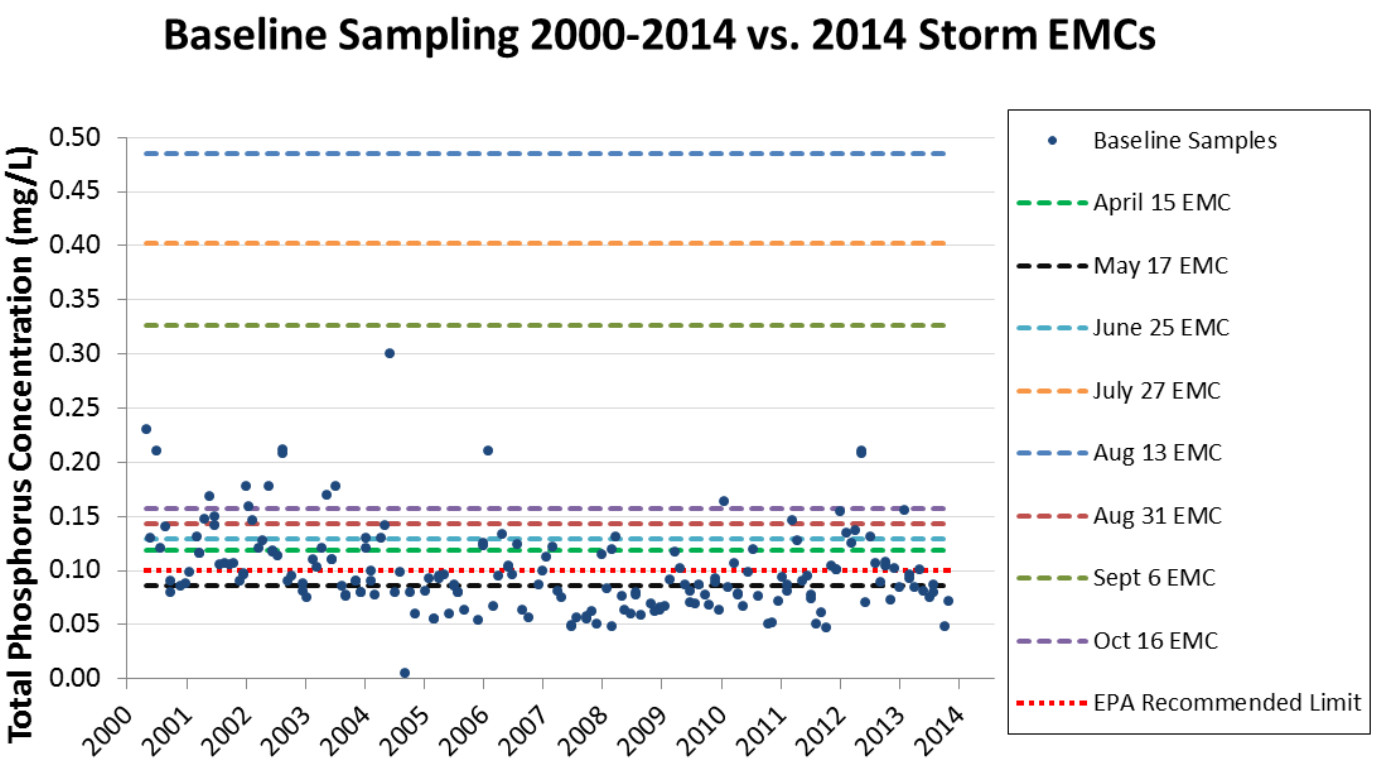

Figure 5. Comparison between Baseline Sampling and 2014 Storm Sampling Results

Modeling Monthly Phosphorus Loads 2007-2014

Although discharge is measured at a sufficiently high frequency at Alewife Brook (15 minute intervals via USGS gage #01103025), constituent concentration is measured less frequently due to the expense and labor of collecting and analyzing water quality samples. Therefore, a combination of the baseline and storm event sampling data presented above was used to model monthly total unfiltered phosphorus loads from 2007-2014. This range was chosen because reliable 15-minute measurements of flow rate at Alewife Brook via a USGS gage are available from 2007-2015.

To examine the effects of discharge, changes in time, and seasonality on total unfiltered phosphorus loads, a seven-parameter regression equation was used (Cohn et al., 1992). As changes in phosphorus loading at Alewife Brook result from different flow regimes and seasonal changes, the regression equation takes the following form:

$$\ln[Load] = \beta_0 + \beta_1 * \ln[Q] + \beta_2 * \ln\left[\frac{Q}{Q_c}\right] + \beta_3 * \left\{\ln\left[\frac{Q}{Q_c}\right]\right\}^2 + \beta_4 * \ln(Q_{t-1}) + \beta_5 * \sin\left[\frac{2\pi T}{365}\right] + \beta_6 * \cos\left[\frac{2\pi T}{365}\right] + \varepsilon \quad (9)$$

where Q is the discharge at the time of the sample, Q_{t-1} represents the previous day's discharge, Q_c[10] is a flow centering term to remove multicollinearity[11], T is day of the year, and ε accounts for error. β_1 through β_6 are coefficients for each term. This model was chosen because it employs a statistical regression in which the constituent concentrations are based on easily acquired data, such as flow rate and day of year. This model format was used to generate a single model, which uses phosphorus concentration

[10] Q_c is determined by taking the average of flow rates in the dataset

[11] Multicollinearity occurs when two or more predictor variables in a multiple regression model are highly correlated, meaning that one can be linearly predicted from the others with a relatively high degree of accuracy.

data (converted into phosphorus loads using corresponding flow rate data from USGS gage #01103025) from both storm samples and monthly baseline samples to estimate phosphorus loads based on flow rate and day of the year. The model developed exhibited low p-values[12] and high explanatory value (or high R^2).

Because access to streamflow data is so readily available via USGS gage, various forms of flow rate were manipulated to best describe total phosphorus load without laborious phosphorus sampling. The previous day's discharge term, Q_{t-1}, accounts for antecedent dry conditions. The flow rate of the day before impacts how phosphorus is mobilized during a storm. If conditions have been dry, flow rates are likely to be lower, which may indicate a period of little to no precipitation. Lack of precipitation allows phosphorus to accumulate on impervious surfaces, leading to increased phosphorus content in the runoff that flows into the brook.

The $[T - Tc]$ and $[T - Tc]^2$ terms account for day of the year, where Tc is a time centering term similar to the flow centering term. The sine and cosine terms are used to fit a first order Fourier series to the seasonal component of variability. These time-dependent terms make up for the lack of time-relevant data, such as seasonal changes in temperature or seasonal use of phosphorus-laden fertilizer to feed lawns.

Numerous variations of (9) were modeled in *R* (Shown in Appendix D) to determine which combination of the model inputs produced the best results for data from seven storms (April through September). This methodology was used to provide cross-

[12] A p-value for a given term tests the null hypothesis that the coefficient is equal to zero (or that the coefficient has no effect on the regression model). A low p-value (<0.05) indicates that the predictor is likely to be a meaningful addition to the model because changes in the predictor's value are related to changes in the response variable.

validation techniques to an unmodeled October storm to verify model fit. While this model form often includes a bias correction factor, one was not included in this analysis. Model fit was improved by eliminating terms with high p-values (>0.05) because lower p-values indicate model coefficients that are more statistically significant than for correspondingly large p-values.

The model fit to all of the available data (both baseline and storm data in 2014) yielded the strongest results when in the form

$$\ln[Load] = \beta_0 + \beta_1 * \ln[Q] + \beta_2 * \ln(Q_{t-1}) + \beta_5 * \sin\left[\frac{2\pi T}{365}\right] + \beta_6 * \cos\left[\frac{2\pi T}{365}\right] + \varepsilon \quad (10)$$

where coefficients are outlined in Table 1. As shown in Table 1, this model produced an R^2 value of 90.3%, with an R^2 predicted value of 89.0%. This finding illustrates that the model has very good predictive power, meaning that it may be used as a surrogate for sampling practices to estimate phosphorus loading at any time.

Table 1. Load Estimator Model Summary Statistics

	Coefficient	P-value	R^2	R^2(adj)	R^2(pred)
Ln(Q)	1.63	0.000	90.3%	89.8%	88.9%
Ln(Q_{t-1})	-0.31	0.001			
Sin(2πT/365)	-0.25	0.000			
Cos(2πT/365)	-0.24	0.001			

As shown in Figure 6, the model sufficiently estimates phosphorus loads for any time or season with the exception of a few extreme events where the model over- or under-estimates predictions in comparison with observed values. The second largest peak in Figure 6 is indicative of an extreme event, which involved a combined sewer overflow.

Because this model only takes into effect flow rate and time of year, other omitted variables such as temperature or precipitation intensity may have impacts on phosphorus loading and therefore the model may be threatened by OVB.

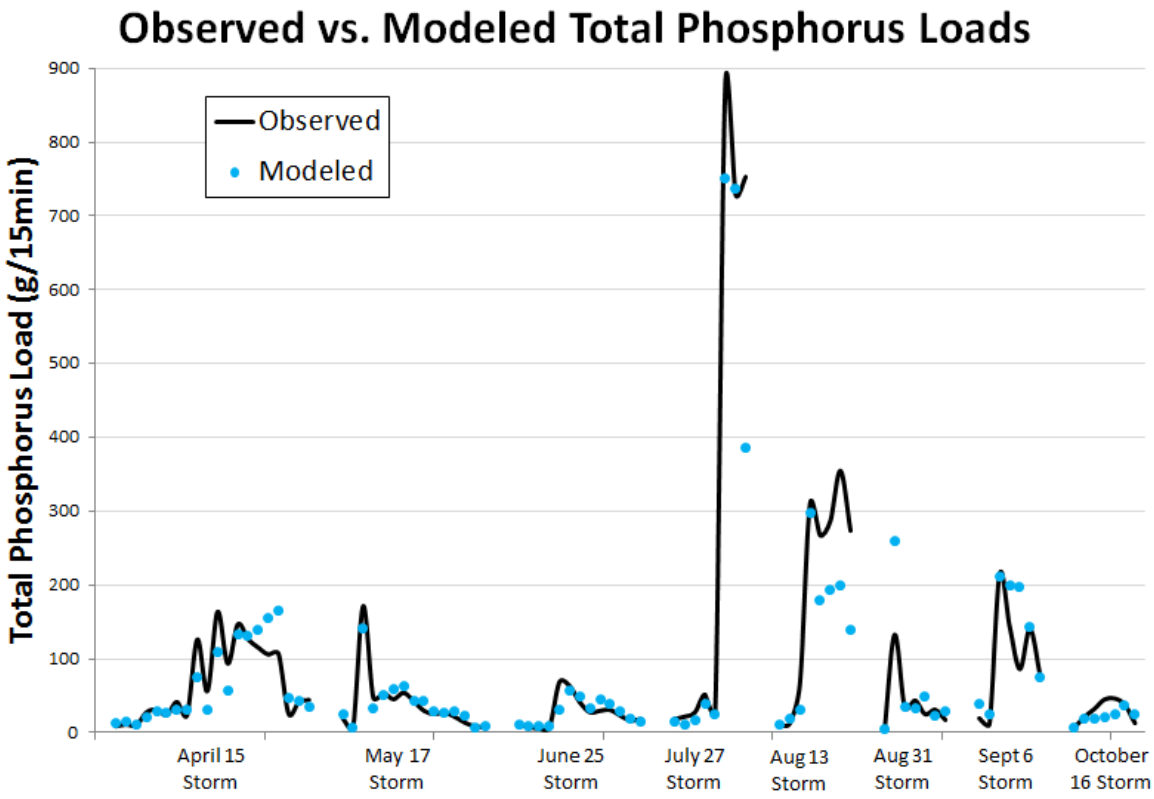

Figure 6. Observed vs. Total Phosphorus Load Estimates from the Load Estimator Model

In order to perform a useful analysis of the sensitivity of total phosphorus to changes in climate, extensive records of phosphorus loads are required. Based on the recommendation of Jiang et al. (2014), monthly average phosphorus loads were desired for the climate elasticity analysis at Alewife Brook. The final model presented in (10) was used to estimate total phosphorus loads for every fifteen minutes from 2007-2014. These estimates were averaged on a monthly scale. Monthly average temperature and

monthly total precipitation data were acquired from the National Climatic Data Center (Station at Logan Airport) and used for the analysis, in addition to USGS flow rate data at Alewife Brook (Gage # 01103025). Additionally, the number of combined sewer overflow (CSO) discharges per month kept on record by the Mystic River Watershed Association since 2007 was used for the sensitivity analysis.

Exploratory Data Analysis

Time-series plots can tell us a great deal about weather patterns in a particular watershed. At Alewife Brook, months with a large amount of precipitation correspond to months with very high estimates of total phosphorus loads, as shown in Figure 7. These trends indicate that water quality in the brook is very sensitive to changes in precipitation; however, gaps in the trend may indicate that other climate factors are influencing sensitivity to climate.

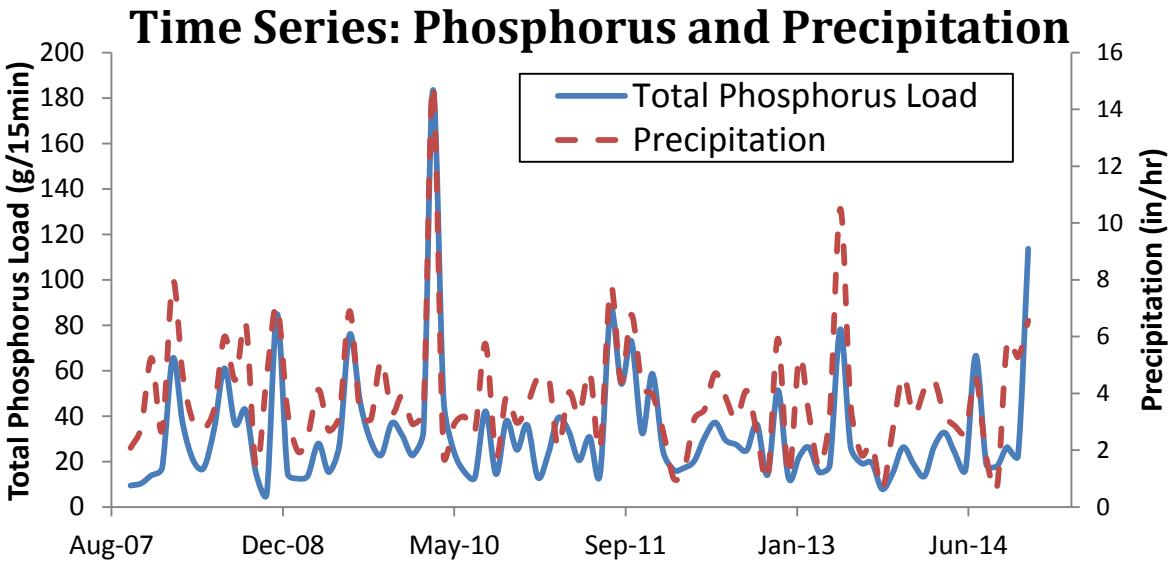

Figure 7. 2007-2014 Time Series of Modeled Total Phosphorus and Precipitation (NCDC Logan Airport Weather Station) at Alewife Brook

The scatterplot in Figure 8 shows the correlation between monthly average phosphorus concentration and monthly total precipitation. Although there is a slight relationship between total phosphorus concentration and precipitation, Figure 9 indicates that estimates of total phosphorus loads and precipitation in the brook exhibit a more obvious linear trend, with high total phosphorus loads corresponding to high precipitation.

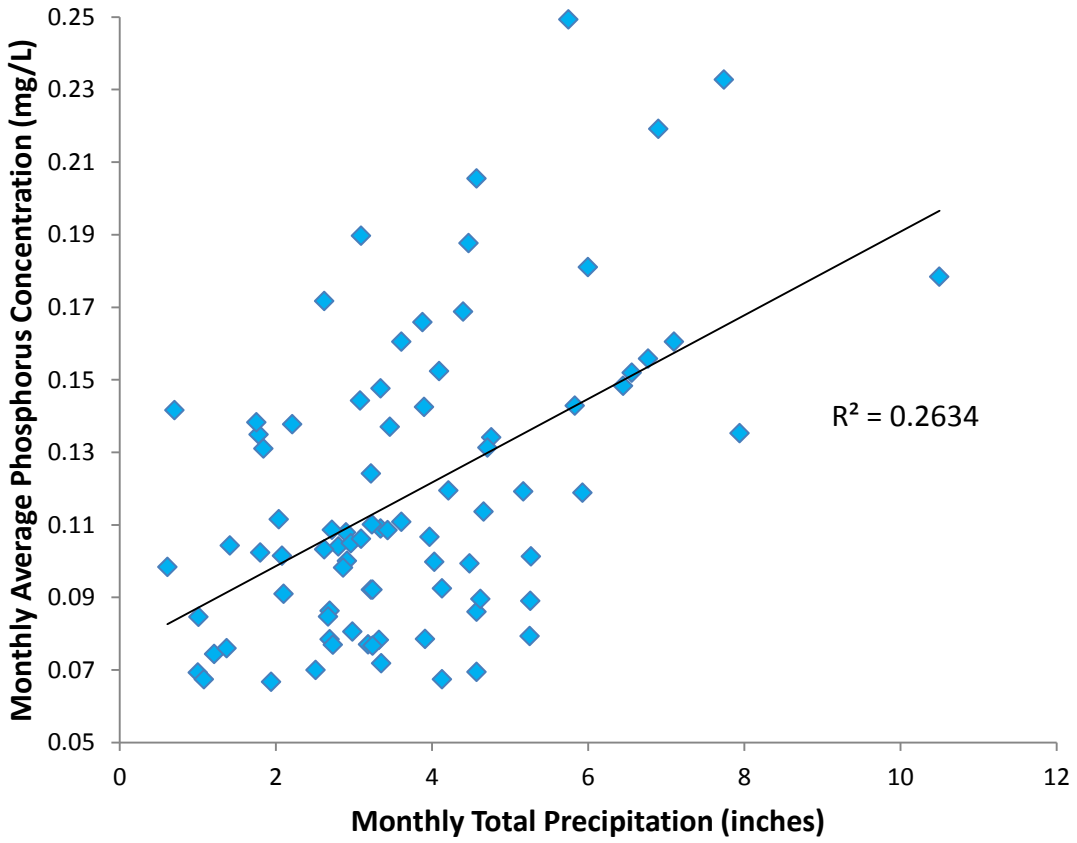

Figure 8. Scatterplot of Modeled Total Phosphorus Concentration and Precipitation (NCDC Logan Airport Weather Station) at Alewife Brook

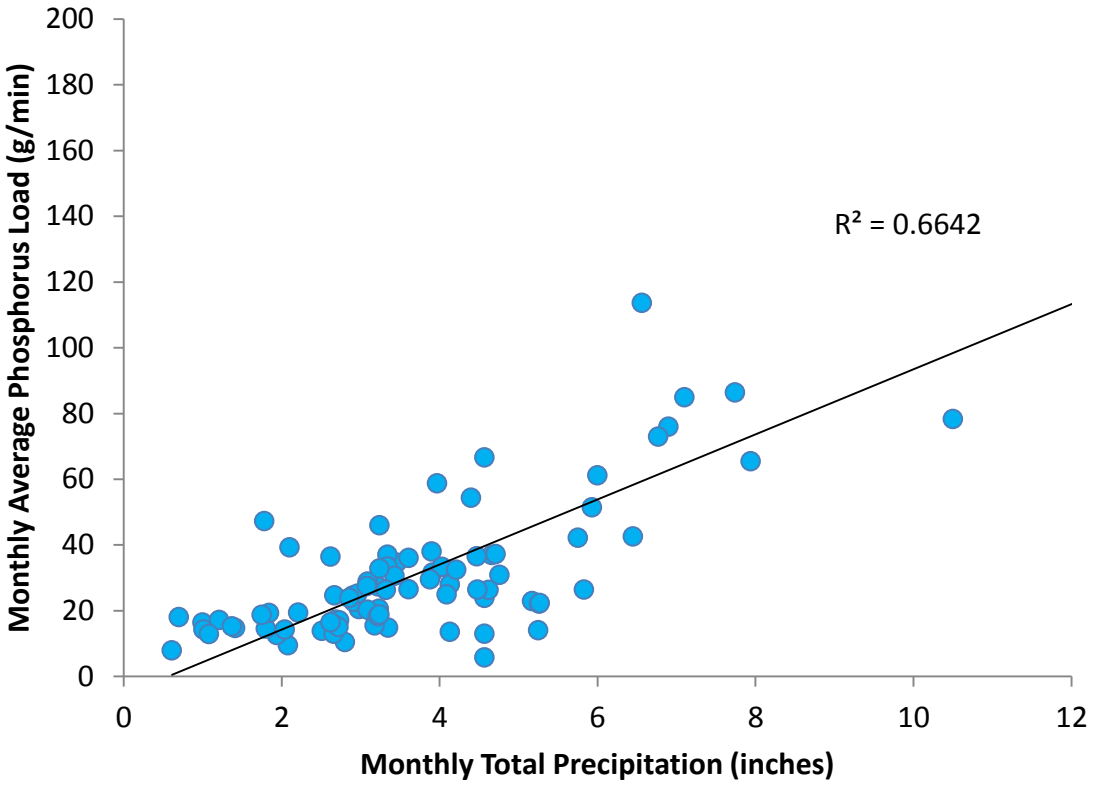

Figure 9. Scatterplot of Modeled Total Phosphorus Load and Precipitation (NCDC Logan Airport Weather Station) at Alewife Brook

Although monthly average temperature has a somewhat sinusoidal shape in relation to monthly average total phosphorus load, as shown in Figure 10, changes in temperature may indicate periods of excessive fertilizer use (late spring and early summer), which could affect phosphorus runoff. Additionally, higher temperatures may be indicative of phosphorus mobilization at a larger scale than lower temperatures based on the increase in microorganism activity with rising temperature (Li et al., 2013). Therefore, temperature is included in the sensitivity analysis.

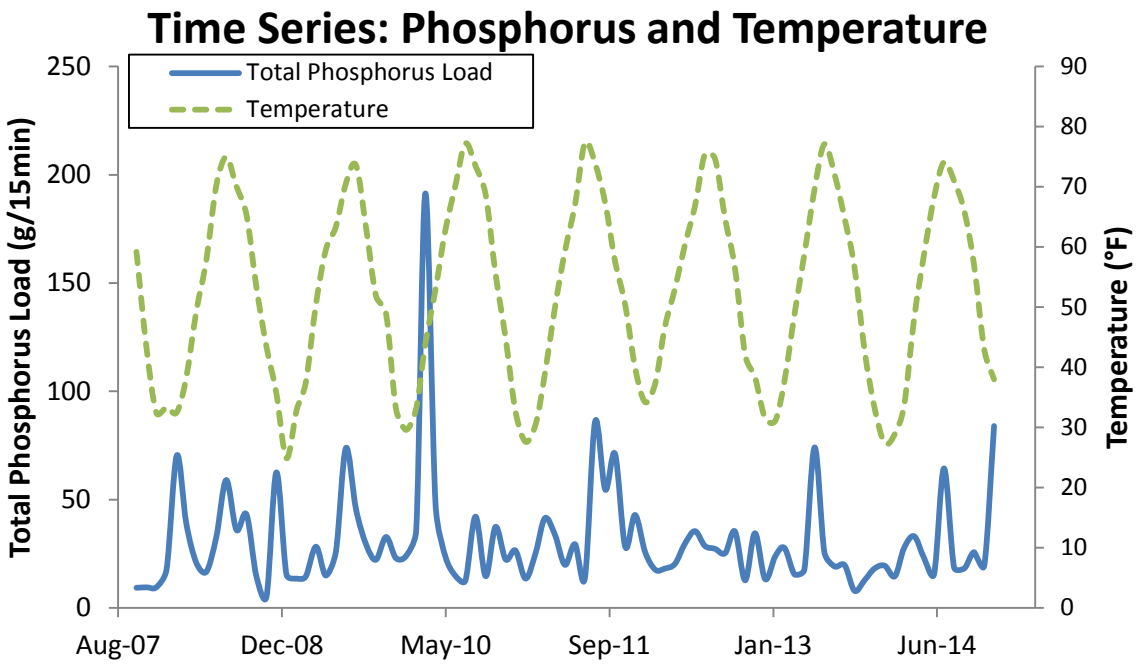

Figure 10. Time Series of Average Monthly Temperature (NCDC) and Modeled Average Monthly Total Phosphorus Load at Alewife Brook

Like precipitation, flow rate is highly correlated with total phosphorus load (Figures 11 and 13). This makes sense because precipitation is one of the main drivers of streamflow. However, streamflow must be considered separately from precipitation to account for groundwater and baseflow conditions, as well as sediment resuspension and near-bank erosion, all of which contribute to phosphorus loading within Alewife Brook. The correlation between monthly average total phosphorus concentration and monthly average flow rate is weak, as shown in Figure 12. This may indicate that phosphorus inputs into Alewife Brook are not solely based on dynamic flow conditions, but rather seasonal cycling of phosphorus. Additionally, correlations between total phosphorus concentration and flow rate may be more linear at a smaller time-scale, such as 15-minute intervals (R^2 near 0.88), but the use of monthly averaged phosphorus concentration and

flow rate might not account for the minute by minute influences that flows may have on concentrations.

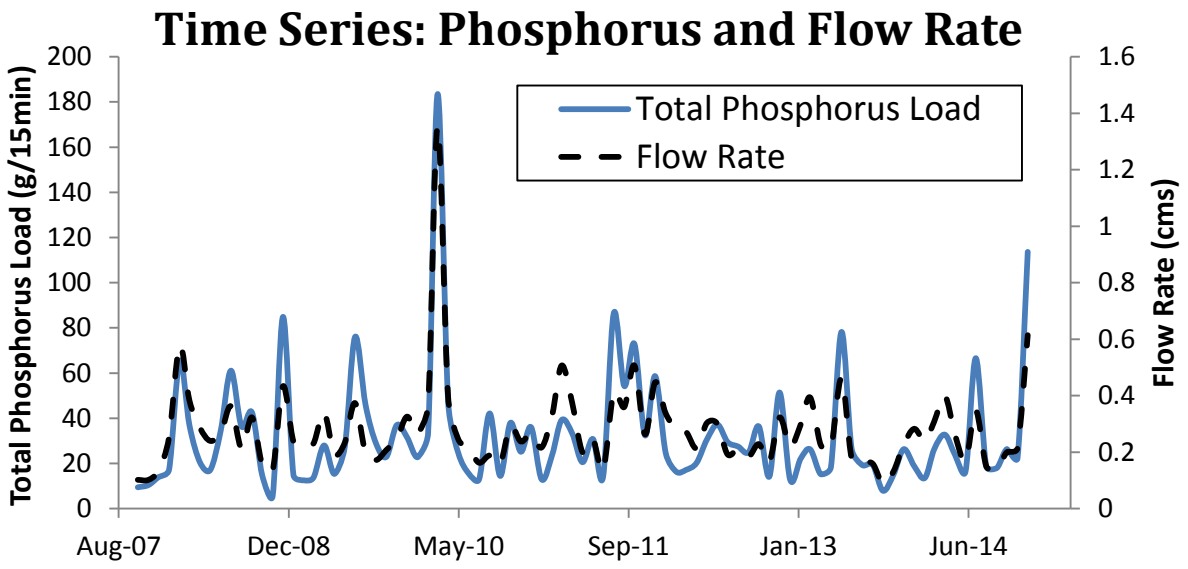

Figure 11. 2007-2014 Time Series of Modeled Total Phosphorus Load and Flow Rate (USGS Gage 01103025) at Alewife Brook

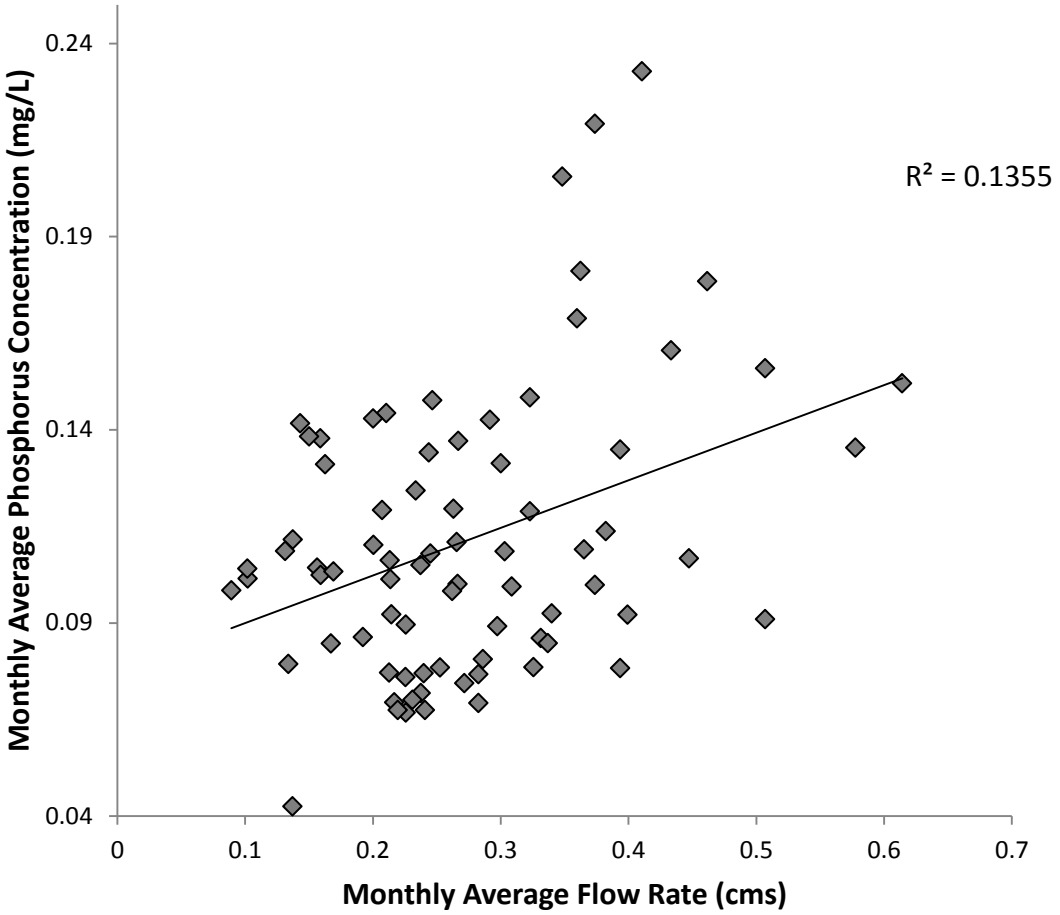

Figure 12. Scatterplot of Total Phosphorus Concentration and Flow Rate (USGS Gage 01103025) at Alewife Brook

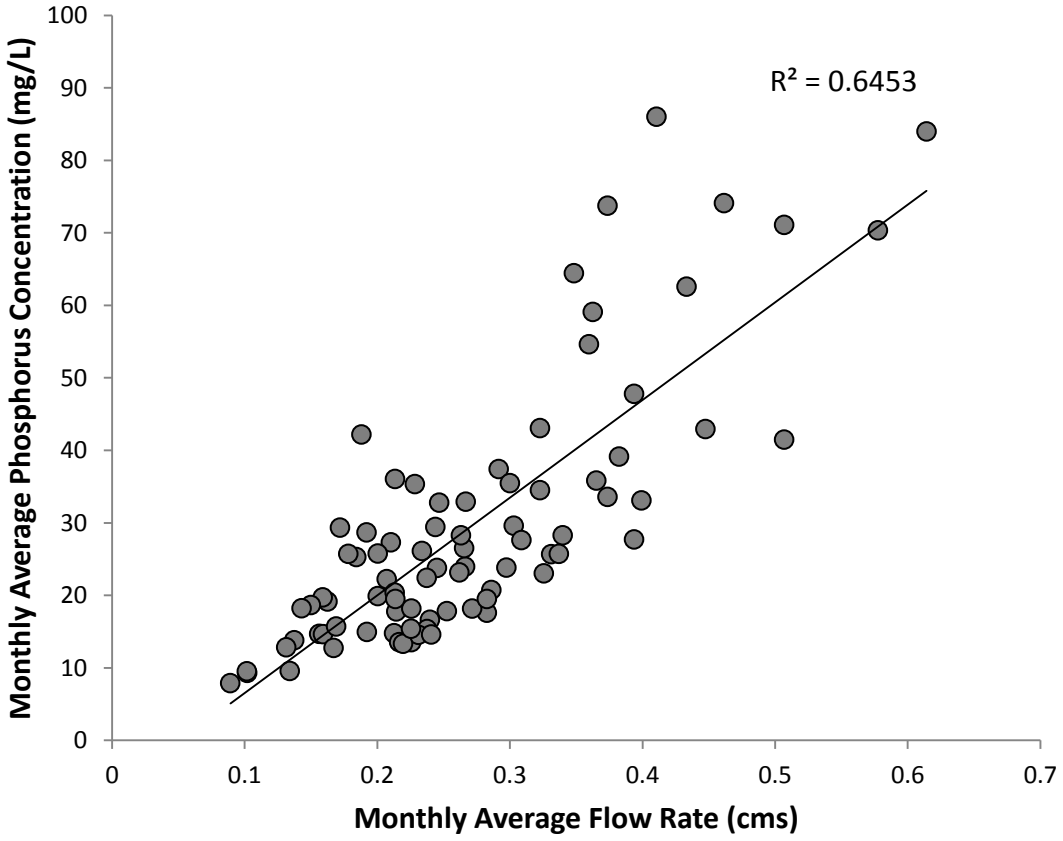

Figure 13. Scatterplot of Total Phosphorus Load and Flow Rate (USGS Gage 01103025) at Alewife Brook

Multivariate Elasticity Methods

Equation (7) is used to estimate total phosphorus load, and a variable for the elasticity of total phosphorus to changes in monthly combined sewer overflow events was added. Equation (8) is also altered to specifically account for changes in total phosphorus as a result of variability in precipitation, temperature, flow rate, and CSOs

simultaneously. Additionally, seasonal fixed effects[13] were added to both models to account for seasonal fluctuations of phosphorus unaccounted for by the temperature variable. These seasonal fixed effects included four additional input variables (spring, summer, fall, and winter). The seasonal inputs were assigned a value of either 1 or 0 depending on the season during which the total phosphorus measurement was taken. For instance, the spring variable input was given a value of 1 if the corresponding total phosphorus value was observed during spring (April, May, or June) or zero if the total phosphorus value was observed during other months. These seasonal fixed effects may account for seasonal changes in the natural phosphorus cycle (Figure 1) that were not accounted for in sampling or modeling procedures. Estimates of elasticity in (7) were obtained using OLS regression, where model residuals were tested to assure that they are uncorrelated, homoscedastic, and well approximated by a normal distribution. Helsel and Hirsch (1992) outline that residuals must follow these patterns in order to obtain unbiased estimators of the dependent variable, test hypotheses, and estimate confidence intervals for regression coefficients. The addition of fixed effects as well as an event-based CSO variable was meant to remove OVB, ensuring that the majority of factors contributing to phosphorus loading were accounted for.

[13] Fixed effects within regression analyses are constants which may assist in controlling for unobserved heterogeneity when this heterogeneity is constant over time and correlated with independent variables.

Results and Discussion

Climate Elasticity of Total Phosphorus

Two models (parametric and nonparametric) estimating the multivariate sensitivities of total phosphorus to changes in precipitation, temperature, streamflow, and number of CSOs were developed using (7) and (8) and the results of these analyses are reported in Table 2. These models were not presented for comparison purposes, but rather to demonstrate two different methods to estimate elasticities – one which assumes a model form and one that does not. Each elasticity estimate is the t-value of each elasticity estimator as well as its p-value. Smaller p-values indicate that values of elasticity are more statistically significant than for correspondingly large p-values. In addition, Table 2 outlines the percentage of the model sum of squares corresponding to each explanatory variable (%SS) and the variance inflation factor (VIF). The %SS may be used to compare the importance of precipitation, temperature, streamflow, and CSO in terms of how much of the variations in phosphorus load is explained by each term. The VIF can be used to identify correlated explanatory variables, with a VIF $\geq$ 10 denoting a multicollinearity problem (Helsel and Hirsch, 1992).

A number of inferences may be drawn from the results in Table 2: The precipitation elasticity of total phosphorus, ε_P, is 0.272 for (7) and 0.100 for (8), which are consistent with results from Jiang et al. (2014) who found that precipitation elasticity of unfiltered phosphorus is generally between zero and 0.4. Jiang et al. (2014) also reported general temperature elasticity results of unfiltered phosphorus in a wider range between 0.1 and 1.0, which is still consistent with our results.

Table 2. Comparison of Climate Elasticity Estimations in Relation to Monthly Average Total Phosphorus Loads

	Result	*Precipitation*	*Temperature*	*CSO*	*Flow Rate*
Equation 7	$\varepsilon_{P,T,CSO,Q}$	0.272	0.556	0.0473	1.12
	t	5.34	3.91	2.85	19.86
	p	0.00	0.00	0.01	0.00
	SS%	67.12%	1.19%	7.14%	19.28%
	VIF	2.52	5.34	1.91	3.15
	R^2	96.2%			
	R^2 (adj)	95.8%			
	R^2 (pred)	95.1%			
Equation 8	$\varepsilon_{P,T,CSO,Q}$	0.100	0.570	0.0155	1.23
	t	2.18	4.29	2.42	19.28
	p	0.03	0.00	0.01	0.00
	SS%	47.42%	4.32%	4.36%	35.64%
	VIF	1.78	4.68	1.48	2.05
	R^2	92.1%			
	R^2 (adj)	91.3%			
	R^2 (pred)	90.2%			

* Although (7) requires that each model be fit without an intercept term, R^2 values are reported for (7) fit with an intercept term only to help identify presence or absence of omitted variable bias.

* **ε** refers to the elasticity estimate, not an error term.

Combined sewer overflows had significant explanatory value, as evidenced by corresponding high t-values and small, yet significant, p-values. Table 2 shows that the CSO elasticity of total phosphorus was only 0.0473 for (7) and 0.0155 for (8), indicating that monthly total phosphorus loads appear to be relatively insensitive to increases in number of CSOs per month compared to other variables. However, the influence of seasonal fixed effects combined with this CSO term improved the model explanatory value while correcting for OVB.

According to economic price elasticity of demand principles, elasticity values less than one represent inelastic behavior, whereas values greater than one represent elastic behavior. Thus, streamflow elasticity estimates in excess of unity imply that the response of total phosphorus loading to changes in flow rate is nonlinear and elastic. Although flow rate is dependent upon precipitation, this finding indicates that nutrient loading at Alewife Brook is much more sensitive to changes in average monthly flow rate than to changes in total monthly precipitation. This may signify that the dynamic streamflow conditions that dictate erosion and sediment recycling within the river exacerbate phosphorus conditions more so than runoff alone.

An attempt was made to determine elasticity estimates for each of the four seasons by estimating separate seasonal sensitivities using fixed effects with interaction terms in both (7) and (8). An interaction term is the multiplication of two independent variables that interact if the effect of one of the variables differs depending on the level of the other variable. In (7) and (8), binary seasonal fixed effects were multiplied by precipitation, temperature, and flow rate to determine whether or not the interactions between climate variables and seasons would produce differing elasticity estimates based on season. Resulting p-values of both models were well within excess of 0.05, leading us to conclude that, even though the magnitude of phosphorus loading changes from season to season, multivariate sensitivities (or elasticity estimates) remain constant.

Elasticity estimates from (7) and (8) are not expected to agree exactly because each has a different interpretation: (7) assumes no model form and is based on mean values, whereas (8) assumes log-linear model form. Both (7) and (8) do, however, lead to the important conclusion that nutrient loading is sensitive to changes in precipitation, temperature, flow rate, and sometimes additional event-based effects, which must all be

considered simultaneously to fully understand the effects of climate change on a watershed. To highlight this point, elasticity estimates were computed based on simple (bivariate) regressions between each explanatory variable separately. That is, the elasticity values were estimated from the following bivariate equations: $l = \bar{\varepsilon}_P * p, l = \bar{\varepsilon}_T * t, l = \bar{\varepsilon}_Q * q,$ and $l = \bar{\varepsilon}_{CSO} * cso$ individually, instead of (7), as well as $L = \theta * P^{\varepsilon_P} * v, L = \theta * T^{\varepsilon_T} * v, L = \theta * Q^{\varepsilon_Q} * v, and\ L = \theta * CSO^{\varepsilon_{CSO}} * v$ instead of (8). These bivariate values were also compared to the bivariate water quality estimators developed by Jiang et al. (2014), which were based on the median of elasticity estimates as indicated in (3).

The resulting elasticity estimates indicate similar results for streamflow elasticity using all methods. However, bivariate methods show increased precipitation and CSO elasticity as well as decreased temperature elasticity, compared to multivariate methods, as indicated in Figure 14. This suggests that bivariate methods predict that total phosphorus loads at Alewife Brook are more sensitive to changes in precipitation and number of CSOs per month than multivariate methods predict. We also illustrate confidence intervals (95%) for bivariate and multivariate methods in Figure 15. As shown in Figure 15, bivariate elasticity estimators yield larger confidence intervals, which indicate more uncertainty concerning the estimates. Table 3 demonstrates the coefficients of determination (R^2 and R^2 predicted) corresponding to bivariate vs. multivariate elasticity estimation methods. The multivariate nonparametric and parametric methods exhibit R^2 values closer to 100%, indicating that the multivariate elasticity models more accurately reflect the data. We therefore conclude that it is necessary to account for the multivariate interactions among precipitation, temperature, and streamflow to successfully understand their impacts on nutrient loading. Single

parameter elasticity methods may represent the general relationship between nutrient loading and a variable of interest in some cases, but these methods cannot reflect the complicated nonlinear relationships inherent among nutrients, precipitation, temperature, and streamflow. Additionally, it is important to include event-based factors that contribute to nutrient loading and seasonal fixed effects in models that estimate elasticity to reduce OVB and confidence intervals while increasing model explanatory value.

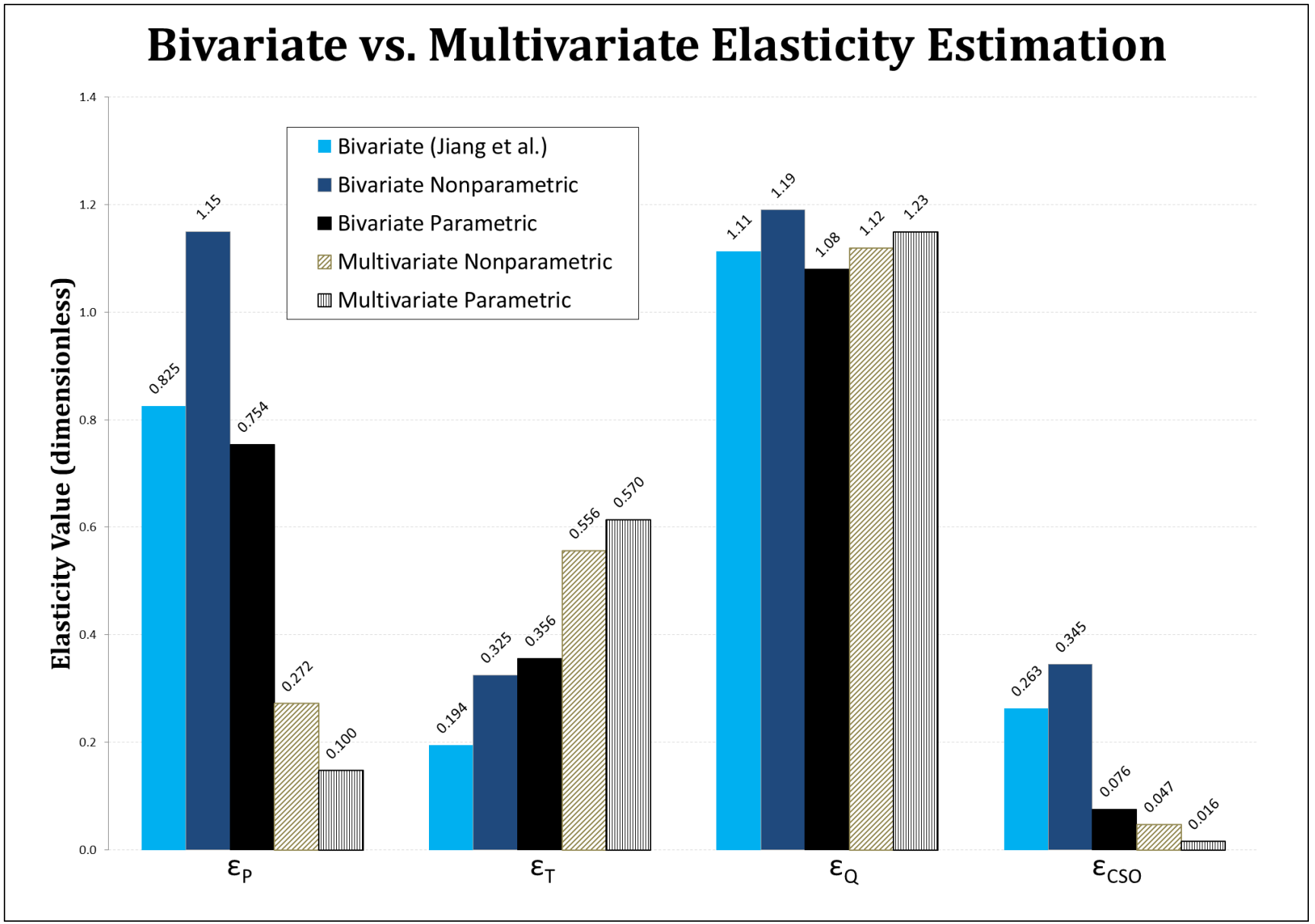

Figure 14. Comparison of Bivariate and Multivariate Elasticity Estimation Methods

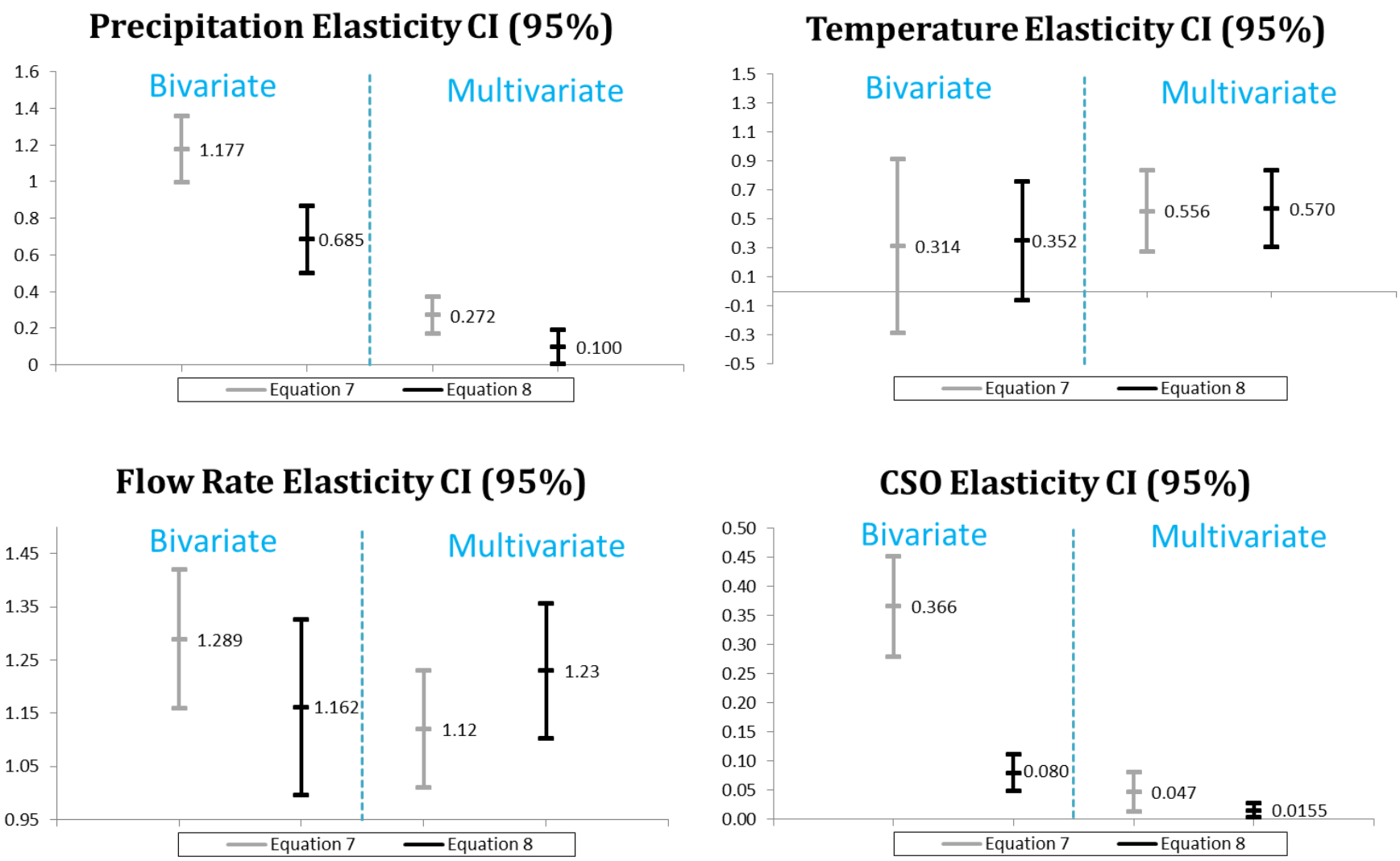

Figure 15. Comparison of Bivariate and Multivariate Elasticity Confidence Intervals (95%)

Table 3. Comparison of Coefficients of Determination (R^2) for Bivariate and Multivariate Elasticity Estimation Methods

	R^2 (R^2 Predicted) [%] for Bivariate and Multivariate Elasticity Methods			
	Bivariate Elasticity		Multivariate Elasticity	
	Nonparametric (7)	Parametric (8)	Nonparametric (7)	Parametric (8)
P	67.1 (58.9)	40.6 (37.2)	96.2 (95.1)	92.1 (90.2)
T	1.30 (0.00)	3.40 (0.00)		
Q	82.2 (81.2)	70.2 (68.9)		
CSO	46.2 (32.0)	23.7 (19.7)		

Unlike common sensitivity analyses, the nonparametric multivariate elasticity approach introduced in (7) is standardized by normalizing each deviation by the mean, rather than the standard deviation. Many sensitivity analyses differ from the approach presented in (7) because they are based on a multivariate regression of an assumed linear model. Such a model assumption limits the analysis, especially when R^2 is low (indicating non-linearity of the assumed linear model), because it is then questionable to use the values of the coefficients for ranking input factors (Saltelli et al., 2004; 2010). Another distinction between the elasticity analysis in (7) and linear regression-based sensitivity analyses is that common sensitivity studies include a constant intercept term, which is not used in the nonparametric sensitivity analysis employed herein. Conversely, the nonparametric sensitivity analysis yields estimates of elasticities using the chain rule definition of the total derivative and elasticity. These estimators have a general nondimensional interpretation, which have been increasing in use among the hydrologic

sciences literature in the last couple of decades and are now starting to receive attention in the water quality realm.

This study demonstrates that the discrepancy between bivariate and multivariate estimates of precipitation elasticity to nutrient loading is a function of omitted variable bias present in bivariate elasticity estimation. The large estimates of precipitation and CSO elasticity shown in the bivariate analysis summarized in Figure 13 are likely compensating for the missing flow rate factor, thus overestimating the effect of precipitation and CSOs on nutrient loading.

An additional benefit of (8) is that the model can provide elasticity estimates while estimating nutrient loads simultaneously. The final model is reported below:

$$L = \theta * P^{0.1001} * T^{0.5702} * Q^{1.230} * CSO^{0.0115}$$

$$\text{Where } \begin{cases} \theta = 11.82 \; if \; spring \\ \theta = 16.41 \; if \; summer \\ \theta = 14.98 \; if \; fall \\ \theta = 12.97 \; if \; winter \end{cases}$$

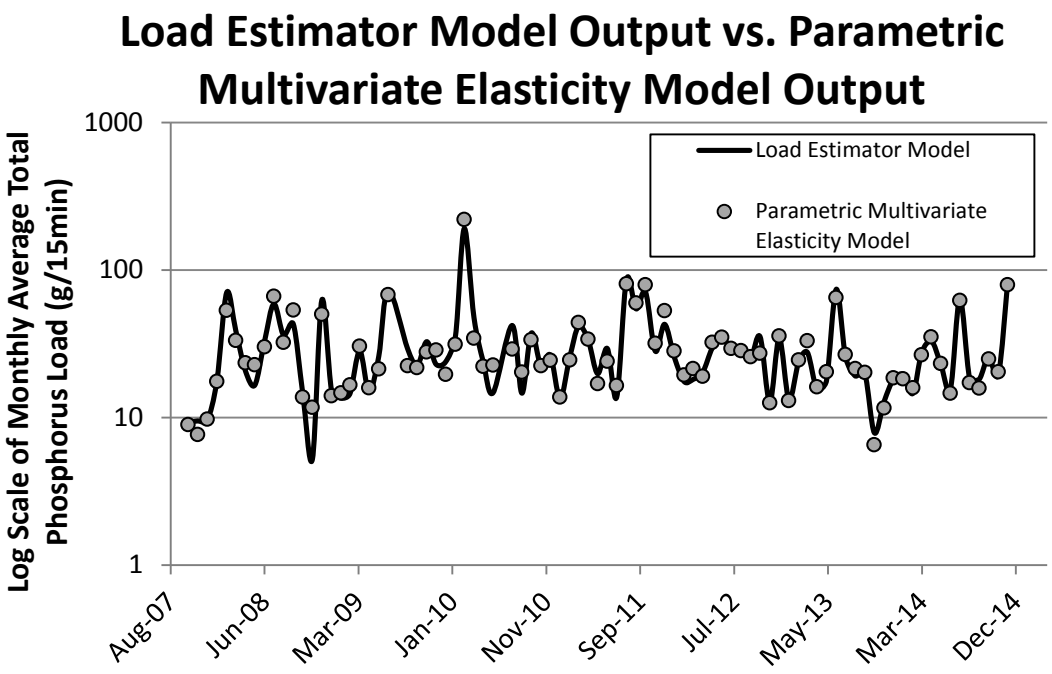

Figure 16. Comparison of Load Estimator Model and Multivariate Parametric Elasticity Model

The influence of seasonal fixed effects are represented in the model intercepts, θ, which demonstrate that phosphorus loads are likely to be higher in the summer and fall seasons, rather than in spring and winter. This is consistent with the total phosphorus estimates provided by the load estimator model, as shown in Figure 16. As documented in Table 2, the parametric model has very high explanatory value (R^2 = 92.1%), which is significantly higher than many other total phosphorus load models, as summarized in Table 4. The comparison of model explanatory value indicates that (8) is a model that can effectively produce elasticity estimates while estimating loads simultaneously.

Table 4. Coefficients of Determination for Multivariate Total Phosphorus Load Models that Include Climate Independent Variables.

Reference	Regression Equation	R^2
Driver and Tasker, 1990	TP = 262 + 0.828(Total storm rainfall) + 0.645(Drainage area) + 0.583(Industrial land use) + 0.181(Commercial land use) - 0.235(Nonurban land use) - 1.376(Mean annual rainfall) + Bias correction factor	72%
Driver and Tasker, 1990	TP = 0.153 + 0.986(Total storm rainfall) + 0.649(Drainage area) + 0.479 (Impervious area) + 1.543(Max precipitation intensity) + Bias correction factor	64%
Driver and Tasker, 1990	TP = 53.2 + 1.019(Total storm rainfall) + 0.846(Drainage area) + 0.189 (Commercial land use) + 0.103(Residential land use) - 0.16(Nonurban land use) - 0.754(Mean minimum January temperature) + Bias correction factor	54%
Arheimer and Liden, 1999	Ln(TP = -1.25 - 0.078(Soil moisture)^2 - 0.63sqrt(Flow rate)	60%
Brezonik and Stadelmann, 2002	TP = -1.205 + 0.801(Precipitation) + 0.244(Precipitation intensity) +0.461(Drainage area)	40%
Smith et al., 2003	Log(TP) = 2.72 + 0.36log(Population) + 0.78log(Runoff)	58%

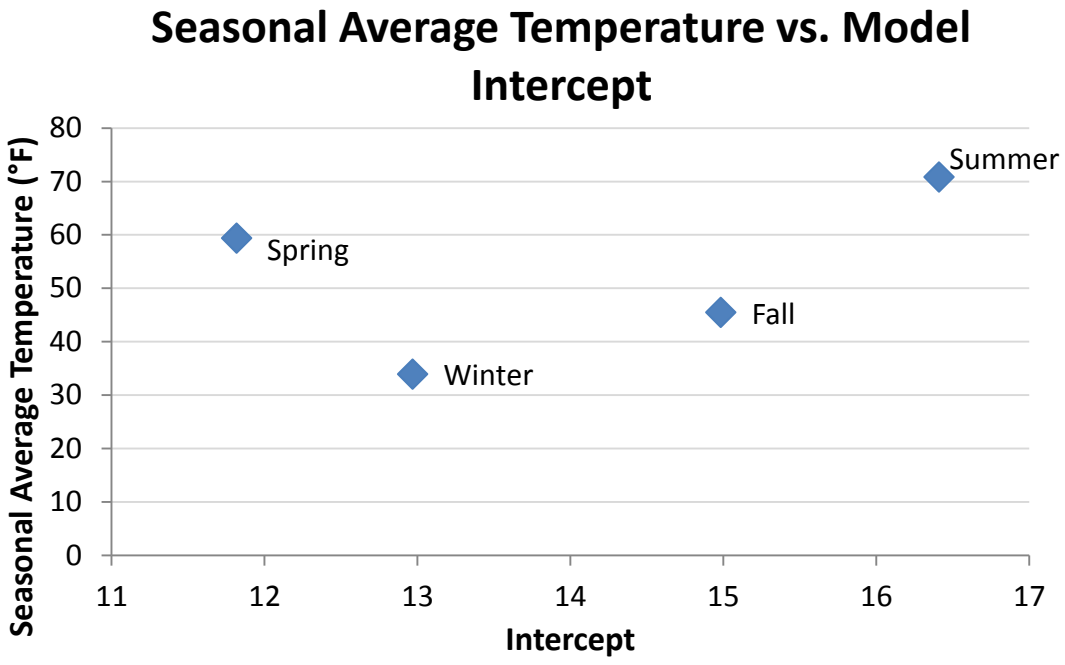

Figure 17. Comparison of Model Intercepts and Seasonal Temperature at Alewife Brook

The model intercepts indicate that season and temperature must both be included in the model to account for temperature changes from month to month as well as seasonal phosphorus cycling in the brook, as indicated in Figure 1. As shown in Figure 16, the intercept values for each model do not produce a linear trend when plotted against temperature. Although spring temperatures are higher than fall and winter temperatures, it is apparent that seasonal phosphorus cycling characteristics dominate phosphorus mobilization in summer and fall, instead of temperature alone. A possible explanation for lower estimates of phosphorus concentration in Alewife Brook during the spring may be leaf-out at the beginning of the growing season, which refers to the emergence of leaves and plants which uptake phosphorus for growth (Polgar and Primack, 2011). This process may be responsible for lower levels of phosphorus in the brook, because plants and trees are utilizing phosphorus for regrowth after their winter dormancy. Thus, because of natural phosphorus cycling within the brook, the model must consider both temperature and seasonal fixed effects.

Low flow rates during fall and summer, as shown in Figure 18, allow phosphorus to be retained in the summer months in DOP form (as described in Figure 1). However, the DOP retained in the sediments react strongly with particulate phosphorus released during high intensity storms. Additionally, the rate of phosphorus release is increased in the summer because of low dissolved oxygen conditions in the sediments. One of the possible reasons that phosphorus loading conditions during the winter months are lower than in fall and summer is because high flow rates due to snowmelt create conditions where less phosphorus can be retained in the sediments.

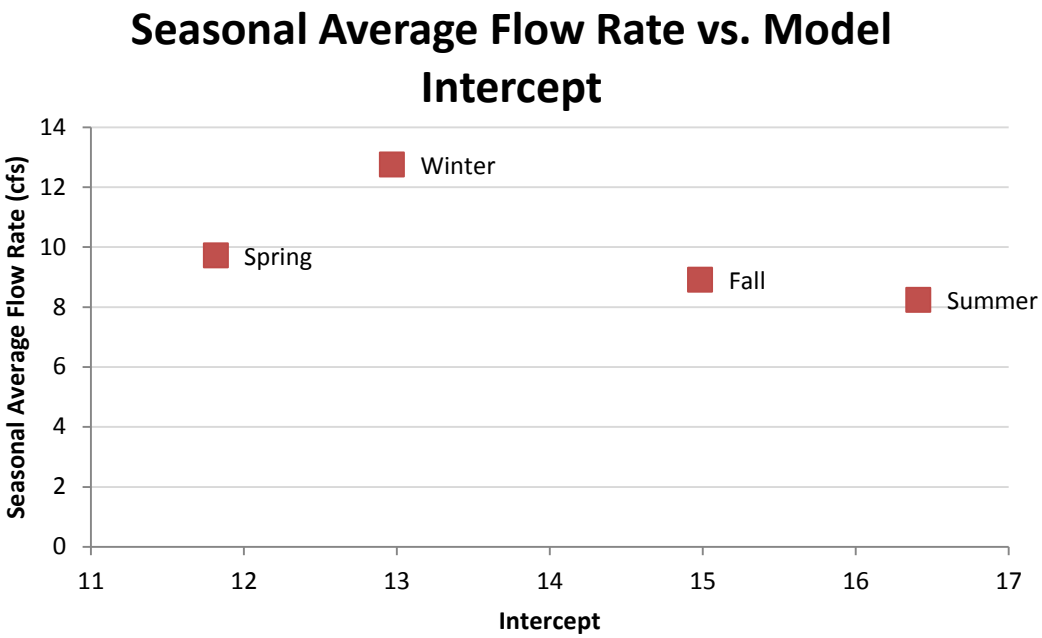

Figure 18. Comparison of Model Intercepts and Seasonal Flow Rate at Alewife Brook

Model Interpretation and Applications

Although the many sources of phosphorus loading into Alewife Brook are difficult to locate, their impacts on phosphorus loading are represented in this work. Elasticity values allow us to estimate how total phosphorus loading may respond to simultaneous changes in precipitation, temperature, flow rate, and number of CSOs. This model enables us to predict how phosphorus conditions at Alewife Brook may respond to various climate scenarios. For instance, Figure 19 demonstrates the percent increases in total phosphorus loading if precipitation (P), temperature (T), flow rate (Q), and number of CSOs per month (CSO) were to all increase by the same increments. As shown, a 1% increase in all of these variables produces an almost 2% increase in total phosphorus loading. However, a 5% increase in these variables is estimated to produce a 10% increase in phosphorus loading. However, we know that the climate variables listed are

not likely to all change by the same percent simultaneously. Thus, Figure 20 offers a few scenarios for which P, T, Q, and CSOs are increasing at different rates. If P, Q, and CSOs increase by 5% while T increases by 1%, total phosphorus at Alewife Brook will increase by approximately 7%. This scenario is more realistic than a 5% change in all of the variables because changes in temperature as a result of climate change are not often noticeable at the local scale.

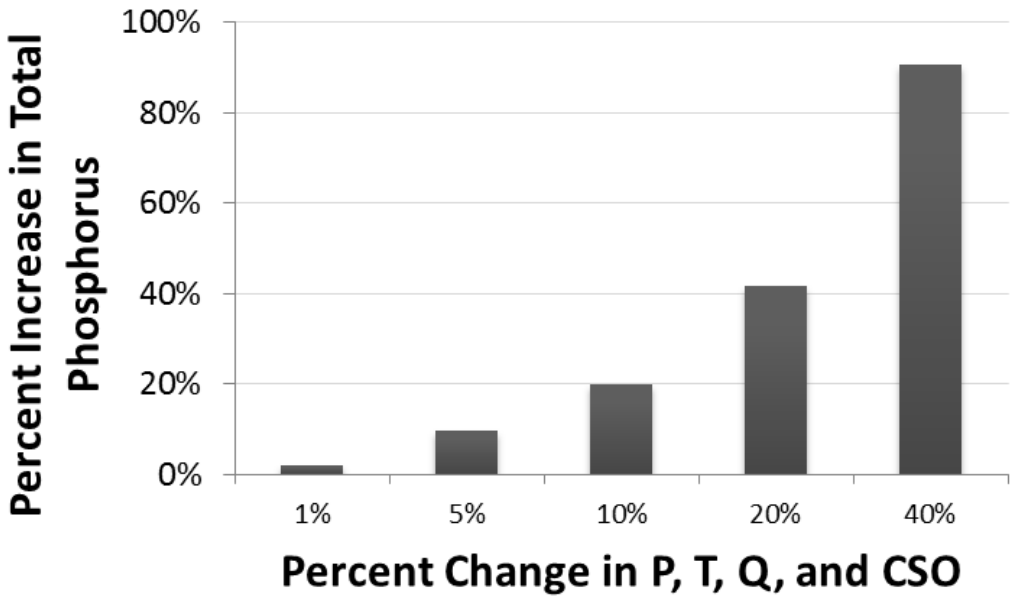

Figure 19. Modeled Percent Change in Total Phosphorus Loads as a Result of Varying Degrees of Climate Variability

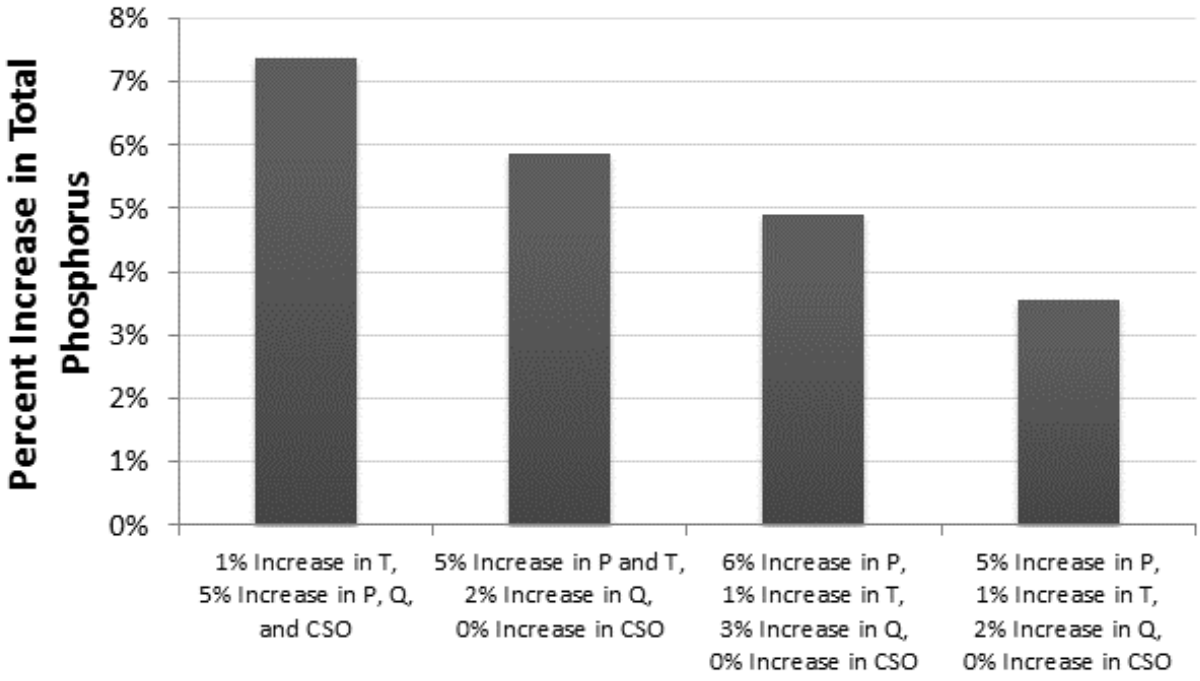

Figure 20. Modeled Phosphorus Response to Varying Climate Scenarios

Figure 20 represents a range over which total phosphorus loads may increase given a variable climate. As shown, the multivariate model predicts that we may see a 3.6% to 7.4% increase in total phosphorus loading at Alewife Brook if small increases in precipitation, temperature, flow rate, and CSOs occur in future years. In particular, the northeastern part of the United States is projected to see an increase in precipitation (10% increase in spring and summer, 15% increase in fall, and 20-30% increase in winter) and the Boston area is expected to see an increase in the number of hot days (up to 24 days of temperatures above 100°F per year). Percent changes in flow rate were estimated for each season based on seasonal regressions between precipitation and flow rate. Figure 21 represents these changes with respect to (8). As shown, spring and summer will see smaller changes in total phosphorus loading (11% and 16% increases, respectively) than fall and winter (34% and 35% increases, respectively). However, the model estimates that

Alewife Brook may experience an overall average of 24% increase in total phosphorus loading if the climate variables in the model increase according to future projections.

These estimates of total phosphorus conditions at Alewife Brook may be useful for future watershed planning. For instance, when a waterbody is impaired, a total maximum daily load (TMDL) is developed along with a plan to restore the waterbody. Development of a TMDL should take into account the effects of a variable climate on nutrient loading. This model is a useful tool to determine how phosphorus conditions may be exacerbated with a changing climate. Although water managers do not have the ability to control future climate, they are capable of creating strategic plans to lessen the impacts of climate variability on phosphorus loading within the basin. For instance, likely increases in frequency and severity of rainstorms may cause increases in CSO events, erosion, sediment resuspension, and runoff. Several remedies may be put in place to alleviate the effects of the changing climate on phosphorus loading. For instance, updating municipal infrastructure to be resilient to intense storms could negate the impacts of CSO inputs of raw sewage into the brook. Decreasing CSO outbreaks may lower the potential for additional inputs of phosphorus into the brook as a result of increased flow rates eroding soil and resuspending sediments. Additionally, initiatives to limit phosphorus fertilizers could alleviate the phosphorus content of runoff into the brook. Best management practices to minimize runoff may be implemented in a number of forms, including implementation of buffer zones, impervious area reduction/restriction, engineered wetlands, and many more (McElmurry et al., 2013).

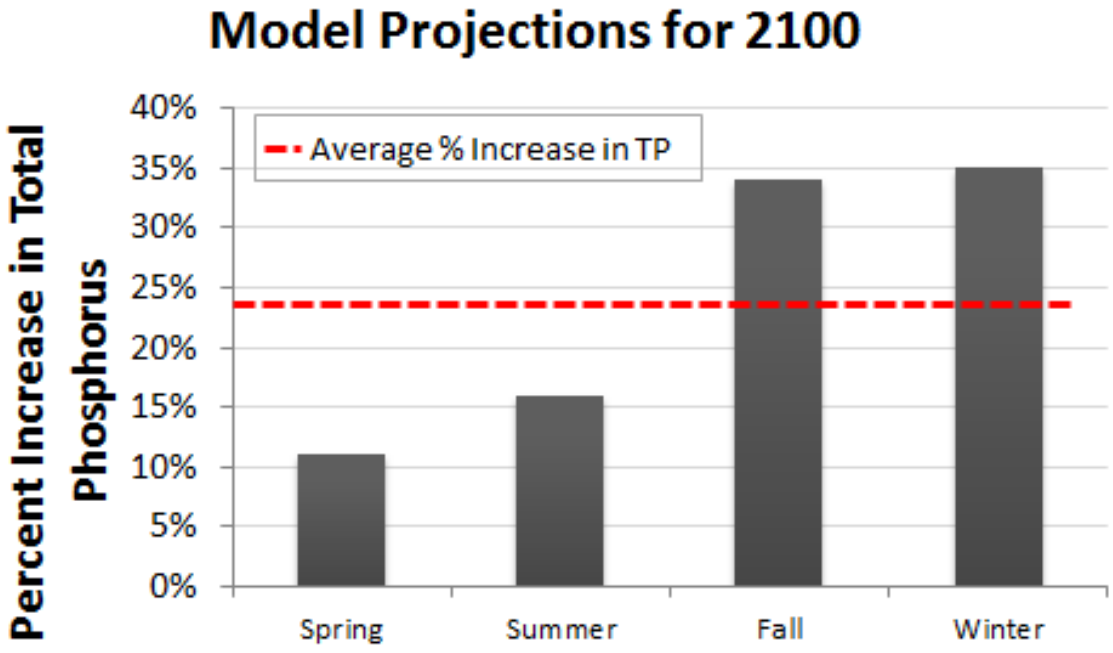

Figure 21. Model Projections for Phosphorus Loads in the year 2100

Limitations

Although the explanatory power of both models (7) and (8) were high, as evidenced by their corresponding values of R^2, several omitted variables may have added to the value of each model. OVB is always present, unless $R^2 = 1$, which is never the case in practice. Some potential omitted variables were not used due to lack of monthly data over the study period including time-series of: impervious coverage, soil compaction, water imports and exports, infrastructure, vegetation removal, population growth, lawn area, and several others. We emphasize, however, that the goal of this study was to elucidate the effects of changing climate variables, rather than direct anthropogenic impacts, on nutrient loading. A limitation of this study may be that the weather station used to characterize climate variables only provides a rough approximation to the weather contributing to the watershed defined by the USGS water quality stations. In addition, there are concerns over scarcity of both sampled total phosphorus and flow rate data, and possible laboratory or sampling errors (i.e. not taking enough samples to represent the full hydrograph of the storm, improper lab analysis techniques, etc.). Further research on this topic should include data from multiple sites in multiple regions, as well as a wider array of nutrients being analyzed. Although there are generally fewer water quality records compared to flow rate records, improved sampling and modeling efforts over time will provide a better examination of long-term climate trends with regard to nutrient loading. Additionally, this thesis lacks a critical evaluation of the assumptions of the climate change scenarios addressed. Future evaluations should assess a number of possible climate scenarios and the effects of various changes in climate on total phosphorus loading in urban streams.

Conclusion

Riverine water quality tends to vary due to a variety influences - anthropogenic, climatic, and otherwise - and therefore all riverine systems exhibit nonstationary behavior. Generally, traditional modeling techniques treat such processes as stationary. This study provides two simple sensitivity analysis techniques to evaluate climatic influences on water quality. A nonparametric multivariate regression method (7) for determining the sensitivity of nutrient loading to changes in climatic factors, such as precipitation, temperature, flow rate, and other possible explanatory variables, was introduced. Compared to other methods of sensitivity analysis, this approach is significantly advantageous due to its multivariate and nonparametric nature. First, the use of a nonparametric regression method does not require any model assumptions because the derivation introduced is based on the chain rule. This derivation results in a multivariate linear model independent of the form of the original model which relates nutrient load to the explanatory variables. Second, confidence intervals and hypothesis tests for the significance of the elasticity estimates can be obtained as long as residuals are homoscedastic and normally distributed.

An additional parametric multivariate regression approach (8) for determining the sensitivity of nutrient loading to changes in climatic factors was presented. Although this method for determining elasticity estimates relies on an assumed log-linear model form, its elasticity estimates are not calculated about the mean. This model may also be used to estimate seasonal total phosphorus loads based on the input variables. It is difficult to determine whether one methodology outperforms another. Instead, this study presents two alternative methods for determining sensitivity of nutrients to changes in climate. It

was found that the difference in elasticity estimates between the two methods was relatively small for each climate variable.

Both methods have advantages over existing sensitivity analysis methods because they avoid the perfunctory complications associated with one at a time (OAT) sensitivity methods by considering several variables that may contribute to water quality changes simultaneously. Accounting for the interactive nature of precipitation, temperature, and streamflow on nutrient loading, both models avoid the negative effects of omitted variable bias so that one variable is not overcompensating for another omitted variable. Additional explanatory variables as well as fixed effects may be included in the analysis to strengthen explanatory power of the model while determining sensitivity of water quality to variables simultaneously.

The multivariate sensitivity methodology introduced in this study was very simple to apply to an urban watershed, such as Alewife Brook, and led to a number of conclusions for the basin. The climatic processes which impact nutrient loading are particularly complex and can influence simultaneous increases or decreases in total phosphorus loading due to the complicated interactions among precipitation, temperature, and streamflow.

For this basin, in terms of percent changes in total phosphorus, nutrient loading is more sensitive to changes in monthly flow rate than monthly precipitation. Although increases in total monthly precipitation will likely have significant impacts on monthly phosphorus loading, an increase in the number of storms per month could produce the dynamic conditions necessary for erosion and sediment resuspension. Future changes in temperature, although less likely to affect total phosphorus loading than streamflow changes, may increase nutrient transport into the river through increased microbial

activity in soil and sediments. The addition of seasonal fixed effects and a combined sewer overflow variable did not alter sensitivity analysis results, but did improve the explanatory value of both models.

This study introduces a methodology that may improve general understanding of the complex interactions among precipitation, temperature, streamflow, and nutrient loading. To improve meaningfulness of such analyses, more extensive records of nutrient loading are needed. Because of sparseness of sampled data and the generation of modeled data, the conclusions of the case study presented are somewhat tentative. This analysis highlights the need for increased sampling efforts to better assess the likely responses of water quality to future climate change.

The most important conclusion as a result of this study is that nutrient loading is sensitive to changes in precipitation, temperature, streamflow, and often event-based factors that should be considered simultaneously to fully understand the impacts of climate change on nutrient loading. This study hopes to inspire extensions of this methodology to a variety of applications, watersheds, and water quality parameters.

References

Allaire, Maura C., Richard M. Vogel, and Charles N. Kroll. "The Hydromorphology of an Urbanizing Watershed Using Multivariate Elasticity." *Advances in Water Resources*, 2015.

Anderson, Donald M., Patricia M. Glibert, and Joann M. Burkholder. "Harmful Algal Blooms and Eutrophication: Nutrient Sources, Composition, and Consequences." Estuaries 25.4 (2002): 704-26.

Arheimer, B., and R. Liden. "Nitrogen and phosphorus concentrations from agricultural catchments—influence of spatial and temporal variables." Journal of Hydrology 227.1 (2000): 140-159.

Barron, Eric, Sally Benson, Leon Clarke, Randall Crane, Andrew Dressler, William Emmanuel, Marvin Geller, Jennifer Hayes, Gabrielle Hegerl, Jeremy Hess, Katherine Jacobs, Ashby Johnson, Jay Lawrimore, Thomas Lovejoy, Robert Webb, and Warren Wiscombe. *Scientific Assessment of the Effects of Global Change on the United States.* Rep. Washington: Committee on Environmental and Natural Resources National Science and Technology Council, 2008.

Barvenik, Susan, Anthony Chirigotis, Dan Engelberg, Linda Fuller, Julie Hamann, and Melba Reed. *EPA Needs to Accelerate Adoption of Numeric Nutrient Water Quality Standards*. Rep. no. 09-P-0223. Washington: U.S. Environmental Protection Agency, 2009.

Bashkin, V. N., and Robert Warren. Howarth. "Fluxes and Pools of Phosphorus in the Biosphere." Modern Biogeochemistry. Dordrecht: Kluwer Academic, 2002. 129-31.

Bennett, Elena M., Stephen R. Carpenter, and Nina F. Caraco. "Human Impact on Erodable Phosphorus and Eutrophication: A Global Perspective." BioScience 51.3 (2001): 227.

Björkman, K., and D. M. Karl. "Bioavailability of inorganic and organic phosphorus compounds to natural assemblages of microorganisms in Hawaiian coastal waters." Marine ecology progress series. Oldendorf 111.3 (1994): 265-273.

Bouraoui, F., L. Galbiati, and G. Bidoglio. "Climate change impacts on nutrient loads in the Yorkshire Ouse catchment (UK)." Hydrology and Earth System Sciences Discussions 6.2 (2002): 197-209.

Bouraoui, F., B. Grizzetti, K. Granlund, S. Rekolainen, and G. Bidoglio. "Impact of Climate Change on the Water Cycle and Nutrient Losses in a Finnish Catchment." Climatic Change 66.1/2 (2004): 109-26.

Brezonik, Patrick L., and Teresa H. Stadelmann. "Analysis and predictive models of stormwater runoff volumes, loads, and pollutant concentrations from watersheds in the Twin Cities metropolitan area, Minnesota, USA." Water Research 36.7 (2002): 1743-1757.

Bukaveckas, P. A., et al. "Effects of point source loadings, sub-basin inputs and longitudinal variation in material retention on C, N and P delivery from the Ohio River basin." Ecosystems 8.7 (2005): 825-840.

Burkholder, Joann, Bob Libra, Peter Weyer, Susan Heathcote, Dana Kolpin, Peter S. Thorne, and Michael Wichman. "Impacts of Waste from Concentrated Animal Feeding Operations on Water Quality." Environmental Health Perspectives 115.2 (2006): 308-12.

Casey, H., and I. S. Farr. "The influence of within-stream disturbance on dissolved nutrient levels during spates." Hydrobiologia 91.1 (1982): 447-462.

Carpenter, S. R., N. F. Caraco, D. L. Correll, R. W. Howarth, A. N. Sharpley, and V. H. Smith 1998. “Nonpoint Pollution of Surface Waters with Phosphorus and Nitrogen.” Ecological Applications 8:559–568.

Carpenter, Stephen R., and David M. Lodge. "Effects of submersed macrophytes on ecosystem processes." Aquatic botany 26 (1986): 341-370.

Cohn, T. A.; Caulder, D. L.; Gilroy, E. J.; Zynjuk, L. D.; Summers, R. M. (1992) The Validity of a Simple Statistical Model for Estimating Fluvial Constituent Loads: An Empirical Study Involving Nutrient Loads Entering Chesapeake Bay. Water Resour. Res., 28, 2353-2363.

Conley, D. J., H. W. Paerl, R. W. Howarth, D. F. Boesch, S. P. Seitzinger, K. E. Havens, C. Lancelot, and G. E. Likens. "Controlling Eutrophication: Nitrogen and Phosphorus." Science 323.5917 (2009): 1014-015.

Chiew, Francis H. S. "Estimation of Rainfall Elasticity of Streamflow in Australia." Hydrological Sciences Journal 51.4 (2006): 613-25.

Draper, N.R., and H. Smith, (1981), *Applied Regression Analysis,* John Wiley, New York.

Driver, Nancy E., and Gary D. Tasker. Techniques for estimation of storm-runoff loads, volumes, and selected constituent concentrations in urban watersheds in the United States. US Government Printing Office, 1990.

Delpla, I., A.-V. Jung, E. Baures, M. Clement, and O. Thomas. "Impacts of Climate Change on Surface Water Quality in Relation to Drinking Water Production." Environment International 35.8 (2009): 1225-233.

Durance, Isabelle, and Stephen James Ormerod. "Climate change effects on upland stream macroinvertebrates over a 25-year period." Global Change Biology 13.5 (2007): 942-957.

Frederick, Kenneth D., and David C. Major. "Climate Change and Water Resources." Climatic Change 37 (1997): 7-23.

Frumhoff, P.C., J.J. McCarthy, J.M. Melillo, S.C. Moser, and D.J. Wuebbles. 2007. *Confronting Climate Change in the U.S. Northeast: Science, Impacts, and Solutions. Synthesis report of the Northeast Climate Impacts Assessment (NECIA*). Cambridge, MA: Union of Concerned Scientists (UCS): 39-46.

Fu, Guobin, Stephen P. Charles, and Francis H. S. Chiew. "A Two-parameter Climate Elasticity of Streamflow Index to Assess Climate Change Effects on Annual Streamflow." Water Resources Research 43.11 (2007): 256-262

Gardner, Leonard R. "Assessing the Effect of Climate Change on Mean Annual Runoff." Journal of Hydrology 379.3-4 (2009): 351-59.

Gleason, Karin L., Jay H. Lawrimore, David H. Levinson, Thomas R. Karl, and David J. Karoly. "A Revised U.S. Climate Extremes Index." Journal of Climate 21.10 (2008): 2124-137

Galloway, James N. "The Global Nitrogen Cycle: Changes and Consequences." Environmental Pollution 102.1 (1998): 15-24.

Gawel, J. E., et al. "Characterization and Cycling of Phosphorus and Arsenic in Spy Pond (Arlington, Massachusetts)." MA Dept. of Environmental Management (2000).

Gilinsky, Ellen, Jon M. Capacasa, Michael G. Baker, and Ephraim S. King. *An Urgent Call to Action - Report of the State-EPA Nutrient Innovations Task Group*. Rep. Washington D.C.: Environmental Protection Agency, 2009.

Gregg, Watson W., and Fred L. Rose. "The effects of aquatic macrophytes on the stream microenvironment." Aquatic botany 14 (1982): 309-324.

Groisman, P.Y., R.W. Knight, T.R. Karl, D.R. Easterling, B. Sun, and J.M. Lawrimore, 2004: “Contemporary changes of the hydrological cycle over the contiguous United States: Trends derived from in-situ observations.” Journal of Hydrometeorology, 5, 64-85.

Gruber, Nicolas, and James N. Galloway. "An Earth-system Perspective of the Global Nitrogen Cycle." Nature 451.7176 (2008): 293-96.

Harrison, Anthony F., et al. "Potential effects of climate change on DOC release from three different soil types on the Northern Pennines UK: examination using field manipulation experiments." Global Change Biology 14.3 (2008): 687-702.

Helsel, Dennis R., and Robert M. Hirsch. Statistical Methods in Water Resources. Amsterdam: Elsevier, 1992. Print.

Holland, A.frederick, Denise M. Sanger, Christopher P. Gawle, Scott B. Lerberg, Marielis Sexto Santiago, George H.m Riekerk, Lynn E. Zimmerman, and Geoffrey I. Scott. "Linkages between Tidal Creek Ecosystems and the Landscape and Demographic Attributes of Their Watersheds." Journal of Experimental Marine Biology and Ecology 298.2 (2004): 151-78.

Howden, S. M., J.-F. Soussana, F. N. Tubiello, N. Chhetri, M. Dunlop, and H. Meinke. "Climate Change and Food Security Special Feature: Adapting Agriculture to Climate Change." Proceedings of the National Academy of Sciences 104.50 (2007): 19691-9696.

Huntington, Thomas G. "Evidence for intensification of the global water cycle: review and synthesis." Journal of Hydrology 319.1 (2006): 83-95.

IPCC, 2007, Climate Change 2007: Synthesis Report. Contribution of Working Groups I, II and III to the Fourth Assessment Report of the Intergovernmental Panel on Climate Change [Core Writing Team, Pachauri, R.K and Reisinger, A. (eds.)]. IPCC, Geneva, Switzerland, 104 pp.

Jeppesen, Erik, Brian Kronvang, Mariana Meerhoff, Martin Søndergaard, and Kristina M. Hansen. "Climate Change Effects on Runoff, Catchment Phosphorus Loading and Lake Ecological State, and Potential Adaptations." Journal of Environment Quality 38.5 (2009): 1930-941.

Jiang, Jiping, Ashish Sharma, Bellie Sivakumar, and Peng Wang. "A Global Assessment of Climate–water Quality Relationships in Large Rivers: An Elasticity Perspective." Science of The Total Environment 468-469 (2014): 877-91.

Johnston, A. E., and I. Steen. Understanding phosphorus and its use in agriculture. European Fertilizer Manufacturers Association, 2000.

Johnston, J, (1984). *Econometric Methods,* McGraw-Hill, New York.

Kalff, Jacob. "Chapter 17: Phosphorus Concentrations and Cycling." Limnology: Inland Water Ecosystems. Upper Saddle River, NJ: Prentice Hall, 2002. 247-69.

Karl, T. R., J. M. Melillo, and T. C. Peterson (eds.). "Global Climate Change Impacts in the United States". United States Global Change Research Program (2009). Cambridge University Press, New York, NY, USA.

Keup, Lowell E. "Phosphorus in flowing waters." Water Research 2.5 (1968): 373-386.

Kleeburg, A., and G.E. Dudel. "Changes in Extent of Phosphorus Release in a Shallow Lake (Lake Groβer Müggelsee; Germany, Berlin) Due to Climatic Factors and Load." *Marine Geology* 139.1 (1997): 67-75. Jan. 1997.

Koklu, Rabia, Bulent Sengorur, and Bayram Topal. "Water Quality Assessment Using Multivariate Statistical Methods—A Case Study: Melen River System (Turkey)." Water Resources Management 24.5 (2010): 959-78.

Kroll, C.N., and J.R. Stedinger, (1998). Regional hydrologic analysis: Ordinary and generalized least squares revisited, *Water Resources Research*, 34(1), 121-128.

Kundzewicz, Zbigniew W., and Valentina Krysanova. "Climate Change and Stream Water Quality in the Multi-factor Context." Climatic Change 103.3-4 (2010): 353-62.

Kundzewicz ZW, Mata LJ, Arnell NW, Döll PK, Jiménez B, Miller KA, et al. Freshwater resources and their management. In: Parry ML, Canziani OF, Palutikof JP, van der Linden PJ, Hanson CE, editors. *Climate Change 2007: Impacts, Adaptation and Vulnerability. Contribution of Working Group II to the Fourth Assessment Report of the Intergovernmental Panel on Climate Change*. Cambridge, UK: Cambridge University Press; 2007. p. 173–210

Kundzewicz, Zbigniew W. "Climate Change Impacts on the Hydrological Cycle." Ecohydrology and Hydrobiology 8.2 (2008): 195-203.

Li, Haiyan, Liang Liu, Mingyi Li, and Xiaoran Zhang. "Effects of PH, Temperature, Dissolved Oxygen, and Flow Rate on Phosphorus Release Processes at the Sediment and Water Interface in Storm Sewer." Journal of Analytical Methods in Chemistry 2013 (2013): 1-7.

Lipp, Erin K., Raymond Kurz, Robert Vincent, Cesar Rodriguez-Palacios, Samuel R. Farrah, and Joan B. Rose. "The Effects of Seasonal Variability and Weather on Microbial Fecal Pollution and Enteric Pathogens in a Subtropical Estuary." Estuaries 24.2 (2001): 266

Ma, Huan, Dawen Yang, Soon Keat Tan, Bing Gao, and Qingfang Hu. "Impact of Climate Variability and Human Activity on Streamflow Decrease in the Miyun Reservoir Catchment." Journal of Hydrology 389.3-4 (2010): 317-24.

Mallin, Michael A., Virginia L. Johnson, and Scott H. Ensign. "Comparative Impacts of Stormwater Runoff on Water Quality of an Urban, a Suburban, and a Rural Stream." Environmental Monitoring and Assessment 159.1-4 (2009): 475-91.

Malmqvist, Björn, and Simon Rundle. "Threats to the running water ecosystems of the world." Environmental conservation 29.02 (2002): 134-153.

Massachusetts Department of Environmental Protection (DEP). (2014). *Massachusetts Year 2014 List of Impaired Waters.* Worcester, Massachusetts.

Mauget, Steven A. "Multidecadal Regime Shifts in U.S. Streamflow, Precipitation, and Temperature at the End of the Twentieth Century." Journal of Climate 16.23 (2003): 3905-916.

McElmurry, S. P., R. Confesor Jr, and R. Peter Richards. "Reducing Phosphorus Loads to Lake Erie: Best Management Practices." A draft literature review prepared for the International Joint Commission's Lake Erie Ecosystem PriorityIJC Great Lakes Regional Office, Windsor, ON (2013).

Meyer, Judy L., et al. "Impacts of Climate Change on Aquatic Ecosystem Functioning and Health." (1999): 1373-1386.

Milly, P. C. D., J. Betancourt, M. Falkenmark, R. M. Hirsch, Z. W. Kundzewicz, D. P. Lettenmaier, and R. J. Stouffer. "CLIMATE CHANGE: Stationarity Is Dead: Whither Water Management?" Science 319.5863 (2008): 573-74.

Mimikou, M.a., E. Baltas, E. Varanou, and K. Pantazis. "Regional Impacts of Climate Change on Water Resources Quantity and Quality Indicators." Journal of Hydrology 234.1-2 (2000): 95-109.

Mueller, David K., and Dennis R. Helsel. Nutrients in the nation's waters: too much of a good thing?. Ed. Mary A. Kidd. US Government Printing Office, 1996.

Mustapha, Adamu, and Ado Abdu. "Application of Principal Component Analysis & Multiple Regression Models in Surface Water Quality Assessment." Journal of Environment and Earth Science 3216.2224 (2012): 16-23.

Nemery, Julien, and Josette Garnier. "Origin and fate of phosphorus in the Seine watershed (France): Agricultural and hydrographic P budgets." Journal of Geophysical Research: Biogeosciences (2005–2012) 112.G3 (2007).

Newson, Malcolm, and John Lewin. "Climatic change, river flow extremes and fluvial erosion-scenarios for England and Wales." Progress in Physical Geography 15.1 (1991): 1-17.

Nasir, Mohd F., Mohd S. Samsudin, Isahak Mohamad, Mohammad R. Awaluddin, Muhd A. Mansor, Hafizan Juahir, and Norlafifah Ramli. "River Water Quality Modeling Using Combined Principle Component Analysis and Multiple Linear Regressions: A Case Study at Klang River, Malaysia." World Applied Sciences Journal 1st ser. 14.201 (2011): 73-82.

Orrett, K., and D. M. Karl. "Dissolved organic phosphorus production in surface seawaters." Limnology and Oceanography 32.2 (1987): 383-395.

Polgar, Caroline A., and Richard B. Primack. "Leaf-out phenology of temperate woody plants: from trees to ecosystems." New Phytologist 191.4 (2011): 926-941.

Praskievicz, S., and H. Chang. "A Review of Hydrological Modelling of Basin-scale Climate Change and Urban Development Impacts." Progress in Physical Geography 33.5 (2009): 650-71.

Saltelli, A., Tarantola, S., Campolongo, F., Ratto, M. (2004). Sensitivity Analysis in Practice: A Guide to Assessing Scientific Models. John Wiley & Sons Publisher

Saltelli, Andrea, and Paola Annoni. "How to Avoid a Perfunctory Sensitivity Analysis." Environmental Modelling & Software 25.12 (2010): 1508-517.

Sankarasubramanian, A., Richard M. Vogel, and James F. Limbrunner. "Climate Elasticity of Streamflow in the United States." Water Resources Research 37.6 (2001): 1771.

Sardans, J., J. Peñuelas, and M. Estiarte. "Warming and Drought Change Trace Element Bioaccumulation Patterns in a Mediterranean Shrubland." Chemosphere 70.5 (2008): 874-85.

Schaake, JC. (1990). From Climate to Flow, Chapter 8. In : Climate Change and U.S. Water Resources. Ed, Waggoner, PE. John Wiley & Sons, Inc

Schindler, David W. "Widespread effects of climatic warming on freshwater ecosystems in North America." Hydrological Processes 11.8 (1997): 1043-1067.

Smith, Stephen V., et al. "Humans, hydrology, and the distribution of inorganic nutrient loading to the ocean." BioScience 53.3 (2003): 235-245.

Stedinger, J.R., and G.D. Tasker (1985). Regional Hydrologic Analysis, 1, Ordinary, weighted, and generalized least squares compared, *Water Resources Research,* 21(9), 1421-1432.

Svendsen, Lars M., and Brian Kronvang. "Retention of nitrogen and phosphorus in a Danish lowland river system: implications for the export from the watershed." Nutrient Dynamics and Retention in Land/Water Ecotones of Lowland, Temperate Lakes and Rivers. Springer Netherlands, 1993. 123-135.

Tsai, Yushiou, and Richard M. Vogel. Climatic and Anthropogenic Influences on Freshwater Availability in the Eastern United States. Rep. N.p.: World Environmental and Water Resources Congress 2010: Challenges of Change, 2010.

U.S. Environmental Protection Agency (1989). Quality Criteria for Water 1986. Rep. no. EPA-440/5-86-001. Washington D.C.: Office of Water Regulations and Standards Division, United States Environmental Protection Agency, Washington D.C.

U.S. Environmental Protection Agency (US EPA). (1992). NPDES Storm Water Sampling Guidance Document. EPA 833-8-92-001.

U.S. Environmental Protection Agency (1998). National Water Quality Inventory: 1996 Report to Congress, EPA841-R-97-008, April 1998, p. ES-13.

U.S. Environmental Protection Agency (2006). Excessive Heat Events Guidebook. EPA 430-B-06-005. 60 pp., U.S. Environmental Protection Agency, Washington, D.C.

Van Der Zee, Clara, and Lei Chou. "Seasonal cycling of phosphorus in the Southern Bight of the North Sea." Biogeosciences 2.1 (2005): 27-42.

Vitousek, Peter M., John D. Aber, Robert W. Howarth, Gene E. Likens, Pamela A. Matson, David W. Schindler, William H. Schlesinger, and David G. Tilman. "Technical Report: Human Alteration of the Global Nitrogen Cycle: Sources and Consequences." Ecological Applications 7.3 (1997): 737.

Vogel, Richard M., Ian Wilson, and Chris Daly. "Regional Regression Models of Annual Streamflow for the United States." Journal of Irrigation and Drainage Engineering 125.3 (1999): 148.

Whitehead, P. G., R. L. Wilby, R. W. Battarbee, M. Kernan, and A. J. Wade. "A Review of the Potential Impacts of Climate Change on Surface Water Quality." Hydrological Sciences Journal 54.1 (2009): 101-23.

Wilby, R. L. "The Influence of Variable Weather Patterns on River Water Quantity and Quality Regimes." International Journal of Climatology 13.4 (1993): 447-59.

Wilby, R. L., et al. "Risks posed by climate change to the delivery of Water Framework Directive objectives in the UK." Environment international 32.8 (2006): 1043-1055.

Withers, P.j.a., and H.p. Jarvie. "Delivery and Cycling of Phosphorus in Rivers: A Review." Science of The Total Environment 400.1-3 (2008): 379-95.

Xu, X., D. Yang, and M. Sivapalan. "Assessing the Impact of Climate Variability on Catchment Water Balance and Vegetation Cover." Hydrology and Earth System Sciences Discussions 8.3 (2011): 6291-329.

Zhu, Guangwei, Fang Wang, Guang Gao, and Yunlin Zhang. "Variability of Phosphorus Concentration in Large, Shallow and Eutrophic Lake Tiahu, China." Water Environment Research 8th ser. 80.9 (2008): 832-39.

Appendices

Appendix A. Sampling Procedures and Guidelines for Measuring Phosphorus Loads Using an ISCO Automated Sampler

Pre-sampling procedures

Presented below is a list of sampling procedures used to measure storm-event phosphorus loads during the 2014 calendar year. Sampling was executed using an ISCO 6712 full size portable autosampler. The list outlines procedures to be taken before, during, and after sampling to promote efficient collection of required measurements. These guidelines were adapted from the 6712 Portable Samplers Installation and Operations Guide to fit the requirements and locational aspects of this study.

The day before sampling:

1. Charge external autosampler battery for 15-18 hours

*Note: DO NOT overcharge.

2. Don purple nitrile gloves and wash bottle caps with Liquinox. Allow to Dry.

3. Place ProPak bags in blue skeletons

4. Secure ProPaks with rubber bands and bottle caps

5. Place blue skeletons with ProPaks bags in sampling base and secure with retaining ring

6. Fill three clean 5-gallon buckets with deionized (DI) water

The day of sampling:

1. Fill cooler with ice and bring a water bottle filled with water for water/ice mixture

2. Make sure you transport all of the following items to the site:

Table A-1. Sampling Checklist

Charged Battery	
Sampling base with secured bottles	
Cooler of ice and water bottle	
Keys to shelter lock	
Bag to hold bottle caps	
Bottle labels and sharpie	

New set of nitrile gloves	
5-gallon buckets	
Graduated cylinder for calibration	

On-site:

1. Check pump tubing for kinks, holes, or debris. Check to see that it is fully submerged.

2. Place battery inside sampling enclosure and plug it into machine

3. Re-name the program to reflect the current date

4. While bottle caps are still on the bottles, place ice in sampler up to the bottom of the retaining ring then add water

5. Remove bottle caps and put sampler top onto sampler base. Secure the top to the base using the three connectors on the sides of the sampler.

Calibration:

1. Disconnect the pump tube (on the left) from the bulkhead fitting.

2. Select Other functions → Manual functions → Calibrate volume → Standard portable

3. Place end of tube over graduated cylinder

4. Collect sample

5. Visually measure the volume of water collected

6. Enter volume into controller when prompted

7. Repeat process until machine accurately reports 1000 mL

DI-blank:

1. Put on the hip waders and wade into the river

*Note: Use walking stick for balance

2. Remove the sample tube from the sampler screen

3. Place sample tube in the first bucket of DI water

4. Remove bulkead fitting from the machine and point toward the autosampler cap

5. Run DI-water through the sample tube and out into the autosampler cap using Other functions → Manual functions → Operate pump → Pump forward

6. Run DI-water from the other two buckets through the pump, but save approximately one-fourth of the DI-water from the last bucket for the DI-blank

7. Reconnect the bulkhead fitting to the machine. With the excess one-fourth of water in the final DI-bucket, take a grab sample and place in the very last sample bottle: Select Other functions →Manual functions → Move distributor arm → Move to bottle 24 (or whatever the last bottle you are using is) and then select Other functions → Grab sample

8. Wade into the river to replace the sample tube onto the sampling screen

9. Move distributor arm back to bottle 1: Other functions → Manual functions → Move distributor arm → Move to bottle 1

Pre-storm sample and programming

Programming the autosampler:

Selections to be made are in **BOLD**. Check to make sure all other options are set to the choices listed below.

UNITS SELECTED:
LENGTH: ft
BUBBLER MODULE:
LEVEL ONLY
CURRENT LEVEL IS
Either + or -4 ft on average

---

5 MINUTE DATA INTERVAL

24, 1000 ml BTLS
28 ft SUCTION LINE
AUTO SUCTION HEAD
0 RINSES, 1 RETRIES

ONE-PART PROGRAM

PACING:
NONUNIFORM TIME, INTERVALS IN MINUTES
**** [*You have to select this to go into the following commands]*

UNIFORM TIME PACED
FLOW PACED
EVENT PACED
NONUNIFORM TIME PACED

NONUNIFORM TIME:
CLOCK TIMES
INTERVAL IN MINUTES
RANDOM INTERVALS

SAMPLE AT START… (This means that one sample will be taken as soon as you hit "run"– we usually deem this the pre-storm sample, but if you have already taken a pre-storm sample, you may make this your first sample if it is raining at the time you are programming)

QUANTITY AT INTERVAL
1. ___ at ___ min
2. ___ at ___ min
3. ___ at ___ min
when you are done with your sampling scheme, set one quantity to zero:
4. 0 at ____min
and it will take you to the next screen.

PACING:
NONUNIFORM TIME, INTERVALS IN MINUTES
**** [*Screen returns to this page – move onto next page now]*

DISTRIBUTION:
SEQUENTIAL

VOLUME:
1000 ml SAMPLES

ENABLE:
NONE PROGRAMMED

ENABLE:
ONCE ENABLED STAY ENABLED
NO SAMPLE AT ENABLE

ENABLE:
0 MINUTE DELAY TO START OF SAMPLING

ENABLE:
0 PAUSES & RESUMES

NO DELAY TO START

PROGRAMMING COMPLETE
RUN THIS PROGRAM NOW?
YES NO

Once you have pressed YES to run the sample, lock the sampler case and put everything back into the car to be taken to the Tufts laboratory.

Post-sampling procedures

First round of sampling collection:

1. At Tufts, fill a big cooler with ice

2. Take the cooler to the site and place samples on ice to be transported to MyWRA for processing

3. Create two labels for each sample: One to be analyzed for TP and one for TURB
- Format: ALB_PHOS_042
- Use military time

4. Pour sample into ¼ of the TURB bottle, then ¼ of the discard bottle, then ¼ of the TP bottle. Repeat until the TURB and TP bottles are full.

5. Label bottles and place them on ice

6. Fill out chain of custody form

7. Put blue skeletons back into autosampler so that it can take more samples

Second round of sample collection:

*Notes:
- You will have to go back to retrieve the second half of the samples
- This time, the program will be finished and you will have to collect data from the machine

1. At Tufts, fill a big cooler with ice

2. Retrieve RTK laptop connection device

3. Go to MyWRA office and retrieve the intern laptop

4. Take laptop and cooler filled with ice to the sampling site

5. Plug laptop connector into machine and connect the USB port to the laptop

6. On the laptop, press START and open the program called Flowlink

7. Select Utilities → Options

8. Click on the tab that says "4100/4200/6700"

9. Make sure the baud rate is at 9600 and the com port is at 4

10. Check "retrieved data gets text reports"

11. Select File → Quick connect

12. Review data

13. Save data to the laptop under Documents/Autosampler files

14. Place samples on ice

15. Take samples back to MyWRA office and process them like before

*Note:

- Make sure you also take sampler base, battery, caps, and laptop connector back so you can put them back in the Tufts lab

16. E-mail the saved data to yourself while in the MyWRA office.

17. Take everything back to Tufts laboratory

18. Clean bottle caps by hand, clean skeletons by hand or in dishwasher rinse cycle

Appendix B: Storm Sampling Times

April Storm						
SampleID	Date	Time	DateTime	Site	Monitors	Notes
ALB_PHOS_001	4/14/2014	4:30:00 PM	4/14/2014 16:30	ALB003	Kate, Andy	Equipment blank
ALB_PHOS_002	4/15/2014	1:45:00 PM	4/15/2014 13:45	ALB003	Kate, Andy	Pre-storm sample
ALB_PHOS_003	4/15/2014	1:45:00 PM	4/15/2014 13:45	ALB003	Kate, Andy	
ALB_PHOS_004	4/15/2014	2:45:00 PM	4/15/2014 14:45	ALB003	Kate, Andy	
ALB_PHOS_005	4/15/2014	3:45:00 PM	4/15/2014 15:45	ALB003	Kate, Andy	
ALB_PHOS_006	4/15/2014	4:45:00 PM	4/15/2014 16:45	ALB003	Kate, Andy	
ALB_PHOS_007	4/15/2014	5:45:00 PM	4/15/2014 17:45	ALB003	Kate, Andy	
ALB_PHOS_008	4/15/2014	6:45:00 PM	4/15/2014 18:45	ALB003	Kate, Andy	
ALB_PHOS_009	4/15/2014	7:45:00 PM	4/15/2014 19:45	ALB003	Kate, Andy	
ALB_PHOS_010	4/15/2014	8:45:00 PM	4/15/2014 20:45	ALB003	Kate, Andy	
ALB_PHOS_011	4/15/2014	9:45:00 PM	4/15/2014 21:45	ALB003	Kate, Andy	
ALB_PHOS_012	4/15/2014	10:45:00 PM	4/15/2014 22:45	ALB003	Kate, Andy	
ALB_PHOS_013	4/15/2014	11:45:00 PM	4/15/2014 23:45	ALB003	Kate, Andy	
ALB_PHOS_014	4/16/2014	1:45:00 AM	4/16/2014 1:45	ALB003	Kate, Andy	
ALB_PHOS_015	4/16/2014	3:45:00 AM	4/16/2014 3:45	ALB003	Kate, Andy	
ALB_PHOS_016	4/16/2014	5:45:00 AM	4/16/2014 5:45	ALB003	Kate, Andy	
ALB_PHOS_017	4/16/2014	7:45:00 AM	4/16/2014 7:45	ALB003	Kate, Andy	
ALB_PHOS_018	4/16/2014	9:45:00 AM	4/16/2014 9:45	ALB003	Kate, Andy	
ALB_PHOS_019	4/16/2014	11:45:00 AM	4/16/2014 11:45	ALB003	Kate, Andy	
ALB_PHOS_020	4/17/2014	8:00:00 AM	4/17/2014 8:00	ALB003	Kate, Andy	
ALB_PHOS_021	4/17/2014	9:45:00 AM	4/17/2014 9:45	ALB003	Kate, Andy	
ALB_PHOS_022	4/17/2014	7:45:00 PM	4/17/2014 19:45	ALB003	Kate, Andy	
ALB_PHOS_023	4/18/2014	7:45:00 AM	4/18/2014 7:45	ALB003	Kate, Andy	

May Storm						
SampleID	Date	Time	DateTime	Site	Monitors	Notes
ALB_PHOS_032	5/16/2014	15:01:00	5/16/2014 15:01:00	ALB003	Kate, Ruhui	Equipment blank
ALB_PHOS_025	5/16/2014	15:35:00	5/16/2014 15:35:00	ALB003	Kate, Ruhui	Pre-storm sample
ALB_PHOS_026	5/17/2014	3:01:00	5/17/2014 3:01:00	ALB003	Kate, Ruhui	
ALB_PHOS_027	5/17/2014	5:01:00	5/17/2014 5:01:00	ALB003	Kate, Ruhui	
ALB_PHOS_028	5/17/2014	7:01:00	5/17/2014 7:01:00	ALB003	Kate, Ruhui	
ALB_PHOS_029	5/17/2014	8:01:00	5/17/2014 8:01:00	ALB003	Kate, Ruhui	
ALB_PHOS_030	5/17/2014	10:01:00	5/17/2014 10:01:00	ALB003	Kate, Ruhui	
ALB_PHOS_031	5/17/2014	11:01:00	5/17/2014 11:01:00	ALB003	Kate, Ruhui	
ALB_PHOS_033	5/17/2014	15:01:00	5/17/2014 15:01:00	ALB003	Kate, Ruhui	
ALB_PHOS_034	5/17/2014	19:01:00	5/17/2014 19:01:00	ALB003	Kate, Ruhui	
ALB_PHOS_035	5/18/2014	3:01:00	5/18/2014 3:01:00	ALB003	Kate, Ruhui	
ALB_PHOS_036	5/18/2014	11:01:00	5/18/2014 11:01:00	ALB003	Kate, Ruhui	
ALB_PHOS_037	5/18/2014	19:01:00	5/18/2014 19:01:00	ALB003	Kate, Ruhui	
ALB_PHOS_038	5/18/2014	23:00:00	5/18/2014 23:00:00	ALB003	Kate, Ruhui	
ALB_PHOS_039	5/18/2014	20:00:00	5/18/2014 20:00:00	ALB003	Kate, Ruhui	Liquinox-washed blank
ALB_PHOS_040	5/18/2014	20:00:00	5/18/2014 20:00:00	ALB003	Kate, Ruhui	Acid-washed blank
ALB_PHOS_041	5/19/2014	11:00:00	5/19/2014 11:00:00	ALB003	Kate, Ruhui	Post-storm grab sample

June Storm

SampleID	Date	Time	DateTime	Site	Monitors	Notes
ALB_PHOS_042	6/25/2014	14:00	6/25/2014 14:00	ALB003	Kate, Ruhui	Equipment blank
ALB_PHOS_043	6/25/2014	14:00:00	6/25/2014 14:00	ALB003	Kate, Ruhui	Prestorm sample
ALB_PHOS_044	6/25/2014	23:00:00	6/25/2014 23:00	ALB003	Kate, Ruhui	
ALB_PHOS_045	6/26/2014	3:00:00	6/26/2014 3:00	ALB003	Kate, Ruhui	
ALB_PHOS_046	6/26/2014	7:00	6/26/2014 7:00	ALB003	Kate, Ruhui	
ALB_PHOS_047	6/26/2014	9:00	6/26/2014 9:00	ALB003	Kate, Ruhui	
ALB_PHOS_048	6/26/2014	11:00	6/26/2014 11:00	ALB003	Kate, Ruhui	
ALB_PHOS_049	6/26/2014	13:00	6/26/2014 13:00	ALB003	Kate, Ruhui	
ALB_PHOS_050	6/26/2014	15:00	6/26/2014 15:00	ALB003	Kate, Ruhui	
ALB_PHOS_051	6/26/2014	19:00	6/26/2014 19:00	ALB003	Kate, Ruhui	
ALB_PHOS_052	6/26/2014	23:00	6/26/2014 23:00	ALB003	Kate, Ruhui	
ALB_PHOS_053	6/27/2014	3:00	6/27/2014 3:00	ALB003	Kate, Ruhui	
ALB_PHOS_054	6/27/2014	7:00	6/27/2014 7:00	ALB003	Kate, Ruhui	
ALB_PHOS_055	6/27/2014	15:00	6/27/2014 15:00	ALB003	Kate, Ruhui	

July Storm

SampleID	Date	Time	DateTime	Site	Monitors	Notes
ALB_PHOS_056	7/27/2014	2:00:00 PM	7/27/2014 14:00	ALB003	Kate, Ruhui	
ALB_PHOS_057	7/27/2014	4:00:00 PM	7/27/2014 16:00	ALB003	Kate, Ruhui	
ALB_PHOS_058	7/27/2014	8:00:00 PM	7/27/2014 20:00	ALB003	Kate, Ruhui	
ALB_PHOS_059	7/27/2014	10:00:00 PM	7/27/2014 22:00	ALB003	Kate, Ruhui	
ALB_PHOS_060	7/28/2014	8:00:00 AM	7/28/2014 8:00	ALB003	Kate, Ruhui	
ALB_PHOS_061	7/27/2014	8:00:00 AM	7/27/2014 8:00	ALB003	Kate, Ruhui	Equipment blank
ALB_PHOS_062	7/27/2014	8:00:00 AM	7/27/2014 8:00	ALB003	Kate, Ruhui	Prestorm sample
ALB_PHOS_063	7/28/2014	12:00:00 PM	7/28/2014 12:00	ALB003	Kate, Ruhui	
ALB_PHOS_064	7/28/2014	3:00:00 PM	7/28/2014 15:00	ALB003	Kate, Ruhui	
ALB_PHOS_065	7/28/2014	9:00:00 PM	7/28/2014 21:00	ALB003	Kate, Ruhui	
ALB_PHOS_066	7/29/2014	9:00:00 AM	7/29/2014 9:00	ALB003	Kate, Ruhui	
ALB_PHOS_067	7/29/2014	11:00:00 AM	7/29/2014 11:00	ALB003	Kate, Ruhui	
ALB_PHOS_068	7/29/2014	11:00:00 AM	7/29/2014 11:00	ALB003	Kate, Ruhui	

August 13 Storm

SampleID	Date	Time	DateTime	Site	Monitors	Notes
ALB_PHOS_069	8/12/2014	7:23:00 PM	8/12/2014 19:23	ALB003	Kate, Ruhui	Equipment blank
ALB_PHOS_070	8/12/2014	7:23:00 PM	8/12/2014 19:23	ALB003	Kate, Ruhui	Prestorm sample
ALB_PHOS_071	8/13/2014	7:00:00 AM	8/13/2014 7:00	ALB003	Kate, Ruhui	
ALB_PHOS_072	8/13/2014	10:00:00 AM	8/13/2014 10:00	ALB003	Kate, Ruhui	
ALB_PHOS_073	8/13/2014	1:00:00 PM	8/13/2014 13:00	ALB003	Kate, Ruhui	
ALB_PHOS_074	8/13/2014	4:00:00 PM	8/13/2014 16:00	ALB003	Kate, Ruhui	
ALB_PHOS_075	8/13/2014	7:00:00 PM	8/13/2014 19:00	ALB003	Kate, Ruhui	
ALB_PHOS_076	8/13/2014	10:00:00 PM	8/13/2014 22:00	ALB003	Kate, Ruhui	
ALB_PHOS_077	8/14/2014	4:00:00 AM	8/14/2014 4:00	ALB003	Kate, Ruhui	Not filtered for PO4

August 31 Storm

SampleID	Date	Time	DateTime	Site	Monitors	Notes
ALB_PHOS_078	8/31/2014	12:23:00 PM	8/31/2014 12:23	ALB003	Kate, Andy	Equipment blank
ALB_PHOS_079	8/31/2014	7:00:00 PM	8/31/2014 19:00	ALB003	Kate, Andy	Prestorm sample
ALB_PHOS_080	8/31/2014	10:00:00 PM	8/31/2014 22:00	ALB003	Kate, Andy	
ALB_PHOS_081	9/1/2014	1:00:00 AM	9/1/2014 1:00	ALB003	Kate, Andy	
ALB_PHOS_082	9/1/2014	4:00:00 AM	9/1/2014 4:00	ALB003	Kate, Andy	
ALB_PHOS_083	9/1/2014	7:00:00 AM	9/1/2014 7:00	ALB003	Kate, Andy	
ALB_PHOS_084	9/1/2014	10:00:00 AM	9/1/2014 10:00	ALB003	Kate, Andy	
ALB_PHOS_085	9/1/2014	1:00:00 PM	9/1/2014 13:00	ALB003	Kate, Andy	

September Storm						
SampleID	**Date**	**Time**	**DateTime**	**Site**	**Monitors**	**Notes**
ALB_PHOS_086	9/6/2014	12:30:00 PM	9/6/2014 12:30	ALB003	Kate, Volunteer	Equipment blank
ALB_PHOS_087	9/6/2014	4:00:00 PM	9/6/2014 16:00	ALB003	Kate, Volunteer	Prestorm sample
ALB_PHOS_088	9/6/2014	6:00:00 PM	9/6/2014 18:00	ALB003	Kate, Volunteer	
ALB_PHOS_089	9/6/2014	8:00:00 PM	9/6/2014 20:00	ALB003	Kate, Volunteer	
ALB_PHOS_090	9/6/2014	10:00:00 PM	9/6/2014 22:00	ALB003	Kate, Volunteer	
ALB_PHOS_091	9/7/2014	12:00:00 AM	9/7/2014 0:00	ALB003	Kate, Volunteer	
ALB_PHOS_092	9/7/2014	6:00:00 AM	9/7/2014 6:00	ALB003	Kate, Volunteer	
ALB_PHOS_093	9/7/2014	12:00:00 PM	9/7/2014 12:00	ALB003	Kate, Volunteer	
ALB_PHOS_094	9/7/2014	6:00:00 PM	9/7/2014 18:00	ALB003	Kate, Volunteer	

October Storm						
SampleID	**Date**	**Time**	**DateTime**	**Site**	**Monitors**	**Notes**
ALB_PHOS_095	10/15/2014	19:52	10/15/2014 19:52	ALB003	Kate, Volunteer	Equipment Blank
ALB_PHOS_096	10/15/2014	19:52	10/15/2014 19:52	ALB003	Kate, Volunteer	Pre-storm Sample
ALB_PHOS_097	10/16/2014	13:00	10/16/2014 13:00	ALB003	Kate, Volunteer	
ALB_PHOS_098	10/16/2014	16:00	10/16/2014 16:00	ALB003	Kate, Volunteer	
ALB_PHOS_099	10/16/2014	19:00	10/16/2014 19:00	ALB003	Kate, Volunteer	
ALB_PHOS_100	10/16/2014	22:00	10/16/2014 22:00	ALB003	Kate, Volunteer	
ALB_PHOS_101	10/17/2014	2:00	10/17/2014 2:00	ALB003	Kate, Volunteer	
ALB_PHOS_102	10/17/2014	6:00	10/17/2014 6:00	ALB003	Kate, Volunteer	
ALB_PHOS_103	10/17/2014	14:00	10/17/2014 14:00	ALB003	Kate, Volunteer	

Appendix C: Additional Storm Sampling Results

Introduction

The following appendix consists of additional storm sampling results not outlined in the main body of this work. Correlations between rain events and weather related characteristics occurring before and during the storm are identified. An analysis to estimate the event mean concentration (EMC) of a storm based on pre-storm and intra-storm conditions is performed. Measurement and modeling of phosphorus will be the first steps in understanding the connection between phosphorus levels and impairments to the river. The accurate measurement of phosphorus loads is imperative to the determination of appropriate levels of nutrients for a healthy urban watershed. The data derived from this project will facilitate collaboration between MyRWA and municipalities to identify targets for phosphorus levels and solutions to stormwater pollution. MyRWA is already heavily involved with the cities of Medford and Somerville on combatting one of the negative outcomes of stormwater pollution – the choking of the Mystic River with invasive plants. This is a concern for Tufts University as well, given the value that the Malden and Mystic Rivers hold for the university crew programs.

Figure C-1 demonstrates the phosphorus and flow rate conditions for each storm sampled. As shown, phosphorus concentrations tend to increase as flow rate increases throughout the storm and then quickly drop off once the hydrograph falls from its highest point. The August 13 storm results may indicate that too few measurements were taken, thus not allowing us to make any assumptions about phosphorus conditions along the falling limb of the hydrograph. For this reason, the August 13 storm was left out of EMC analyses.

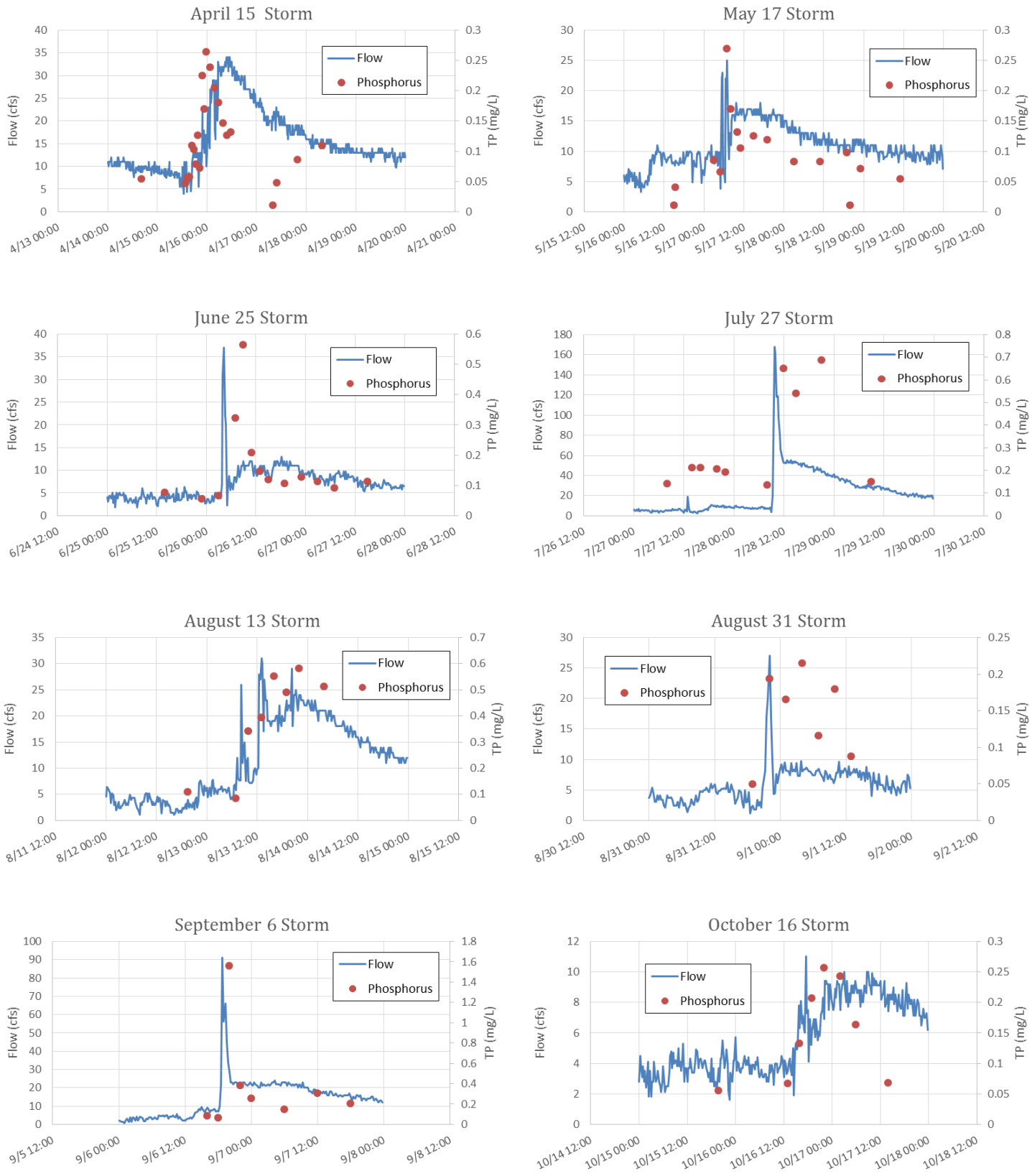

Figure C-1. Comparison of Total Phosphorus and Flow Rate Values During Each Storm

Total Phosphorus

The eight storms sampled show an array of total phosphorus statistics. In later sections, these total phosphorus measurements are analyzed in conjunction with several different factors that contribute to pollutant loading. It is evident from Table C-2 that maximum total phosphorus concentrations are highest in the summer months, possibly due to higher temperatures influencing microbial activity. However, event mean concentrations do not necessarily follow a seasonal pattern, as the August 31st storm EMC value is similar to both the October storm EMC and the June storm EMC.

Table C-2. 2014 Total Phosphorus Stormwater Results

Storm	Maximum TP (mg/L)	Minimum TP (mg/L)	Time for TP to reach peak (hr)	FWM Concentration (mg/L)	Event Mean Concentration (mg/L)
Apr 15	0.264	0.010	16	0.132	0.118
May 17	0.269	0.040	16	0.115	0.086
Jun 25	0.563	0.055	4.5	0.192	0.129
July27	0.687	0.134	33	0.477	0.402
Aug 13	0.580	0.083	17	0.459	0.485
Aug 31	0.215	0.049	7	0.164	0.144
Sep 6	1.560	0.065	1.25	0.527	0.326
Oct 16	0.256	0.067	7	0.169	0.157

Table C-3 provides statistical information regarding total phosphorus concentrations for each storm. Similar to event mean concentrations listed above, the mean and median total phosphorus concentrations were highest for the July, August 13th,

and September storms. These storms also show rather high variance values, meaning that total phosphorus values are fairly spread out compared to other storms. The small variances of the April, May, August 31, and October storms indicate that most of the total phosphorus measurements tend to be very close to the mean total phosphorus concentrations of each storm. Additionally, negative kurtosis values indicate flatter distributions. The storms with higher variances and standard deviations are likely to contain outliers or extremes total phosphorus values.

Skewness identifies distribution shape. In the case of the sampled storms, positive skew indicates that the right tail of the distribution is longer, generally. If skewness is high, this may indicate that precipitation was intense initially and therefore produced high phosphorus concentrations within the river which then tapered off as precipitation decreased. This is true of both June and September storms, which both exhibited high rainfall intensity at the beginning of the storms.

Table C-3. 2014 Total Phosphorus Statistics

Storm	Mean TP	Median TP	Variance TP	Standard Deviation TP	Skewness TP	Kurtosis TP
Apr 15	0.123	0.109	0.005	0.069	0.499	-0.529
May 17	0.112	0.097	0.003	0.057	1.977	4.695
Jun 25	0.169	0.116	0.020	0.143	2.277	5.417
July27	0.331	0.212	0.051	0.226	0.904	-1.280
Aug 13	0.421	0.489	0.029	0.172	-1.469	2.186
Aug 31	0.140	0.148	0.004	0.066	-0.291	-1.815
Sep 6	0.417	0.256	0.265	0.515	2.422	6.118
Oct 16	0.162	0.163	0.006	0.078	-0.146	-1.732

Figure C-2 demonstrates that peak maximum total phosphorus concentrations do not necessarily lead to the highest EMC values. In particular, the September storm exhibits an extremely large maximum total phosphorus value that does not correspond to an extremely large event mean concentration. Because EMC is a function of both concentration and flow rate, the September storm may have significant factors other than flow rate that explain the excessive maximum total phosphorus concentration. However, pre-storm total phosphorus conditions, as shown in Figure C-3, may reveal a pattern between phosphorus conditions prior to the storm and overall event mean concentration.

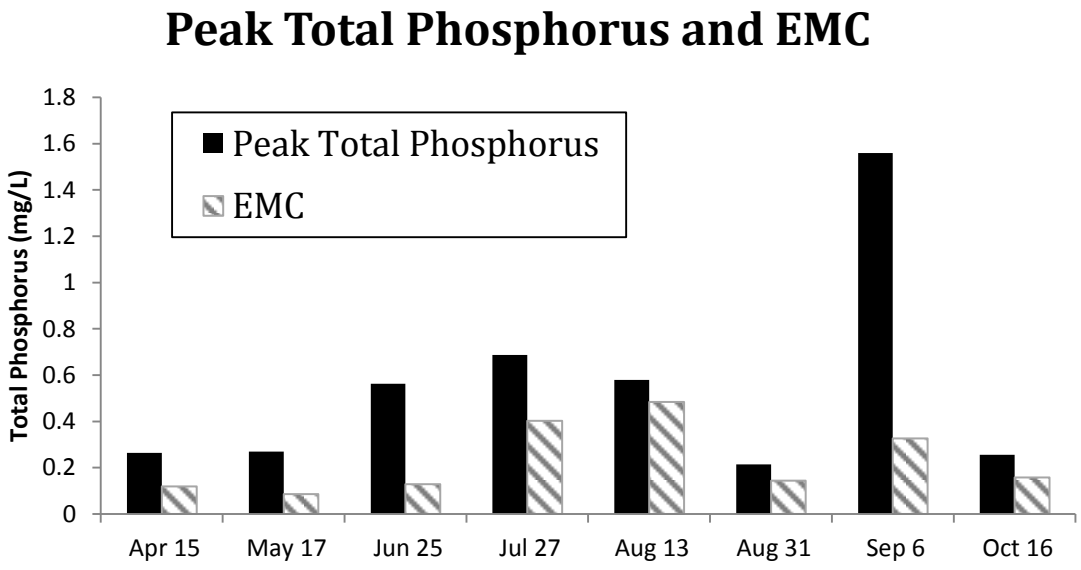

Figure C-2. Comparison of Peak Total Phosphorus Concentration and Event Mean Concentration

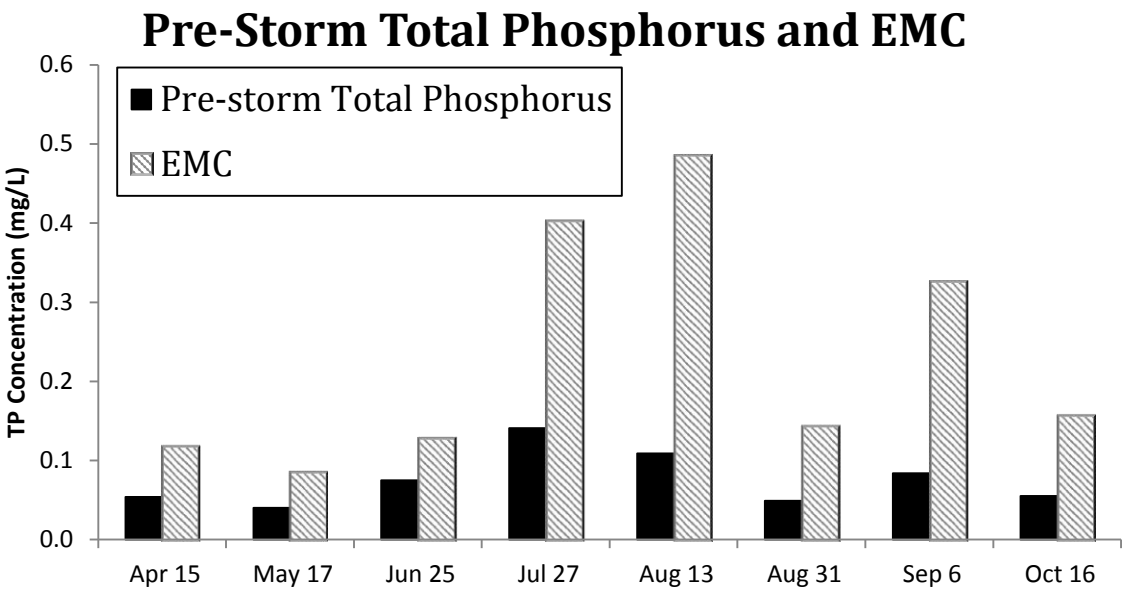

Figure C-3. Comparison of Pre-Storm Phosphorus Conditions and Storm Event Mean Concentration

Flow Rate

The rate of discharge during a storm can provide a great deal of information about total phosphorus loading. It is clear that increased precipitation leads to greater flow rates within Alewife Brook. Rainfall runs off of impervious surfaces into the river, carrying phosphorus-containing pollutants. Table C-4 contains information on maximum, minimum, total, and average discharge per storm. This information, coupled with total phosphorus statistics per storm, provides an enhanced understanding of the effects of flow rate on total phosphorus within the brook.

Table C-4. Flow Rate Statistics During Sampled Storms

Storm	Maximum Discharge (cfs)	Minimum Discharge (cfs)	Total Discharge (cfs)	Mean Discharge (cfs)
Apr 15	34	4.00	1229.60	11.79
May 17	25	3.30	722.70	9.9
Jun 25	37	1.80	542.00	7.28
July27	168	2.60	1063.70	10.97
Aug 13	31	1.10	1112.30	5.18
Aug 31	27	1.10	120.00	5.73
Sep 6	91	0.80	1025.00	22.97
Oct 16	11	1.60	316.40	4.56

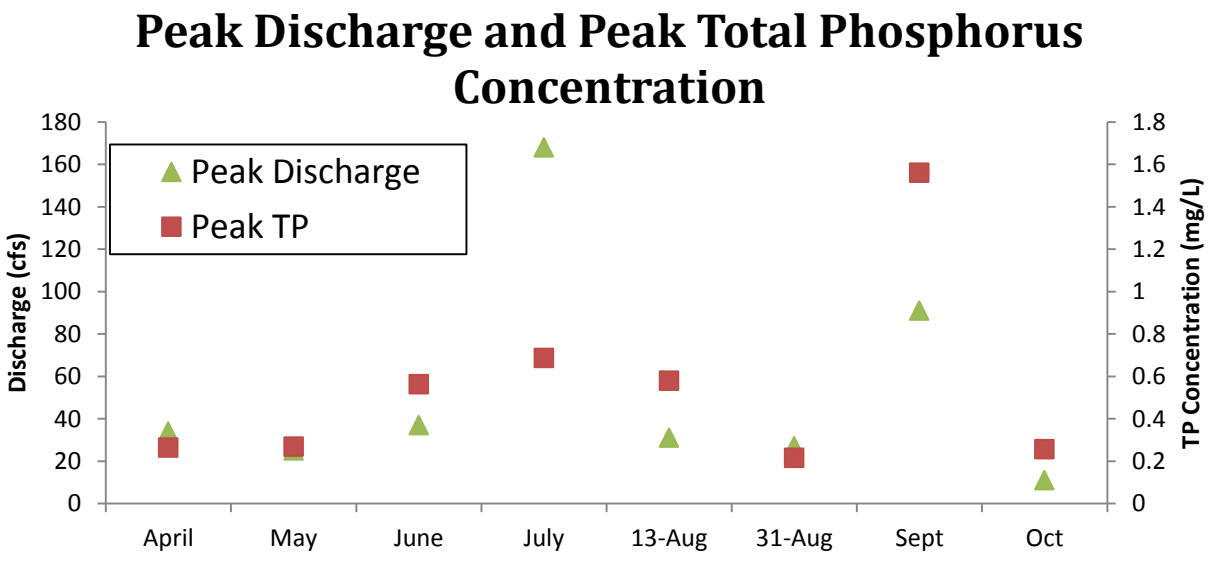

Figure C-4. Comparison of Peak Discharge and Peak Total Phosphorus Concentration

As shown in Figure C-4, maximum discharge somewhat correlates with maximum total phosphorus concentration for most storms. However, the July and September storms are outliers, because these storms exhibited significantly higher peak flow rates than the other six storms. High precipitation intensity during these two storms drove additional inputs of sewage water into the river via CSO, directly impacting both flow rate and total phosphorus levels.

Precipitation

Rain events facilitate excessive phosphorus loading into the Alewife Brook by loosening phosphorus-containing particles from impervious surfaces and carrying them down gradient into rivers. If a storm has a large number of dry weather days prior to the event, phosphorus has more time to accumulate on these surfaces, thus exacerbating the phosphorous conditions within the river during and after rainfall. Table C-5 summarizes dryness and precipitation data, showing that the July storm had both the highest number of preceding dry days as well as the highest peak precipitation intensity. Although some storms had longer precipitation duration than others, precipitation intensity may have a stronger impact on event mean concentration within the river because intense rainfall can trigger CSO outbreaks.

Table C-5. Summary of Precipitation and Dry Period Data

Storm	Preceding Dry Period (days)	Precipitation Duration (hr)	Total Precipitation (in)	Peak Precipitation Intensity (in/hr)
Apr 15	1.79	23	0.98	0.19
May 17	5.71	18	0.71	0.38
Jun 25	8.83	17	0.28	0.14
July27	11.67	22	0.46	0.28
Aug 13	6.58	17	1.06	0.14
Aug 31	3.96	2	0.54	0.27
Sep 6	4.25	9.17	0.37	0.22
Oct 16	4.67	15.35	0.63	0.22

Seasonal and Event-Based Factors

Phosphorus pollution may be a function of seasonal changes, during which air temperature influences water temperature, possibly affecting phosphorus mobilization. Increases in temperature increase microbial activity on land surfaces, creating a larger availability of phosphorus which can run off of impervious surfaces into Alewife Brook. Additionally, fertilization of residential lawns generally occurs in the spring and sometimes summer months, which may contribute to inputs of phosphorus in the form of storm event runoff. Finally, combined sewer overflows (CSO) will add additional inputs of phosphorus in the form of raw sewage directly into the river. These CSO outbreaks are most often triggered by intense rainfall in short time periods, which can occur regardless of seasonality. Event-based factors are summarized in Table C-6.

Table C-6. Summary of Event-Based Factors During Sampled Storms

Storm	Day of Year	Average Air Temperature (°F)	Average Water Temperature (°F)	Season	CSO (YES/NO)
Apr 15	105	52.12	N/A	Spring	NO
May 17	136	62.94	66.07	Spring	NO
Jun 25	177	70.82	78.25	Summer	NO
July27	208	70.57	72.72	Summer	YES
Aug 13	225	66.25	N/A	Summer	NO
Aug 31	243	73.80	N/A	Summer	NO
Sep 6	294	71.79	75.70	Fall	YES
Oct 16	289	65.59	65.47	Fall	NO

Storms without CSO outbreaks exhibit maximum flow rates of approximately 40 cfs and lower. However, the September storm had a maximum flow rate greater than 90 cfs and the July storm produced a maximum flow rate of almost 170 cfs. This extra input of phosphorus from sewer water had a profound effect on the phosphorus levels within Alewife Brook during those storms. Thus, as shown in Figure C-7, the September and July storms consequently had two of the highest EMCs.

Table C-7. Comprehensive Table of Factors Related to Storms Sampled During 2014

		2014 Storm Sampling Date							
Contributing Factor	*Units*	*15-Apr*	*17-May*	*25-Jun*	*27-Jul*	*13-Aug*	*31-Aug*	*6-Sep*	*16-Oct*
Event Mean TP Concentration	(mg/L)	0.118	0.086	0.129	0.402	0.485	0.144	0.326	0.157
Pre-storm TP Concentration	(mg/L)	0.054	0.040	0.075	0.141	0.109	0.049	0.084	0.055
Mean TP Concentration	(mg/L)	0.123	0.112	0.169	0.331	0.421	0.140	0.417	0.162
Median TP Concentration	(mg/L)	0.109	0.097	0.1155	0.212	0.489	0.1475	0.256	0.163
Peak TP Concentration	(mg/L)	0.264	0.269	0.563	0.687	0.58	0.215	1.56	0.256
Precipitation Duration	(hr)	23	18	17	22	17	2	9	15
Total Precipitation	(in)	0.98	0.71	0.28	0.46	1.06	0.54	0.37	0.63
Peak Precip Intensity	(in/hr)	0.19	0.38	0.14	0.28	0.14	0.27	0.22	0.22
Preceding Dry Period	(days)	1.8	5.7	8.8	11.7	6.6	4.0	4.3	4.7
CSO?	(YES/NO)	NO	NO	NO	YES	NO	NO	YES	NO
Average CSO Flow Rate	(cfs)	0	0	0	137.5	0	0	28.6	0
Peak Flow Rate	(cfs)	34	25	37	168	31	27	91	11
Mean Flow	(cfs)	11.8	9.9	7.3	11.0	5.2	5.7	23.0	4.6
Median Flow	(cfs)	9.6	9.1	5.3	7.7	5.6	4.6	22.0	4.0
Peak Velocity	(fps)	1.0	0.8	1.0	3.2	1.0	0.8	2.0	0.4
Lowest Velocity	(fps)	0.1	0.1	0.1	0.1	0.0	0.0	0.0	0.1
Peak Gage Height	(ft)	2.7	2.3	2.6	4.5	2.2	2.4	3.3	2.2
Lowest Gage Height	(ft)	1.8	1.8	2.1	2.1	1.9	2.0	1.9	1.5
Average Temperature	(°F)	52.1	62.9	70.8	70.6	66.3	73.8	71.8	65.6
Day of Year	(Day/365)	105	136	177	208	225	243	249	289
Average Wind Speed	(mph)	17	12	11	10	14	8	9	13

[14]

Event Mean Concentration

Calculation of the event mean concentration (EMC) is a practical method for characterizing phosphorus concentrations in Alewife Brook from a runoff event. The EMC is used to reflect the average concentration over the course of each storm event and can be used to estimate pollutant loads. EMC is weighted by the flow volume, and is calculated as follows:

$$EMC = \frac{\sum_{i=1}^{n} C_i V_i}{\sum_{i=1}^{n} V_i}$$

[14] This data came from USGS flow records, NCDC weather records, and storm-event sampling performed by the author.

Where C_i is the concentration measured in sample i, and V_i is the flow volume associated with that sample. The flow volumes were computed by integrating the flow measurements between samples. EMC results are shown in Figure C-5.

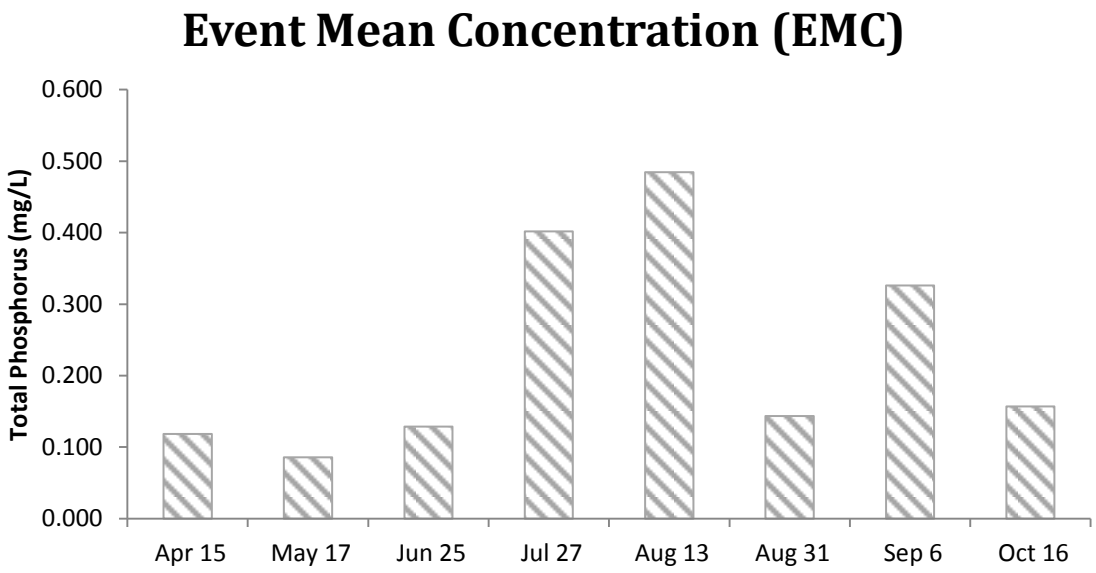

Figure C-5. Event Mean Concentrations per Storm

Variability in Event Mean Concentration

One of the main objectives of this work was to identify which factors contribute most to event mean concentration at Alewife Brook. Thus, the data summarized above was used to determine correlation values relative to event mean concentration values of each storm. Correlation values take the form of the following equation

$$r\ (\%) = 100 * \left[\frac{a * b}{\sqrt{a^2 * b^2}}\right]$$

Where $a = EMC\ value - Mean\ EMC\ value$ and $b = various\ variable\ value - mean\ variable\ value$. The closer the correlation (r) value is to 100%, the higher the

correlation. Table C-8 depicts the variables with the highest correlation to EMC. As shown, pre-storm total phosphorus, average CSO flow rate, slope of hydrograph, and peak high flow indicate the highest correlation to EMC. This shows that pre-storm nutrient conditions and flow conditions greatly influence storm event mean concentration. Variables with high correlation to EMC were then used to develop a regression model for EMC based on these characteristics. The following subsections describe the impacts of these variables on EMC.

Table C-8. Event Mean Concentration Correlations

Variable	Correlation Percent
Pre-storm Total Phosphorus (mg/L)	90.5%
Average CSO Flow Rate (cfs)	87.5%
Slope of Hydrograph	84.9%
Peak High Flow (cfs)	73.1%
Average Temp (K)	40.7%
Total Flow Rate per Storm (cfs)	20.9%
Preceding Dry Period (days)	16.5%
Runoff Volume per storm (cubic ft)	14.2%
Day of Year	12.0%

Pre-Storm Total Phosphorus Conditions

One of the most telling features of how much total phosphorus will exist within a river during a storm is the quantity existing within the river before the storm. A variety of factors will increase the pre-event phosphorus to its storm-event levels, but the pre-storm

concentration serves as a baseline for future phosphorus levels. Figure C-5 in the previous section showed both pre-storm total phosphorus and the event mean concentrations for each storm. Pre-storm phosphorus measurements are generally taken 4 to 10 hours before rainfall occurs. The patterns relevant between pre-storm total phosphorus levels and event mean concentrations imply that one cannot merely focus on intra-storm events to characterize EMC. Conditions prior to storm events play a significant role in phosphorus loading during storms.

Active Combined Sewer Overflow Discharge

Combined sewer overflows have a powerful impact on phosphorus conditions within Alewife Brook. The two storms that experienced CSO discharges contributed to significant increases in both flow rate and phosphorus concentration within the river. As shown in Figure C-6, the average flow rate of the July CSO is very similar to the peak flow rate for the storm as a whole. However, the average CSO flow rate of the September storm is less than half of the magnitude of the peak flow rate for that storm, which coincides with a smaller EMC than the July storm. Not only do CSO outbreaks increase flow rates, but they increase gage height, eroding soil from areas surrounding the river. CSOs also provide a direct input of phosphorus in the form of raw sewage into Alewife Brook. The storms with active CSOs stand out in an event mean concentration context because they have large additional direct inputs of phosphorus-laden sewage into the river, whereas other storm inputs mainly come from non-point sources.

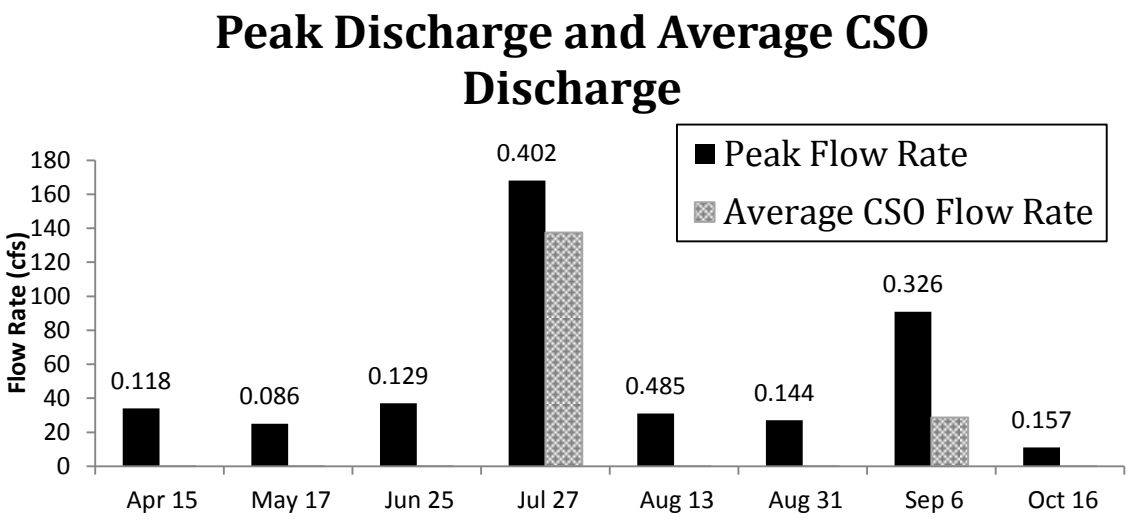

Figure C-6. Comparison of Peak Discharge and Average CSO Flow Rates, (EMC values listed above each bar)

Slope of Hydrograph

The slope of the hydrograph of a storm provides information about storm intensity. Peak flow rate certainly indicates enormity of a storm and its ability to produce high flow scenarios, but the slope of the hydrograph offers information about the peak high flow and what amount of *time* it took to achieve that maximum. Figure C-7 identifies each storm's slope of hydrograph, referring to the ratio of the rise of the flow rate to maximum discharge to the time it took to achieve maximum discharge. The figure also labels each storm's correlated EMC. As shown, the July and September storms have very high slopes. This indicates that the storm intensity was very high for these storms and the additional input of CSO flow contributed to an overall flow rate in a very short amount of time at the USGS flow gauge location. April, August, and October storms exhibit very small slopes, indicating that it either took a longer amount of time to achieve

the maximum flow rate, or that maximum flow rate was small in comparison to other storms.

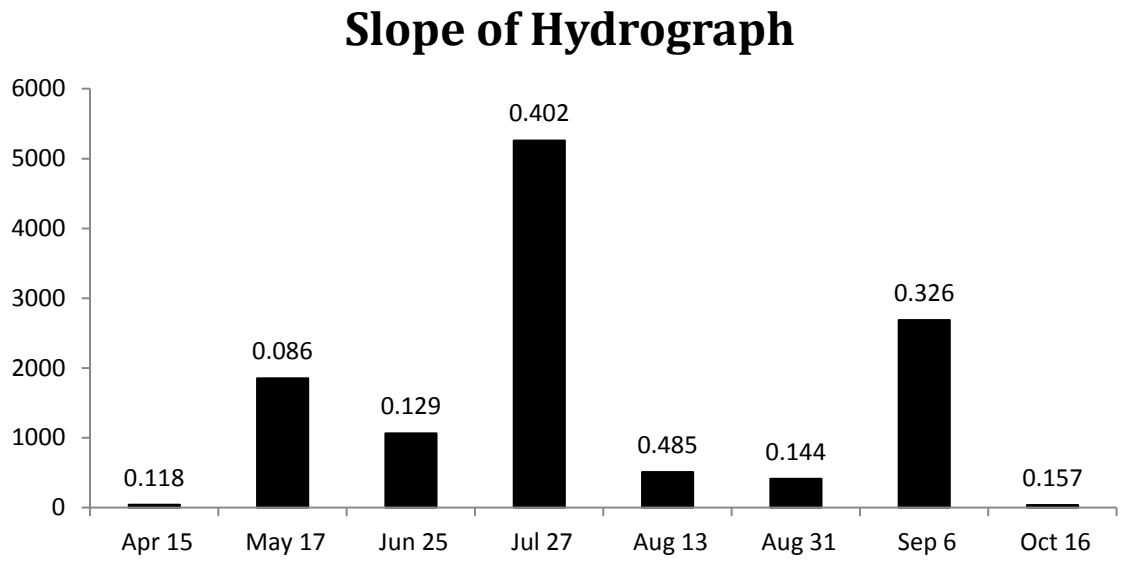

Figure C-7. Slope of Each Storm's Hydrograph (EMC values listed above each bar)

Peak High Flow Rate

Increase in discharge during storm events is a function of many different variables, such as precipitation, precipitation intensity, inputs of constituents carried into the river via runoff, active CSOs, and a number of other factors. As shown in Figure C-8, peak discharge was very high for both July and September storms. Figure C-6 previously indicated that the two storms with highest peak discharge were subject to active CSO outbreaks. In regression modeling, these high peak discharge rates may indirectly account for extreme events, such as CSOs, during a storm.

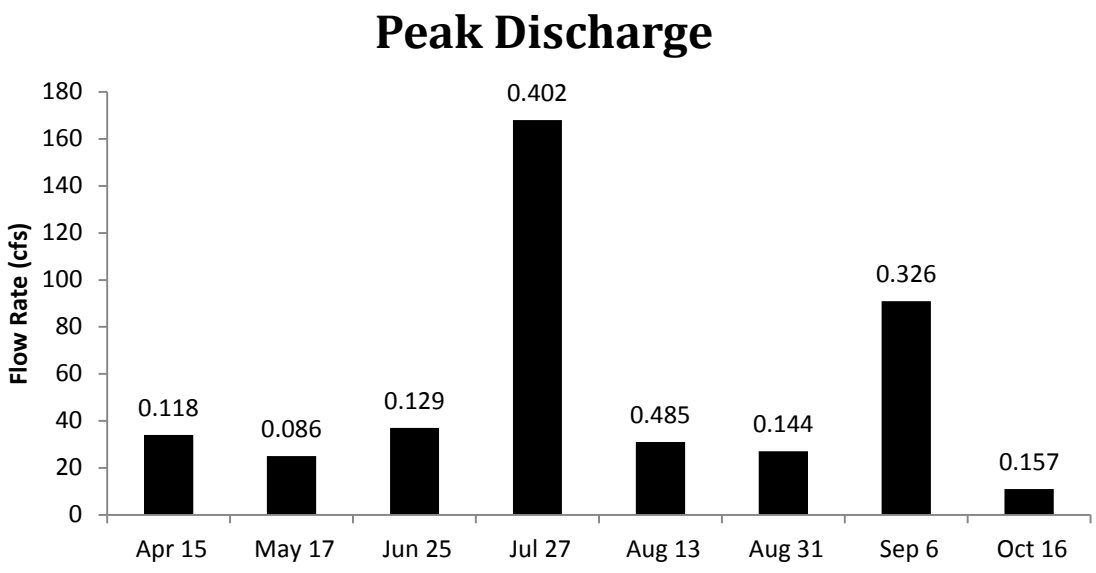

Figure C-8. Maximum Discharge during Each Storm (EMC values listed above each bar)

Average Air Temperature

Air temperature has a profound impact on microbial activity. Higher temperatures mobilize microbes and allow for soil organic matter to decay at higher rates. In the winter, such microbial processes do not work as quickly because colder temperatures do not enhance mobilization of microbes. As temperature increases, microbial activity increases, allowing phosphorus to move right into the river system during storm events. If air temperature is coupled with preceding dry period, assumptions can be made about microbial activity and phosphorus accumulation prior to storm events. Figure C-9 provides average temperatures during each storm event.

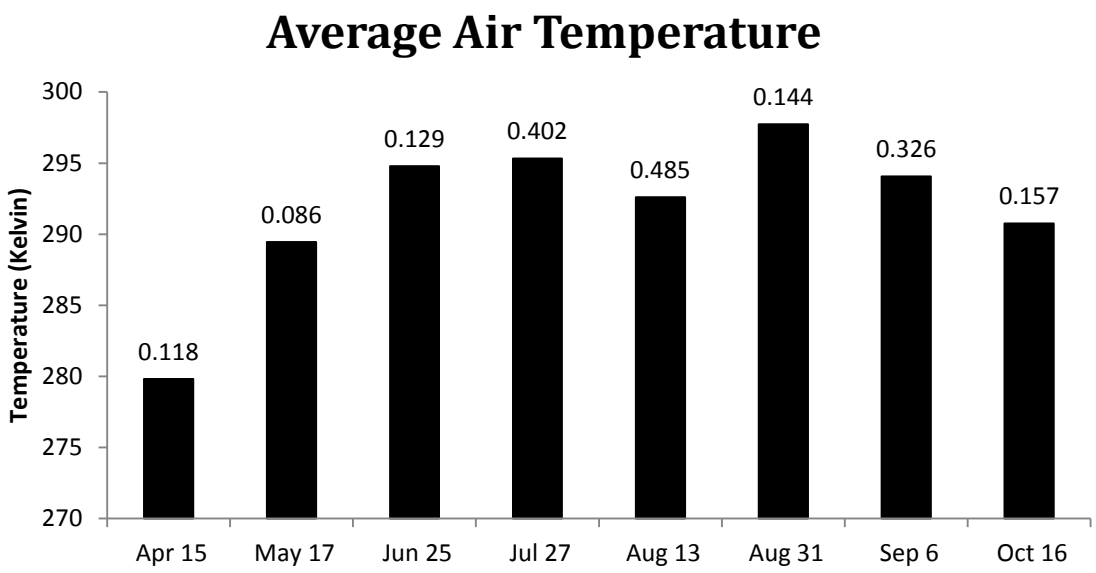

Figure C-9.Average Air Temperature during Sampled Storms (EMC value listed above each bar)

Preceding Dry Period

A number of factors contribute to accumulation of phosphorus near and around a waterway, such as pet waste, decay of soil organic matter, improper waste of phosphate-containing cleaning supplies, and fertilizer. Generally, rain storms with intensity greater than 0.10 inches per hour wash these sources of phosphorus into the river. However, the period of dry weather before a storm may influence just how much phosphorus is input into the river system. Figure C-10 indicates number of dry days preceding each storm sampled with the event mean concentration for each storm labeled above the dry period value. Now that we know that both July and September storms experienced CSO outbreaks, we can use this figure to point to another possible reason why the July storm experienced a higher EMC than the September storm. As shown, the July storm had

almost 12 days of dry weather before the rain event occurred. This means that phosphorus was able to accumulate on surfaces surrounding Alewife Brook for several days longer than the September storm, allowing a larger quantity of phosphorus to be washed into the river.

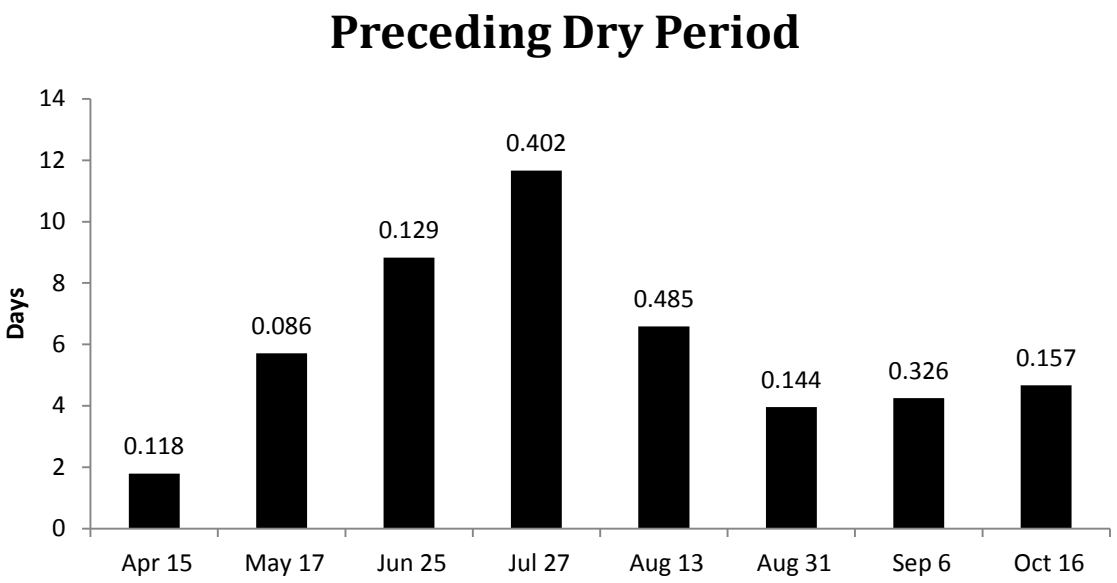

Figure C-10. Antecedent Moisture Conditions (EMC value listed above each bar)

EMC Regression Model

Two regression models were developed using the above characteristics relating to event mean concentrations. The model took the general form of

$$EMC = \beta_0 + \beta_1 Variable\ 1 + \beta_2\ Variable\ 2 + \beta_3\ Variable\ 3 + \cdots$$

Where β_0 through β_n are model coefficients and the variables are summarized below. The August 13 storm was omitted from analysis because inadequate sampling techniques

(not enough samples taken to represent the rise *and* fall of the hydrograph) inflated its EMC value.

A multivariate regression model is required as it is unrealistic to focus solely on the response of EMC to just one variable at a time. As noted above, many forces work together to produce each event mean concentration and the combination of these variables into a regression model can provide essential information on the impacts of each variable on phosphorus loading in Alewife Brook.

The first regression model takes into account pre-storm conditions as indicators of event mean concentration. These pre-storm variables include antecedent dry period (days of dry weather prior to storm), season (dummy variable indicating spring, summer, or fall seasons), day of year, and the pre-storm phosphorus concentration. The second regression model uses intra-event conditions to describe EMC. The intra-event variables include peak high flow, average CSO flow rate, slope of hydrograph, and average temperature. Although the majority of these variables are flow-related, the temperature component of this model can be used as a seasonal factor, addressing the difference in EMC values based on warmth or coldness of air temperature.

As shown in Figure C-11, the pre-storm model more accurately predicts observed event mean concentration values than the intra-storm model. This tells us that conditions prior to a storm greatly influence event mean concentration and may be used to identify impacts of rain events on total phosphorus concentrations within Alewife Brook. The intra-storm event model was more accurate than the pre-storm model in three instances, although it greatly underestimated the EMCs of both fall storms. Overall, both models

indicate the importance of flow rate, temperature, pre-event conditions, and season in determining differences in event mean concentration storm-to-storm.

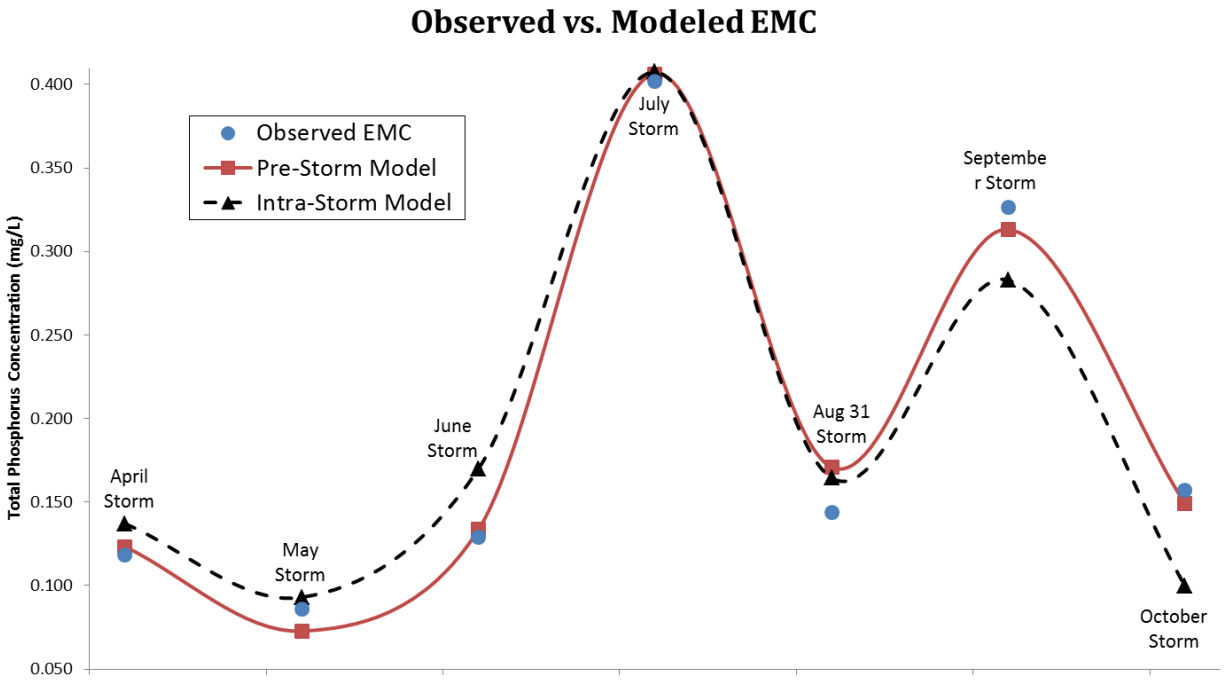

Figure C-11. Observed EMC Values vs. Pre-Storm and Intra-Storm Models

A third regression model was developed which excludes pre-storm total phosphorus concentration. This model can be used to estimate approximate event mean concentration of total phosphorus without taking and analyzing samples. The model includes both pre-storm and intra-storm conditions, such as slope of hydrograph, preceding dry period, peak high flow, season, and average temperature. Such data can easily be determined from online sources such as the National Climatic Data Center (for temperature and preceding dry period) and the United States Geological Survey (for flow rate).

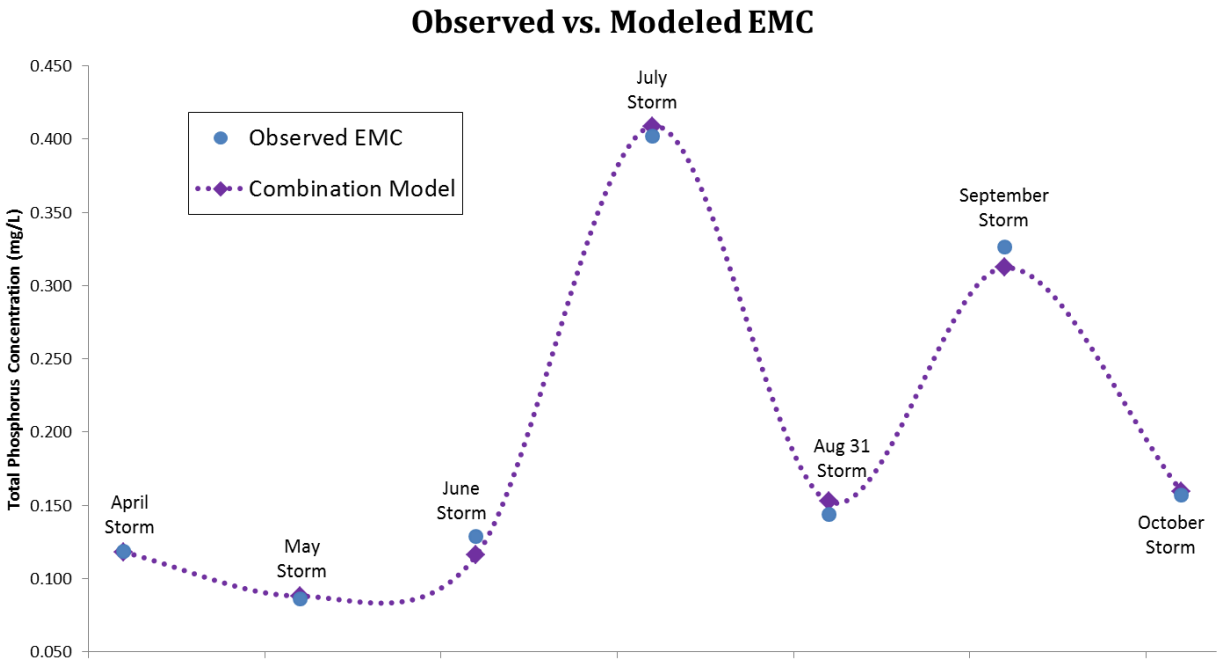

Figure C-12. Combination Model to Predict EMC

As shown in Figure C-12, the combination model fairly accurately predicts each EMC value, only subtly overestimating the EMC of the August 31 storm and underestimating EMC of the September and June storms. Summary statistics and model coefficients for all three models are found in Table C-9. The combination model actually outperforms both the separate pre-storm and intra-storm models based on low residual error and high R^2 values.

Table C-9. Summary Statistics for Three EMC Models

	Model		
Summary Statistic	**Pre-Storm**	**Intra-Storm**	**Combination**
S	0.025	0.062	0.022
R^2	98.6%	91.1%	99.4%
R^2 (adjusted)	95.8%	73.2%	96.6%
Residual Error	0.001	0.008	0.001

Annual Budget 2014

Combining sampling data from storm events and regular monthly baseline sampling data, a model was created that can determine total phosphorus loading at any time of year. Because access to flow data is available for every fifteen minutes via flow gage at Alewife Brook, phosphorus loading is easily estimated using the model introduced in section 4.3. As shown in Table C-10, applying this model to flow gage data for the entire 2014 calendar year, it is estimated that 16,000 kg of phosphorus was input into Alewife Brook. Total Phosphorus load estimates for previous years are also shown in Table C-10.

Table C-10. Estimates of Annual Total Unfiltered Phosphorus Loads from 2009-2014 (from Load Estimator Model, Using USGS Flow Rate Data)

Year	Estimated Annual Total Phosphorus Load (kg)
2009	14400
2010	15800
2011	18600
2012	16600
2013	15700
2014	16000

Appendix D: R Code

Load Estimator Model

```
> # Load Estimator Model
> # Alewife Storm Sampling April - October 2014
> # Multiple linear regression load estimation
>
> # Check to make sure regression packages have been loaded
> library(QuantPsyc)
> library(car)
> library(boot)
>
> # Upload data from working directory
> R_EST_MODEL = read.csv("/Users/kmunso01/Documents/R/R_EST_MODEL.csv",
header = TRUE)
>
> # Save this data
> write.csv(R_EST_MODEL, "R_EST_MODEL.csv")
>
> # Run regression model
> R_EST_MODEL = lm(formula = Load~Q+Qt+sin+cos, data = R_EST_MODEL)
>
> # View results of model
> summary(R_EST_MODEL)

Call:
lm(formula = Load ~ Q + Qt + sin + cos, data = R_EST_MODEL)

Residuals:
     Min       1Q   Median       3Q      Max
-0.83617 -0.23598 -0.00178  0.26747  0.80472

Coefficients:
            Estimate Std. Error t value Pr(>|t|)
(Intercept)  4.86990    0.16702  29.158  < 2e-16 ***
Q            1.62659    0.05321  30.571  < 2e-16 ***
Qt          -0.31242    0.08743  -3.573 0.000532 ***
sin         -0.25416    0.06901  -3.683 0.000365 ***
cos         -0.24240    0.06923  -3.501 0.000679 ***
---
Signif. codes:  0 ‘***’ 0.001 ‘**’ 0.01 ‘*’ 0.05 ‘.’ 0.1 ‘ ’ 1

Residual standard error: 0.3736 on 106 degrees of freedom
Multiple R-squared:  0.9018,    Adjusted R-squared:  0.8981
F-statistic: 243.3 on 4 and 106 DF,  p-value: < 2.2e-16

>
> # View coefficients of parameters
> coefficients(R_EST_MODEL)
(Intercept)           Q          Qt         sin         cos
  4.8698971   1.6265931  -0.3124161  -0.2541584  -0.2424028
```

```
>
> # View analysis of variance (ANOVA)
> anova(R_EST_MODEL)
Analysis of Variance Table

Response: Load
          Df  Sum Sq Mean Sq F value    Pr(>F)
Q          1 120.710 120.710 864.944 < 2.2e-16 ***
Qt         1  11.834  11.834  84.793 3.395e-15 ***
sin        1   1.550   1.550  11.105 0.0011861 **
cos        1   1.711   1.711  12.258 0.0006791 ***
Residuals 106  14.793   0.140
---
Signif. codes:  0 ‘***’ 0.001 ‘**’ 0.01 ‘*’ 0.05 ‘.’ 0.1 ‘ ’ 1
>
> # Plot residuals to look for homoscedasticity
> plot(R_EST_MODEL)
>
> # Confidence intervals for model parameters
> confint(R_EST_MODEL)
                2.5 %     97.5 %
(Intercept)  4.5387651  5.2010291
Q            1.5211055  1.7320808
Qt          -0.4857581 -0.1390741
sin         -0.3909768 -0.1173400
cos         -0.3796671 -0.1051384
>
```

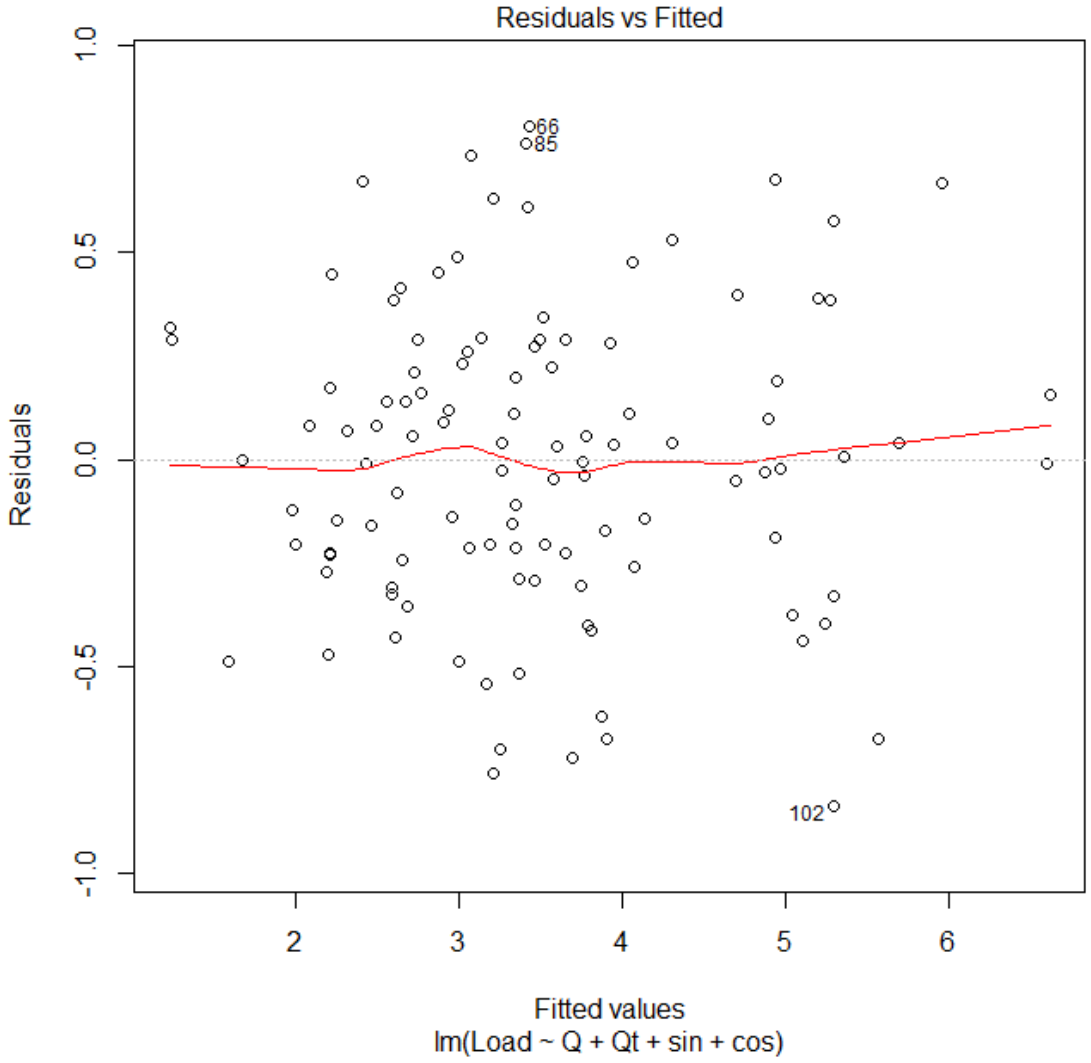

Figure D-1. Residuals vs. Fitted: Load Estimator Model

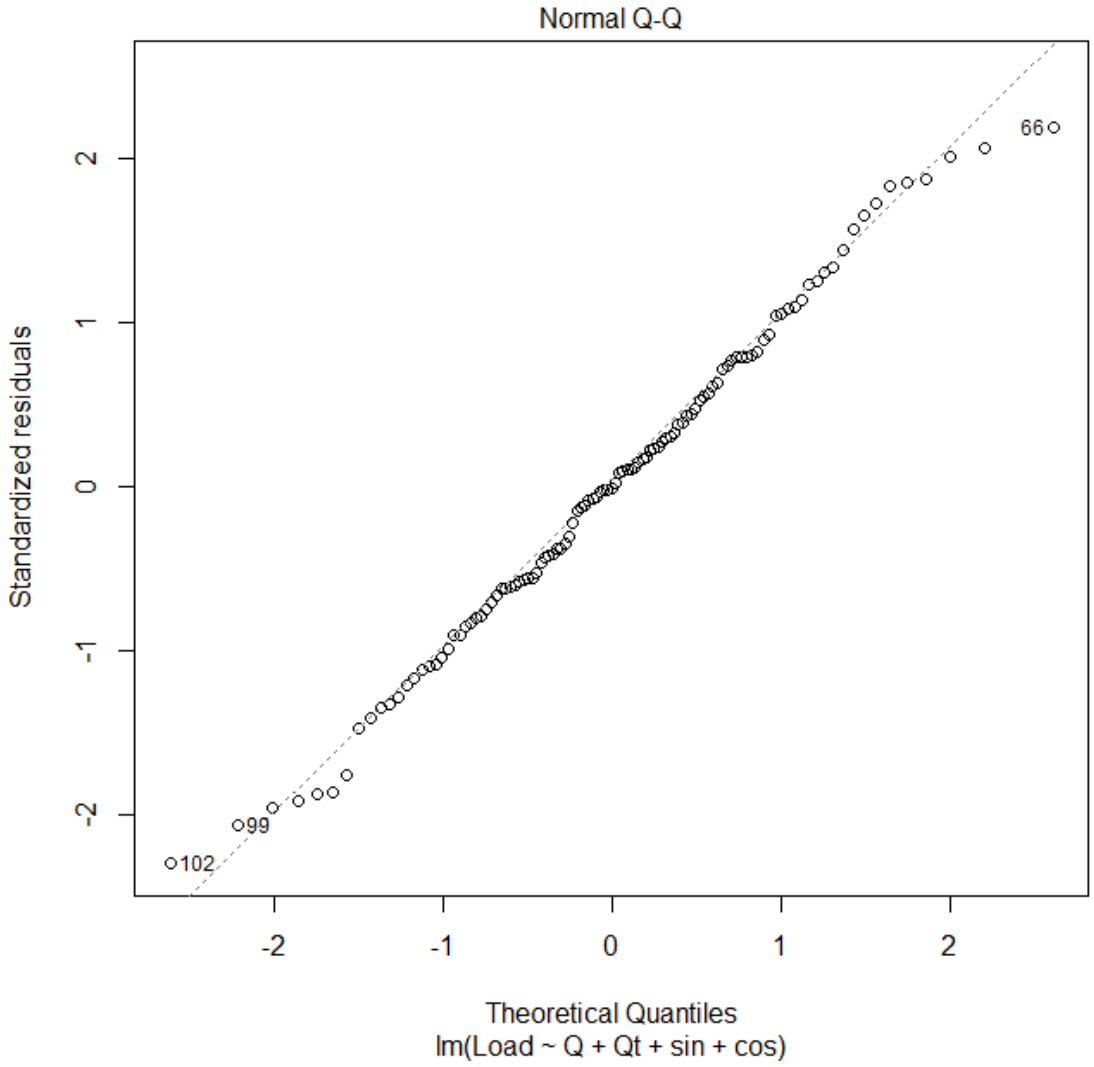

Figure D-2. Normal Q-Q Plot for Load Estimator Model

Climate Elasticity Models

Nonparametric – Equation 7

```
> # Climate Elasticity Model
> # Based on modeled monthly water quality data as well as NCDC and
USGS weather data
> # Multivariate Sensitivity of total phosphorus to changes in
precipitation, temperature, and flow rate
> # Fixed effects = seasonal dummy variables
>
> # Check to make sure regression packages have been loaded
> library(QuantPsyc)
> library(car)
> library(boot)
>
> # Upload data from working directory
> ELAST_MODEL = read.csv("/Users/kmunso01/Documents/R/ELAST_MODEL.csv",
header = TRUE)
>
> # Save this data
> write.csv(ELAST_MODEL, "ELAST_MODEL.csv")
>
> # Run first regression model: Nonparametric equation 7
> ELAST_MODEL_7 = lm(formula =
TP7~P7+T7+Q7+CSO7+Spring+Summer+Fall+Winter, data = ELAST_MODEL)
>
> # View results of model
> summary(ELAST_MODEL_7)

Call:
lm(formula = TP7 ~ P7 + T7 + Q7 + CSO7 + Spring + Summer + Fall +
    Winter, data = ELAST_MODEL)

Residuals:
     Min       1Q   Median       3Q      Max
-0.33186 -0.12716  0.02531  0.10147  0.41056

Coefficients: (1 not defined because of singularities)
            Estimate Std. Error t value Pr(>|t|)
(Intercept) -0.06984    0.06223  -1.122 0.265234
P7           0.27219    0.05094   5.344 8.99e-07 ***
T7           0.55583    0.14219   3.909 0.000198 ***
Q7           1.11946    0.05637  19.858  < 2e-16 ***
CSO7         0.04733    0.01662   2.848 0.005635 **
Spring      -0.07681    0.08618  -0.891 0.375565
Summer       0.20051    0.11314   1.772 0.080305 .
Fall         0.14155    0.06194   2.285 0.025053 *
Winter            NA         NA      NA       NA
---
Signif. codes:  0 ‘***’ 0.001 ‘**’ 0.01 ‘*’ 0.05 ‘.’ 0.1 ‘ ’ 1
```

```
Residual standard error: 0.1655 on 77 degrees of freedom
Multiple R-squared:  0.9617,    Adjusted R-squared:  0.9582
F-statistic: 275.9 on 7 and 77 DF,  p-value: < 2.2e-16

>
> # View coefficients of parameters
> coefficients(ELAST_MODEL_7)
(Intercept)          P7          T7          Q7        CSO7      Spring
Summer        Fall      Winter
-0.06983930  0.27218967  0.55582622  1.11946228  0.04732827 -0.07681316
0.20050937  0.14154665          NA
>
> # View analysis of variance (ANOVA)
> anova(ELAST_MODEL_7)
Analysis of Variance Table

Response: TP7
          Df Sum Sq Mean Sq   F value    Pr(>F)
P7         1 36.927  36.927 1347.8646 < 2.2e-16 ***
T7         1  0.653   0.653   23.8340 5.562e-06 ***
Q7         1 14.020  14.020  511.7441 < 2.2e-16 ***
CSO7       1  0.516   0.516   18.8342 4.283e-05 ***
Spring     1  0.645   0.645   23.5592 6.203e-06 ***
Summer     1  0.002   0.002    0.0845   0.77207
Fall       1  0.143   0.143    5.2222   0.02505 *
Residuals 77  2.110   0.027
---
Signif. codes:  0 ‘***’ 0.001 ‘**’ 0.01 ‘*’ 0.05 ‘.’ 0.1 ‘ ’ 1
>
> # Confidence intervals for model parameters
> confint(ELAST_MODEL_7)
                 2.5 %     97.5 %
(Intercept) -0.19375561 0.05407701
P7           0.17075923 0.37362012
T7           0.27269721 0.83895523
Q7           1.00721079 1.23171378
CSO7         0.01423995 0.08041660
Spring      -0.24842860 0.09480229
Summer      -0.02477520 0.42579394
Fall         0.01820767 0.26488563
Winter              NA         NA

>
> # Plot residuals
> plot(ELAST_MODEL_7)
```

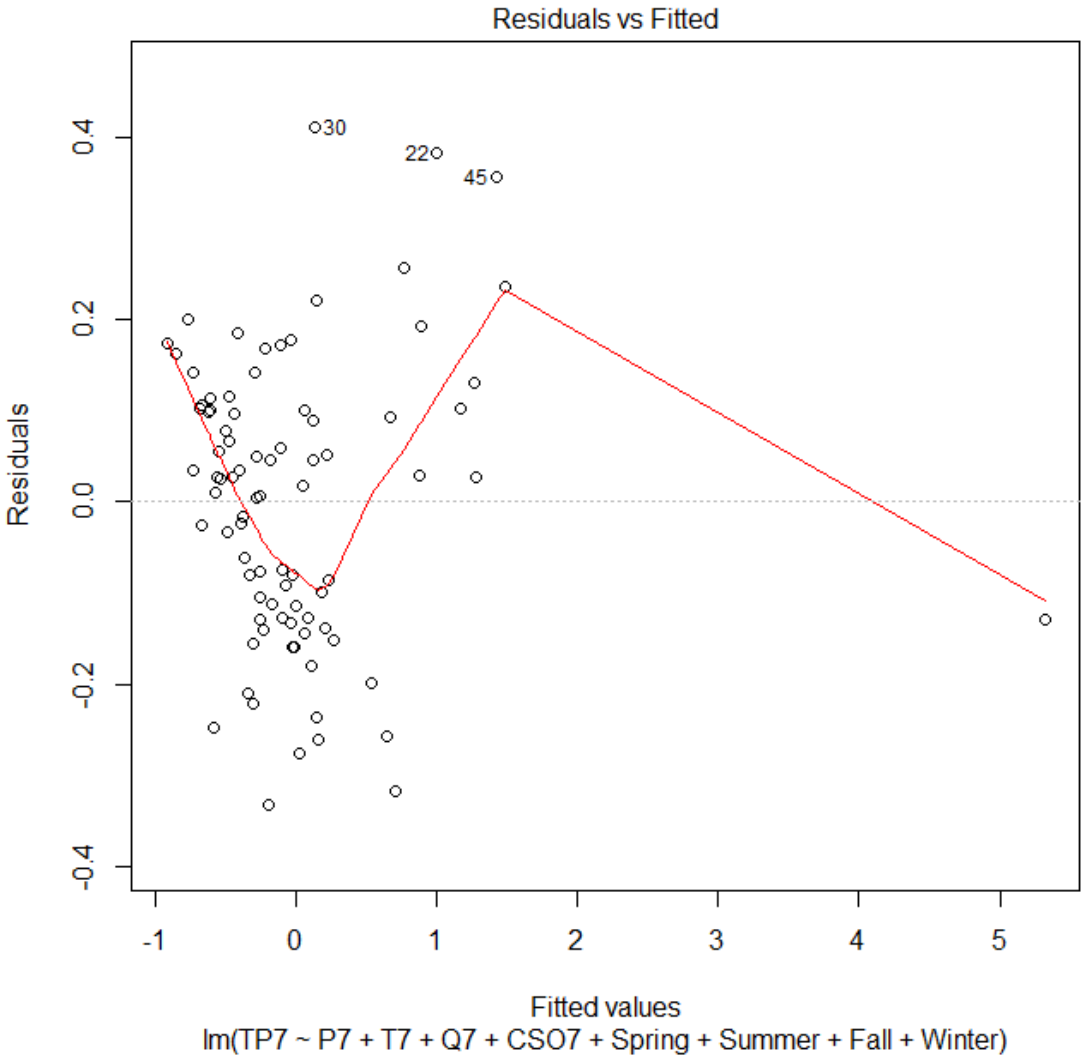

Figure D-3. Residuals vs. Fitted: Nonparametric Elasticity Model

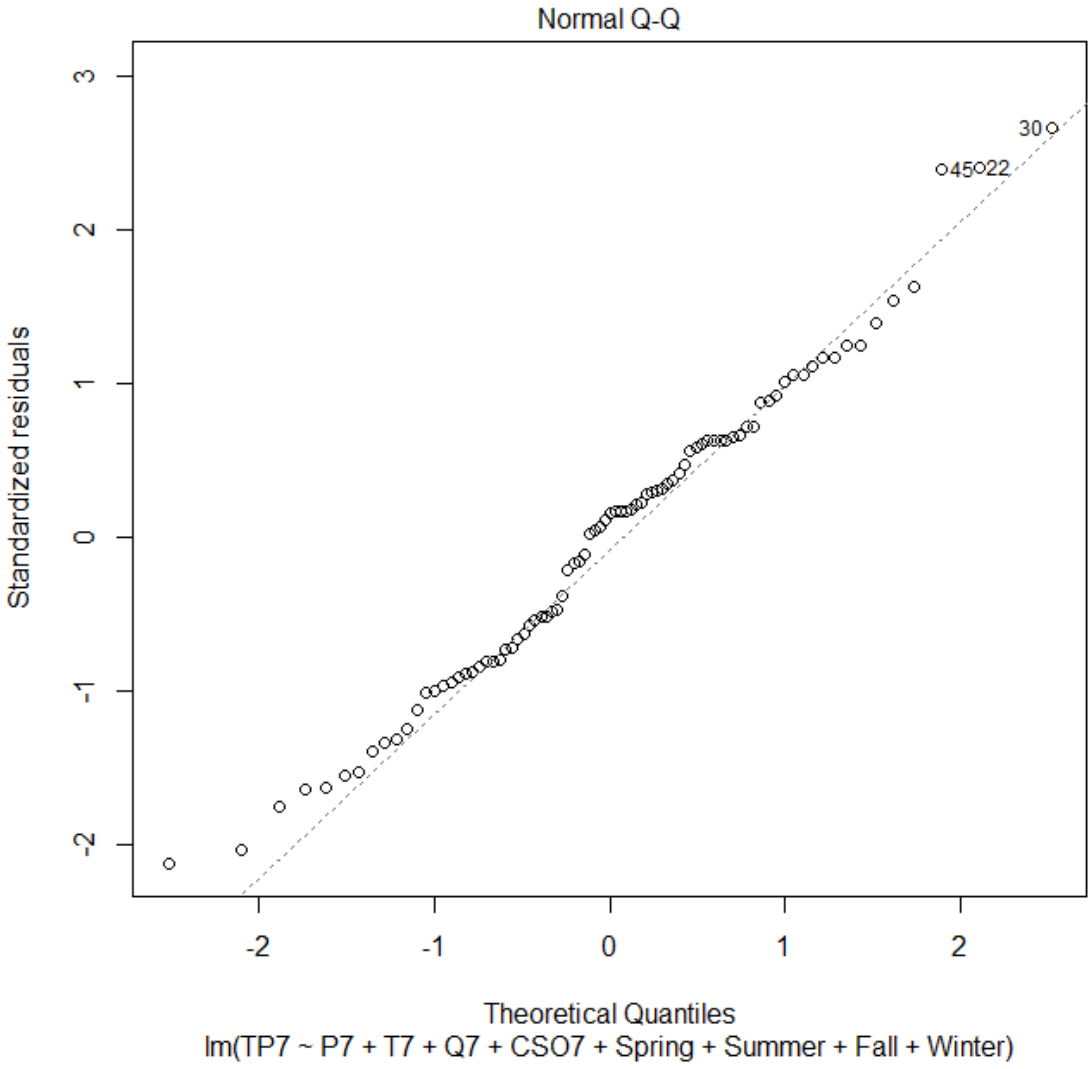

Figure D-4. Normal Q-Q Plot for Nonparametric Elasticity Model

Parametric – Equation 8

```
> # Run second regression model: Parametric equation 8
> ELAST_MODEL_8 = lm(formula =
TP8~P8+T8+Q8+CSO8+Spring+Summer+Fall+Winter, data = ELAST_MODEL)
>
> # View results of model
> summary(ELAST_MODEL_8)

Call:
lm(formula = TP8 ~ P8 + T8 + Q8 + CSO8 + Spring + Summer + Fall +
    Winter, data = ELAST_MODEL)

Residuals:
     Min       1Q   Median       3Q      Max
-0.80205 -0.08553  0.00166  0.08866  0.37381

Coefficients: (1 not defined because of singularities)
             Estimate Std. Error t value Pr(>|t|)
(Intercept)  2.562907   0.493095   5.198 1.61e-06 ***
P8           0.100113   0.046013   2.176   0.0326 *
T8           0.570213   0.132855   4.292 5.10e-05 ***
Q8           1.229814   0.063781  19.282  < 2e-16 ***
CSO8         0.015516   0.006423   2.416   0.0181 *
Spring      -0.093011   0.093579  -0.994   0.3234
Summer       0.235269   0.118370   1.988   0.0504 .
Fall         0.144369   0.070979   2.034   0.0454 *
Winter             NA         NA      NA       NA
---
Signif. codes:  0 ‘***’ 0.001 ‘**’ 0.01 ‘*’ 0.05 ‘.’ 0.1 ‘ ’ 1

Residual standard error: 0.1771 on 77 degrees of freedom
Multiple R-squared:  0.9206,    Adjusted R-squared:  0.9134
F-statistic: 127.5 on 7 and 77 DF,  p-value: < 2.2e-16

>
> # View coefficients of parameters
> coefficients(ELAST_MODEL_8)
(Intercept)          P8          T8          Q8        CSO8      Spring
Summer        Fall      Winter
 2.56290688  0.10011293  0.57021256  1.22981367  0.01551565 -0.09301127
0.23526866  0.14436866          NA
```

```
>
> # View analysis of variance (ANOVA)
> anova(ELAST_MODEL_8)
Analysis of Variance Table

Response: TP8
          Df  Sum Sq Mean Sq  F value    Pr(>F)
P8         1 12.3660 12.3660 394.0485 < 2.2e-16 ***
T8         1  1.1983  1.1983  38.1846 2.836e-08 ***
Q8         1 12.8582 12.8582 409.7343 < 2.2e-16 ***
CSO8       1  0.6117  0.6117  19.4922 3.251e-05 ***
Spring     1  0.8357  0.8357  26.6314 1.867e-06 ***
Summer     1  0.0167  0.0167   0.5328    0.4676
Fall       1  0.1298  0.1298   4.1370    0.0454 *
Residuals 77  2.4164  0.0314
---
Signif. codes:  0 ‘***’ 0.001 ‘**’ 0.01 ‘*’ 0.05 ‘.’ 0.1 ‘ ’ 1
>
> # Confidence intervals for model parameters
> confint(ELAST_MODEL_8)
                   2.5 %     97.5 %
(Intercept)  1.5810293987 3.54478435
P8           0.0084890314 0.19173683
T8           0.3056643352 0.83476078
Q8           1.1028089092 1.35681842
CSO8         0.0027252706 0.02830602
Spring      -0.2793510671 0.09332853
Summer      -0.0004366052 0.47097393
Fall         0.0030315078 0.28570582
Winter                NA         NA
>
> # Plot residuals
> plot(ELAST_MODEL_8)
```

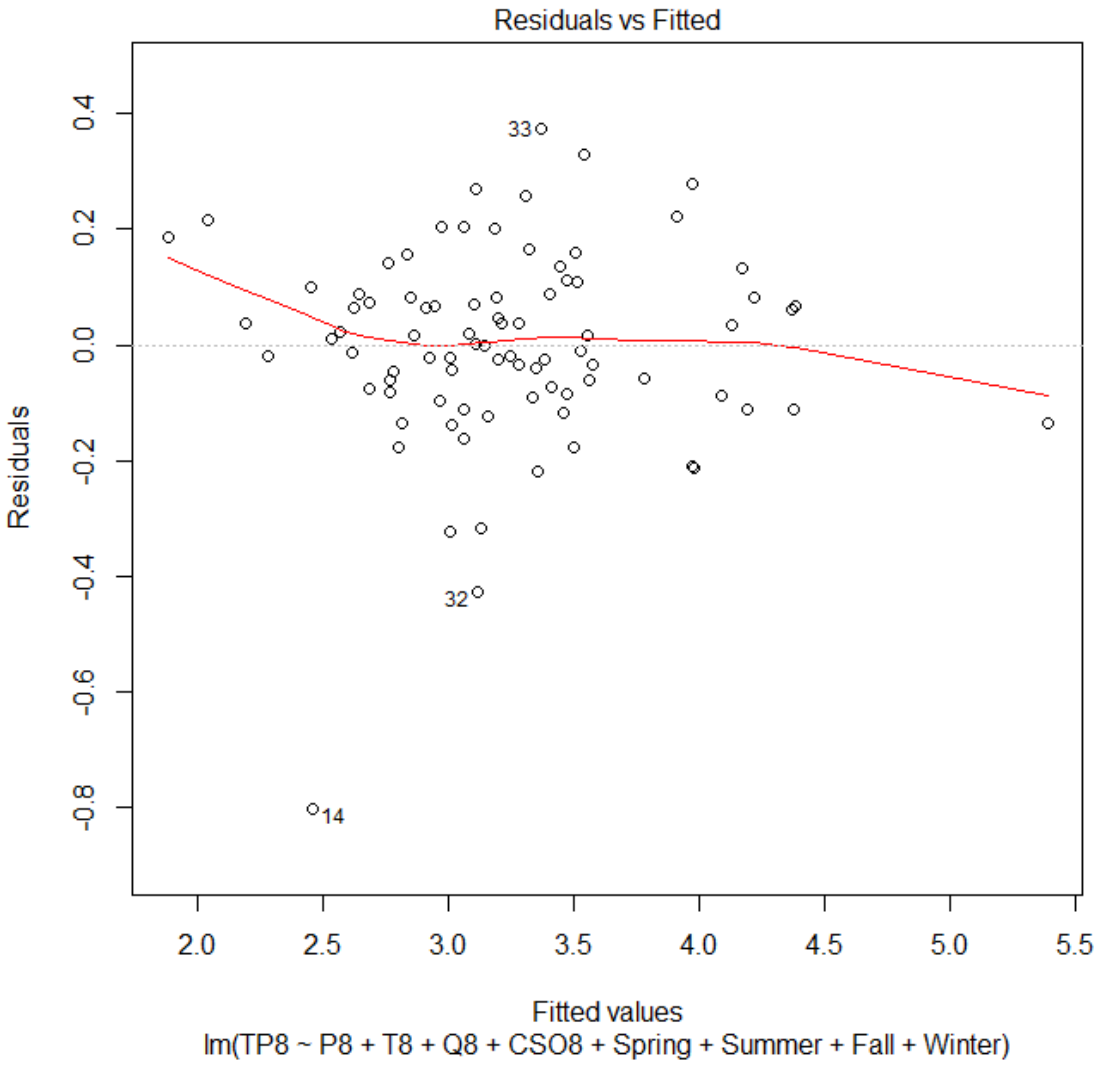

Figure D-5. Residuals vs. Fitted: Parametric Elasticity Model

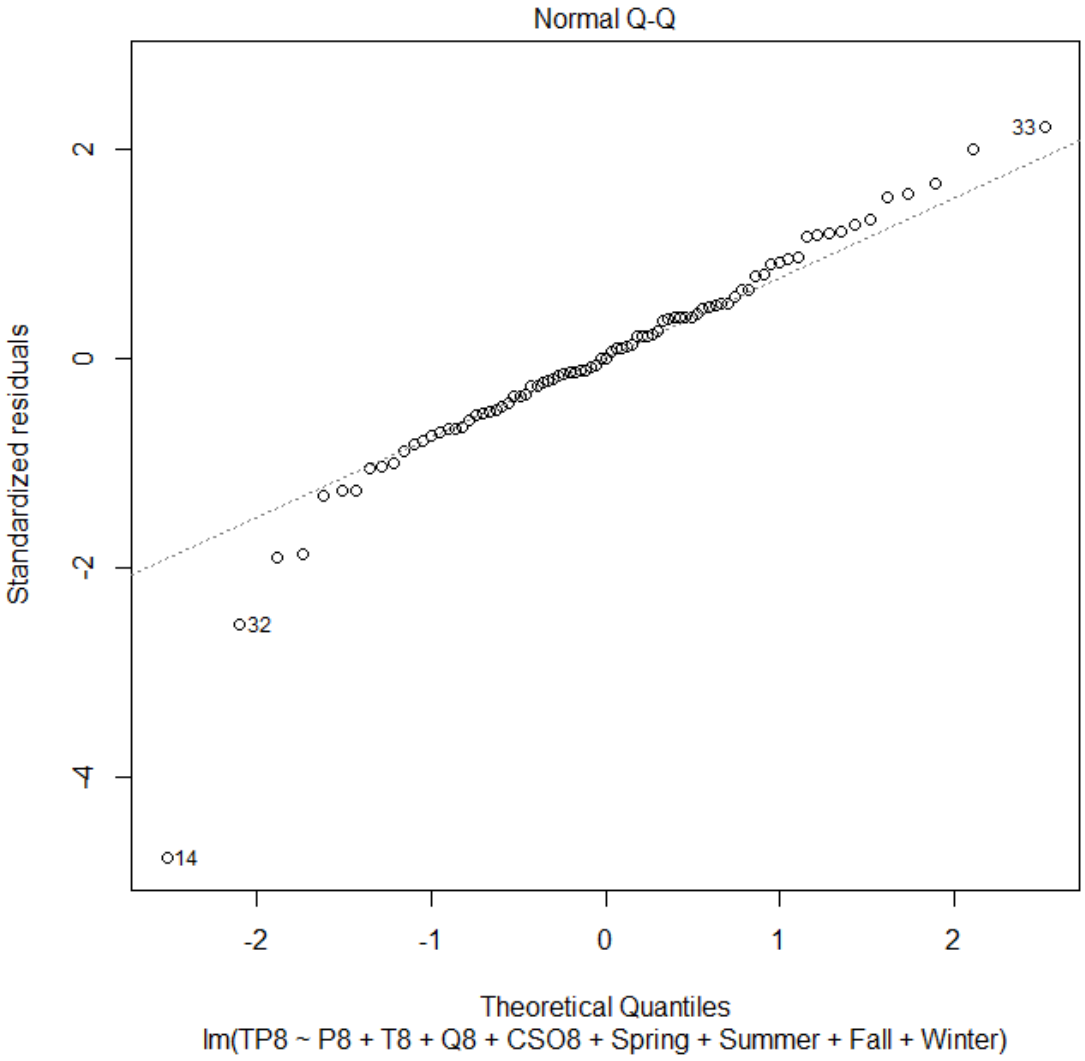

Figure D-6. Normal Q-Q Plot for Parametric Elasticity Model